Impact of the environmental conditions on the stoichiometry of magnetite nanoparticles

Phoomipat Jungcharoen

UNIVERSITÉ DE RENNES 1

THESE DE DOCTORAT DE

L'UNIVERSITE DE RENNES 1

ECOLE DOCTORALE N° 600
Ecole doctorale Ecologie, Géosciences, Agronomie et Alimentation
Spécialité : Sciences de la Terre et de l'Environnement

Par

Phoomipat JUNGCHAROEN

Impact des conditions environnementales sur la stoechiometrie de nanoparticules de magnétite

Thèse présentée et soutenue à Rennes, le 24 Septembre 2021

Unité de recherche : Géosciences Rennes

Rapporteurs avant soutenance :

Alexandre GELABERT - Maître de Conférences - Institut de Physique du Globe de Paris
Grégory LEFEVRE - Chargé de Recherche CNRS - Chimie ParisTech

Composition du Jury :

Président :

Fabien GRASSET - Directeur de Recherche CNRS - Institut des Sciences Chimiques de Rennes

Examinateurs :

Aline DIA - Directrice de Recherche CNRS - Géosciences Rennes
Fabienne GAUFFRE - Directrice de Recherche CNRS - Institut des Sciences Chimiques de Rennes
Alexandre GELABERT - Maître de Conférences - Institut de Physique du Globe de Paris
Grégory LEFEVRE - Chargé de Recherche CNRS - Chimie ParisTech
Khalil HANNA - Professeur des Universités - Université de Rennes 1

Directeur et co-directeur de thèse :

Rémi MARSAC - Chargé de Recherche CNRS - Géosciences Rennes
Mathieu PÉDROT - Maître de Conférences - Géosciences Rennes

Acknowledgements

My academic endeavor would have never been possible without the scholarship from the faculty of Engineering at Khon Kaen University in Thailand via Campus France and together with the NanoBioGeochemistry (NBG) team at Geosciences from the University of Rennes 1.

First and foremost, I would like to express my sincere gratitude and heartfelt appreciation to my beloved supervisors: Dr. Rémi Marsac and Dr. Mathieu Pédrot for their guidance, enthusiastic encouragements, and support like my real family who took care of me for the first time. I still remember the deep appreciations when I first met them. For example, Dr. Pédrot took me from the train station (Rennes) to his house for 2 days and he wrote a paper about the plan for my French life, cook food, went to our department, and back to his house like my father when I was young. And another hero is Dr. Marsac, he often took me to many supermarkets to buy my stuff and went to his home. Indeed, his mother cooked a lot of food and I felt very warm. Although my words cannot convey my appreciation, I would like to look after them when they will visit me as a visiting scholar in Thailand in order to do some projects such as agricultural innovations and environmental sustainability.

My deepest gratitude also goes to Dr. Marc Jolivet, Dr. Amelie Juhin, Prof. Oliver Dauteuil, and Prof. Malanie Davranche who did not only support for scientific research but they also show their pure souls and teach me how to work efficiently and stay motivated under pressure.

I am thankful to Prof. Khalil Hanna, Dr. Fadi Choueikani, Dr. Mathieu Pasturel, and Dr. Frank Heberling for their generosity, recommendations, and support throughout my experiments and academic writing. I feel extremely fortunate to have had the golden opportunity to work together with them.

I would like to acknowledge the jury members: Fabienne GAUFFRE, Alexandre GELABERT, Grégory LEFEVRE, Aline DIA, Fabien GRASSET for their valuable time, critical comments, suggestions, and encouragements.

Throughout 3 years of my Ph.D. life, it was a great opportunity to work in unfamiliar environments with people from diverse backgrounds, cultures, nationalities and cultivate a creative problem solving and turning worst case scenarios into growth opportunities. I feel very happy to be a part of this team and work with my lovely friends: Alice Pradel (Pi Alice), Florent Blancho (Pi Florent), Aurelie Wahl, Marawit Tesfa, Lea Mounier, Margaux Kerdiles, Anne-Catherine Pierson-Wickman, Patrice Petitjeam, Delphine Masson, Valentine Bouju, France Polette, Charlotte Le Traon, Alexandre Coche, Maxime Bernard, Thomas Bernard, Coralie Dode, and Jan Westerweel. In addition, I would like to thank to my Asian friends: Dr. Wei Cheng, Dr. Gu Sem, Dr. Wen Zhang, Keran Zhang (Pi Keran), Junmin Deng, Qinzhi Li, Lian Zhou, and Xuemei Chen. Moreover, I would like to thank my Thai friends who study at the University of Rennes 1: Dr. Jompol Thongpaen, Tunyawan Getyeam, Wish Yardparga, Wimonsiri Huadsai, Chakkrit Netkaew, Sitthichok Kasemthaveechok, Thanaphon Khrueawatthanawet, Satawat Tongdee. Thank you for your support and for taking care of me.

I am grateful to thank to Prof. Apirat Siritaratiwat, Assoc. Prof. Dr. Jin Anotai, Assoc. Prof. Dr. Chantra Tongcumpou, Assoc. Prof. Dr. Ekawan Luepromchai, Assoc. Prof. Dr. Ratchaphon Suntivarakorn, Asst. Prof. Dr. Prapat Pongkiatku, Asst. Prof. Dr. Nonglak Boonrattanakij, Asst. Prof. Dr. Penradee Chapiwat, Wanpen Sirapat, Saowanee Namthachan, Netdao Chamroendararasmee, Niramon Pookrongnak, Khaneeros Pocharoen, and Vinaroj Supsongsuk for their great encouragements. Indeed, they not only taught me about academic activities both in the

lab and field scales for industries and outreach communities but they also teach me about improving soft skills by staying honesty.

Last but not least, I also would like to thank all of my warmest friends that I have met during my research life in 6 universities (3 national and 3 international universities). Therefore, I would like to thank Dr. Clare Kennedy, Dr. Sajjad Eghdamirad, Dr. Dipayan Choudhury, Dr. Jeerapong Silasuwan, Dr. Thanchanok Sutjarittham, Dr. Amarin Siripanich, Dr. Kanyawee Keeratimahat, Dr. Kunlapat Thongkaew, Dr. Tanit Chavalit, Dr. Pipat Piewngam, Pharm. Chanthima Jintakaweephan, Pimsiri Pumpuang, Panupan Maksuwan, Thanyarat Sriphuttisit, Karnsinee Lertratwattana, Chawin Tawiwaradilok, Chayut Orapinpatipat, Jirayu Sarakul, Nuttinee Sriwaleerut, Narakorn Inkamma, Phatraphorn Kinnala, Napaatcha Tanatanadol, Chotiwat Jantarakasem, Apirata Komenrung, Pattaranun Sitthirit, Kanokkorn Horkaew, Sujinan Yimkomkam, Naruemol Wasukran, Nafisa Kemden, Piyathida Schmid, Jittapol Prukpatarakul, Prakaithip Kitikhun, Boontarika Ubonyaem, Thanita Boonmee, Satika Boonkaewwan, Parichaya Tiralerdpanich, Sarasanant Bungadaeng, Woongbae Lee, Sangki Choi, Dongwhi Lee, Shinyun Park, Soyoung Kim, Kristal Aubrey Bornillo, Hyungmyoun Moon, and Yunyi Choi for showing, giving pure friendship and looking after me during my happy and sad times. Although time flies so fast, our friendship remains strong.

Most of all, I could have never reached my dreams without unconditional love, overwhelmingly support, and positive encouragement from my family: Tara Jungcharoen, Manchusa Saekua, Phenpim Jungcharoen, and Phoorich Jungcharoen and relatives: Yuttasak Thammarattananan, Mayuree Thuamphong, Chatchawan Thammarattananan, Somboon Meesombay, Siripen Thammarattananan, Alisa Thammarattananan, and Suppached Siwananthakorn.

Abstract

Magnetite (Fe_3O_4) nanoparticles are commonly found in soil and has been broadly used in numerous applications (e.g., environmental remediation, catalysis, energy storage, magnetic resonance imaging, medicine therapy) due to their interesting physical and chemical properties (e.g., magnetic, redox, high surface area, optic, semiconductor). Many of these properties are related to the presence of Fe(II) in the crystallographic structure. Stoichiometric magnetite exhibits Fe(II)/Fe(III) ratio (R) of 0.5. However, at acidic pH or the presence of oxygen lead to the transformation of magnetite into maghemite (Fe_2O_3) with R = 0. If most of the interesting properties of nanomagnetites are dependent on their stoichiometry (R), the impact of environmental factors on its transformation to maghemite and the formation of intermediate compounds (magnetite-maghemite solid-solutions) has been poorly characterized. This thesis aimed to get proper measurement for the determination of magnetite stoichiometry by synchrotron techniques and to develop predictive models of magnetite solubility under environmentally relevant conditions (pH, redox condition, presence of dissolved Fe(II) and organic ligands).

The first part of the thesis work is focused on, the effect of redox conditions and dissolved Fe^{2+} on nanomagnetite stoichiometry by wet chemistry, XRD, XAS, and XMCD. XMCD signals have been used to further characterize the complex reactions involved in the magnetite/maghemite system upon oxidation and recharge processes, *e.g.* decreasing R from 0.5 to 0.1 using H_2O_2 or increasing from 0.1 to 0.5 through dissolved Fe^{2+} amendment. Indeed, surface recrystallization processes, induced by oxidation as well as Fe^{2+} diffusion into the solid phase and/or redistribution of electron equivalents between the aqueous solution and the magnetite bulk, led to decreased spin canting effects, altering XMCD signals. By accounting for these effects, a more accurate method for the determination of magnetite stoichiometry by XMCD is proposed.

The second part of the thesis work is focused on the impact of pH on magnetite solubility. In the absence of O_2, the H^+-promoted dissolution process was responsible for the preferential release of Fe(II) over Fe(III) to the solution, which led to the partial transformation of magnetite into maghemite. Long term kinetic studies (560 days) revealed that while a small magnetite core is hardly affected over a few years in acidic conditions (pH < 5), a thin shell at the surface can be formed even at circumneutral pH and rapidly equilibrates with the aqueous solution. A thermodynamic model for the magnetite-maghemite solid-solution was calibrated. It is capable of predicting the stability and redox-reactivity of nano-magnetite.

The last part of the thesis work investigated the effects of dissolved organic ligands (acetate, lactate, citrate, and EDTA) on Fe solubility and on the stoichiometry of nano-magnetite. These ligands are either natural organic molecules present in soils (e.g. in the rhizosphere) or used to modify the behaviour of iron oxide nanoparticles for enhancing nanotechnology applications. If acetate and lactate did not show significant change, citrate and EDTA significantly increased the solubility of Fe. Especially, citrate and EDTA affected magnetite stoichiometry because of the preferential complexation with Fe(II) than Fe(III). The findings suggest that ligand-controlled dissolution processes should be considered for the chemical stability of magnetite.

This study indicates that magnetite stoichiometry strongly depends on physico-chemical conditions such as pH, E_h and ligands concentration, which explains the variability of geochemical behaviors of magnetites in the environment. This work also recommends that magnetite stoichiometry should be carefully considered when applying magnetite nanoparticles for any applications including environmental remediation, biomedical process and catalysis.

Keywords: magnetite, maghemite, stoichiometry, solubility, solid-solution, geochemical speciation modeling, XMCD

Résumé

Les nanoparticules de magnétite (Fe_3O_4) sont couramment trouvées dans le sol et sont largement utilisées dans de nombreuses applications (par exemple, assainissement de l'environnement, catalyse, stockage d'énergie, imagerie par résonance magnétique, thérapie médicale) en raison de leurs propriétés physiques et chimiques intéressantes (par exemple, magnétique, redox, grande surface, optique, semi-conducteur). Beaucoup de ces propriétés sont liées à la présence de Fe(II) dans la structure cristallographique. La magnétite stœchiométrique présente un rapport Fe(II)/Fe(III) (R) de 0,5. Cependant, un pH acide ou la présence d'oxygène conduisent à la transformation de la magnétite en maghémite (Fe_2O_3) avec R = 0. Si la plupart des propriétés intéressantes des nanomagnétites dépendent de leur stœchiométrie (R), l'impact des facteurs environnementaux sur sa la transformation en maghémite et la formation de composés intermédiaires (solutions solides de magnétite-maghémite) ont été mal caractérisées. Cette thèse vise à obtenir des mesures appropriées pour la détermination de la stœchiométrie de la magnétite par des techniques synchrotron et à développer des modèles prédictifs de la solubilité de la magnétite dans des conditions environnementales pertinentes (pH, condition redox, présence de Fe(II) dissous et de ligands organiques).

La première partie du travail de thèse est axée sur l'effet des conditions redox et du Fe^{2+} dissous sur la stœchiométrie de la nanomagnétite par étude de chimie des solutions, XRD, XAS et XMCD. Les spectres XMCD ont été utilisés pour caractériser davantage les réactions complexes impliquées dans le système magnétite/maghémite lors des processus d'oxydation et de recharge, par exemple, en diminuant R de 0,5 à 0,1 par ajout de H_2O_2 ou en l'augmentant à nouveau de 0,1 à 0,5 par ajout de Fe^{2+} dissous. En effet, les processus de recristallisation de surface, induits par l'oxydation ainsi que la diffusion de Fe^{2+} dans la phase solide et/ou la redistribution d'équivalents

d’électrons entre la solution aqueuse et le cœur de la magnétite, conduisent à une diminution des effets liés à l’inclinaison des spins (« spin canting », en anglais), altérant le signal XMCD. Cette étude fournit une compréhension des processus fondamentaux se produisant dans le système magnétite/maghémite lors de l'altération des conditions redox et offre une méthode plus précise pour la détermination de la stœchiométrie de la magnétite par XMCD.

La deuxième partie du travail de thèse est centrée sur l'impact du pH sur la solubilité de la magnétite. En l'absence d'O_2, le processus de dissolution, favorisé par la présence de H^+, est responsable de la libération préférentielle du Fe(II) par rapport au Fe(III) dans la solution, ce qui conduit à la transformation partielle de la magnétite en maghémite. Des études cinétiques à long terme (560 jours) ont révélé que Si un cœur de magnétite peut persister pendant plusieurs années dans des conditions acides (pH < 5), une couche de maghémite peut se former à la surface en s'équilibrant rapidement avec la solution aqueuse même à pH neutre. Finalement, un modèle thermodynamique pour la solution-solide magnétite-maghémite capable de prédire la stabilité et la réactivité redox de nano-magnétites a pu être proposé.

La dernière partie du travail de thèse a étudié les effets de ligands organiques dissous (acétate, lactate, citrate et EDTA) sur la solubilité du Fe et sur la stœchiométrie de la nano-magnétite. Ces ligands sont soit des molécules organiques naturelles présentes dans les sols (par exemple dans la rhizosphère), soit utilisés pour modifier le comportement des nanoparticules d'oxyde de fer afin d'améliorer les applications des nanotechnologies. Si l'acétate et le lactate n'ont pas montré de changement significatif, le citrate et l'EDTA ont augmenté de manière significative la solubilité du Fe. En particulier, le citrate et l'EDTA ont affecté la stœchiométrie de la magnétite en raison de la complexation préférentielle avec le Fe(II) qu'avec le Fe(III). Les résultats suggèrent

que les processus de dissolution contrôlés par le ligand devraient être pris en compte pour la stabilité chimique de la magnétite.

Cette étude indique que la stœchiométrie de la magnétite dépend fortement des conditions physico-chimiques telles que le pH, le potentiel redox et la concentration en ligands, ce qui explique la variabilité des comportements géochimiques des magnétites dans l'environnement. Ce travail recommande également que la stœchiométrie de la magnétite soit soigneusement prise en compte lors de l'application de nanoparticules de magnétite pour toutes applications, y compris pour l'assainissement de l'environnement, biomédicales et en catalyse.

Mots clés : magnétite, maghémite, stoechiométrie, solubilité, solution solide, modélisation de la spéciation géochimique, XMCD

Table of contents

Chapter 1 Introduction

1.1 Magnetite and maghemite

Magnetite (Fe_3O_4) is commonly found in natural systems. Magnetite crystallizes in a inverse spinel structure (Figure 1) (Bliem et al., 2014). The oxygen ions closely pack face-centered cubic lattices and iron ions are located in the interstices between oxygen ions. There are two different types of interstices, tetrahedral sites and octahedral sites. Magnetite contains Fe^{2+} in the octahedral sites ($Fe^{2+}{}_{Oh}$), Fe^{3+} in the octahedral sites ($Fe^{3+}{}_{Oh}$), and Fe^{3+} in the tetrahedral sites ($Fe^{3+}{}_{Td}$) in a 1:1:1 ratio. The formula of this composition is $Fe^{3+}{}_{Td}[Fe^{3+}Fe^{2+}]_{Oh}O_4{}^{2-}$. The unit cell edge length of magnetite is a = 8.408 Å under Curie temperature of 580 -600 °C (Cornell and Schwertmann, 2003).

Stoichiometric magnetite (R = Fe(II)/Fe(III) = 0.5) can only be presented under certain physico-chemical conditions. It exists in its stoichiometric form when it is present in an anoxic medium (Cornell and Schwertmann, 2003) but, under more oxidizing conditions or acidic pH, magnetite oxidizes gradually by releasing Fe(II) (Jolivet and Tronc, 1988; White et al., 1994). Its transformation leads to the formation of maghemite (γ-Fe_2O_3). Maghemite contains only Fe^{3+} (R = 0), which is located in octahedral sites ($Fe^{3+}{}_{Oh}$) as well as in tetrahedral sites ($Fe^{3+}{}_{Td}$). The chemical formula of maghemite can be written as $Fe^{3+}[Fe_{5/3}{}^{3+}\square_{1/3}]O_4{}^{2-}$. The symbol '$\square$' symbolizes vacancies which are required for charge neutrality (Darbandi et al., 2012; Bourgeois et al., 2013). Magnetite and Maghemite form a solid-solution, i.e. magnetite with different stoichiometries ($0 < R < 0.5$) can exist (Gorski and Scherer, 2009, 2010; Cheng et al., 2018).

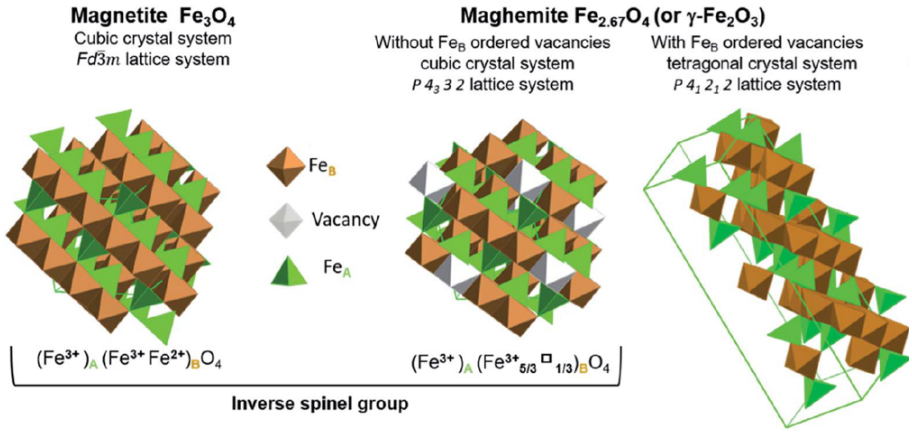

Figure 1. The crystal structures of magnetite and maghemite (with ordered and disordered vacancy distributions) (adapted from (Li et al., 2019)).

1.2 Presence in the natural environment

Abiogenic magnetite nanoparticles are present in several geological environments which are ranging between igneous such as layered ultrabasic rocks and basalts and sedimentary rocks such as banded iron formations and beach sands. The crust of the earth is composed of rocks which are the primary sources of magnetite and supply most of iron cycled by ecosystems (He et al., 2015). Lithogenic magnetite is commonly found in the coarse, heavy mineral fraction of soils. In addition, two other routes of magnetite formation exist, via abiotic (Maher and Taylor, 1988) and biotic processes (Fassbinder et al., 1990). Pedogenic formation of the magnetite can occur through redox changes induced by redox fluctuations, for instance, alternating soil drying and soil flooding following rainfall events (Ahmed and Maher, 2018). Iron oxide nanoparticles are crucial to all living organisms with several bacteria having developed pathways to access iron as an electron acceptor or donor which are dependent on their mobility, oxidation state, and bioavailability

(Melton et al., 2014). Thus, magnetite can be also produced by the influence of (i) bacterial Fe(III) reduction or (ii) mixed-valent iron minerals by bacterial Fe(II) oxidation (Usman et al., 2018). For example, Fe(II)-oxidizing bacteria are capable of promoting electrons electron transfer by oxidizing ferrous ions to ferric iron (Konhauser et al., 2011). Magnetite is important for many micro-organisms because the oxidation and reduction of magnetite nanoparticles can be affected by growing Fe-metabolizing bacterial (Byrne et al., 2015). Magnetite can be reduced by microbial reduction which occurs in natural environments such as sediments and soils (Kostka and Nealson, 1995; Brown et al., 1997; Kostka et al., 2002; Melton et al., 2014; Usman et al., 2018). Moreover, biogenic magnetite, chemically pure magnetite crystals, also occurs in the bodies of various organism within the kingdoms of the Monera, Protista, and Animalia including magnetotactic bacteria, mollusks, insects, fish, birds, and mammals (Kirschvink et al., 2001). In those organisms, magnetite forms the basis for one type of biophysical mechanism of magnetic field detection which affects orientation and navigation (Mouritsen and Ritz, 2005; Kirschvink et al., 2010).

1.3 Example of applications

Magnetite and maghemite nanoparticles are also widely used in nanotechnology (Teja and Koh, 2009). There are several applications of magnetite and maghemite nanoparticles because the magnetic properties and size-related behavior of such particles enable interesting applications (for example, adsorption, catalytic degradation, and disinfection). It can be used in a variety of environmental remediation applications, especially for the removal of organic and inorganic contaminants by different processes. Firstly, it can lead to the degradation of organic contaminants by reduction, such as for nitroaromatic compounds (Gorski and Scherer, 2009; Gorski et al., 2010).

It can also remove contaminants by sorption, such as in the case of antibiotics or americium (Cheng et al., 2018; Morelová et al., 2020). Combination of U(VI) or Cr(VI) reduction and subsequent sorption of U(IV) or Cr(III) can efficiently eliminate these contaminants from groundwaters (Peterson et al., 1997; Latta et al., 2012). Moreover, Fenton-like processes could be involved with hydrogen peroxide as oxidizing agents and iron ions as a catalyst to provide strongly chemical species which are •OH radicals. This process has been significantly used for removing organic contaminants (Lin and Gurol, 1998; Rahim Pouran et al., 2014).

Magnetite is a conductor and also has magnetic properties (Sherman, 1987; Goss, 1988; Walz, 2002). The control of the surface reactivity is one of the most significant topics (Laurent et al., 2008) because numerous applications require the interactions with different ions, biomolecules, or polymers with magnetite (Ito et al., 2005; Schwaminger et al., 2017; Yew et al., 2020; Abushrida et al., 2020). To prevent the oxidation or agglomeration of magnetite nanoparticles and/or to modify the surface properties, they are often modified by organic or inorganic molecules (Laurent et al., 2008), which can form surface complexes with Fe atoms at the surface. This may prevent the generation of ROS, the release of toxic ions, the oxidation of proteins and the adsorption of pollutants (Auffan et al., 2009; Liu et al., 2013; Usman et al., 2018; Norouzi et al., 2020). For example, EDTA is commonly used for this purpose (Blesa et al., 1984; Yi et al., 2014; Ramos-Guivar et al., 2021). Another coating of magnetite nanoparticles with sodium oleate can create biocompatible, stable colloids (Roth et al., 2016; Marín et al., 2016) as shown in Figure 2. Moreover, the surfactant/polymer, silica coating, and carbon coating of nanomagnetite have been applied for their applications in both catalysis for the removal of organic pollutants and a field of wastewater treatment (Nidheesh, 2015), and biotechnology (Lu et al., 2007) as presented in Figure 2.

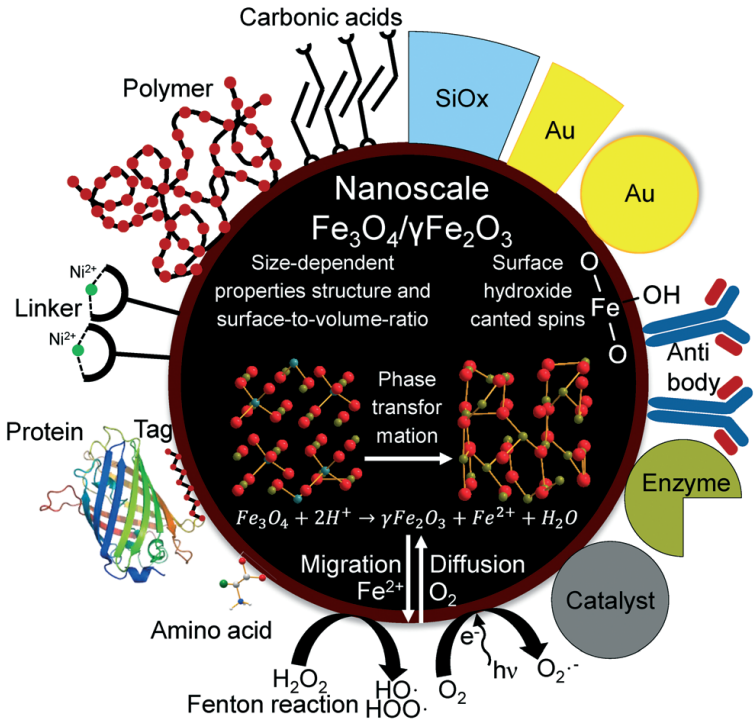

Figure 2. Various applications, structural transformations, and surface interactions of iron oxide nanoparticles (adapted from (Schwaminger et al., 2017).

Magnetite has also some biomedical applications as shown in Figure 3. For example, it can be used at the same time for therapy and diagnosis of cancer (Li, 2014; Weissleder et al., 2014; Quinto et al., 2015; Zanganeh et al., 2016). Magnetite nanoparticles associated with drugs are injected into the patient, and it is used as a drug delivery system to transport the drug to the tumoral cells (Figure 3a). Then, magnetite nanoparticles can be used as contrast agents for the diagnosis of cancer by magnetic resonance imaging (MRI) or by magnetoimpedance (MI) sensor (Figure 3b). Finally, by applying an alternating magnetic field, the nanoparticles can be used for additional therapy by hyperthermia, which can kill the tumoral cells by the heat produced by the movement of the nanoparticles (Quinto et al., 2015) (Figure 3c). Several other biomedical applications, such as

thermal therapy (Mahmoudi et al., 2011; F. Hasany et al., 2013; Ikoba et al., 2015) and DNA/ RNA purification (Turcu et al., 2015), are under consideration owing to their low toxicity, superparamagnetic properties, and simple preparation.

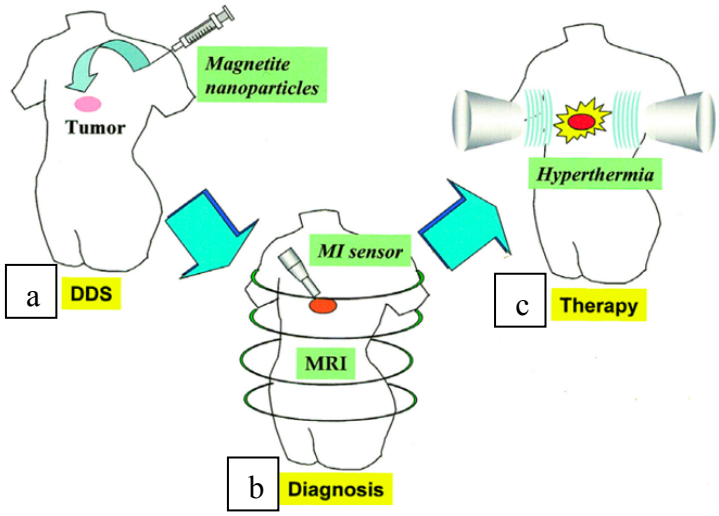

Figure 3. Illustration of the therapeutic methods using magnetite nanoparticles. (a) drug delivery system (DDS), (b) magnetic resonance imaging (MRI), (c) hyperthermia (Adapted from Ito et al., 2005).

1.4 Synthesis and characterization of magnetite nanoparticles

The impact of shapes of nanoparticles is tremendous on their properties such as catalysis (Park et al., 2005; Fortin et al., 2007). The shape can affect crystal facets and the atomic arrangement has a reflective effect on their properties (Dadashi et al., 2015). Therefore, several protocols for desired morphology, size, and shape have been developed (Laurent et al., 2008; Ravikumar and Bandyopadhyaya, 2011; Kolhatkar et al., 2013; Naseem and Farrukh, 2015; Roth et al., 2016). Table 1 shows a comparison of different synthesis methods. Briefly, magnetite nanoparticles can

be synthesized by physical, chemical, and biological methods. Physical methods are elaborate procedures that suffer from the inability to control the nano-size of nanoparticles (Lin and Samia, 2006; Roldan Cuenya, 2010). Chemical methods are relatively simple and efficient in which the size, shape, and composition can be controlled (Jolivet and Tronc, 1988; Laurent et al., 2008; Soenen et al., 2009; Ravikumar and Bandyopadhyaya, 2011; Wu et al., 2011). The chemical methods are strongly dependent on the type of salt used, ratio of Fe(II) to Fe(III), pH, and ionic strength (Laurent et al., 2008; Ravikumar and Bandyopadhyaya, 2011). (iii) Biological methods ensure low cost, reproducibility, and high yield (Carvallo et al., 2008; Narayanan and Sakthivel, 2010). However, microbial methods have been shown rather slow and laborious (Narayanan and Sakthivel, 2010).

Among these methods, the chemical coprecipitation methods are highly effective owing to low price, high yield, and the small size of the nanoparticles that are produced (≈10nm, (Park et al., 2004; Gorski and Scherer, 2010; Demangeat et al., 2018; Cheng et al., 2018)). The chemical reaction of Fe_3O_4 precipitation is revealed in Equation 1.

$$Fe^{2+} + 2Fe^{3+} + 8OH^- \rightarrow Fe_3O_4 + 4H_2O \quad (1)$$

Under anaerobic conditions, complete precipitation of Fe_3O_4 is between pH 8 and 14 which can maintain a molar ratio of Fe(II) to Fe(III) (0.5). The solid phase dissolution (e.g. with 5 M HCl) under anaerobic conditions followed by dissolved Fe(II) and Fe(III) analysis allows an accurate determination of magnetite stoichiometry (Gorski and Scherer, 2010).

Table 1. A comparison of the synthesis of iron oxide nanoparticles by three different routes.

Techniques		Product morphology	Benefits	Drawbacks
1.Physical	Electron beam lithography (Lin and Samia, 2006)	Spheres and rods	Well-controlled interparticle spacing	Highly complex machines
	Deposition of gas phase (Roldan Cuenya, 2010)	Spheres and irregular spheres	Easy to execute	Hard to control the size of particles
2.Chemical	Chemical coprecipitation (Ravikumar and Bandyopadhyaya, 2011; Wu et al., 2011; Cheng et al., 2018)	Spheres	Effective and easy	Large aggregation
	Oxidation (Woo et al., 2004; Soenen et al., 2009)	Small spheres	Uniform size	Ferrite colloids of small size
	Hydrothermal (Wu et al., 2008)	Compact irregular spheres	Easily controlled	High pressure and temperature
	Electrochemical (Laurent et al., 2008)	Spherical nanoparticles,	Controllable size	Inability to reproduce

		nanorods, and fecets		
3.Biological	Microbial incubation (Narayanan and Sakthivel, 2010)	Irregular and spherical spheres	High yield and low cost	Slow and laborious

The individual particle size, shape and morphology of biogenic and abiogenic magnetite nanoparticles can be analyzed by high resolution transmission electron microscopy (HR-TEM). For instance, Figure 4a,b compares biogenic and abiogenic magnetite nanoparticles with similar sizes (31 ± 7.2 nm and 22.5 ± 12.5 nm, respectively) (Carvallo et al., 2008). The biogenic nanomagnetite particles had an octahedral shape, the abiotic ones had an undefined spheroidal shape. Figure 4c,d compares magnetite nanoparticles before (Figure 4c) and after (Figure 4d) oxidation to maghemite. Both magnetite and maghemite nanoparticles show rounded shapes and relatively similar sizes (7 ± 2 nm and 6 ± 2 nm, respectively). The results suggested that the nanomagnetite transformation to maghemite nanoparticles did not affect much the particle size (Demangeat et al., 2018). These comparisons also show that (HR)TEM cannot differentiate magnetite and maghemite nanoparticles.

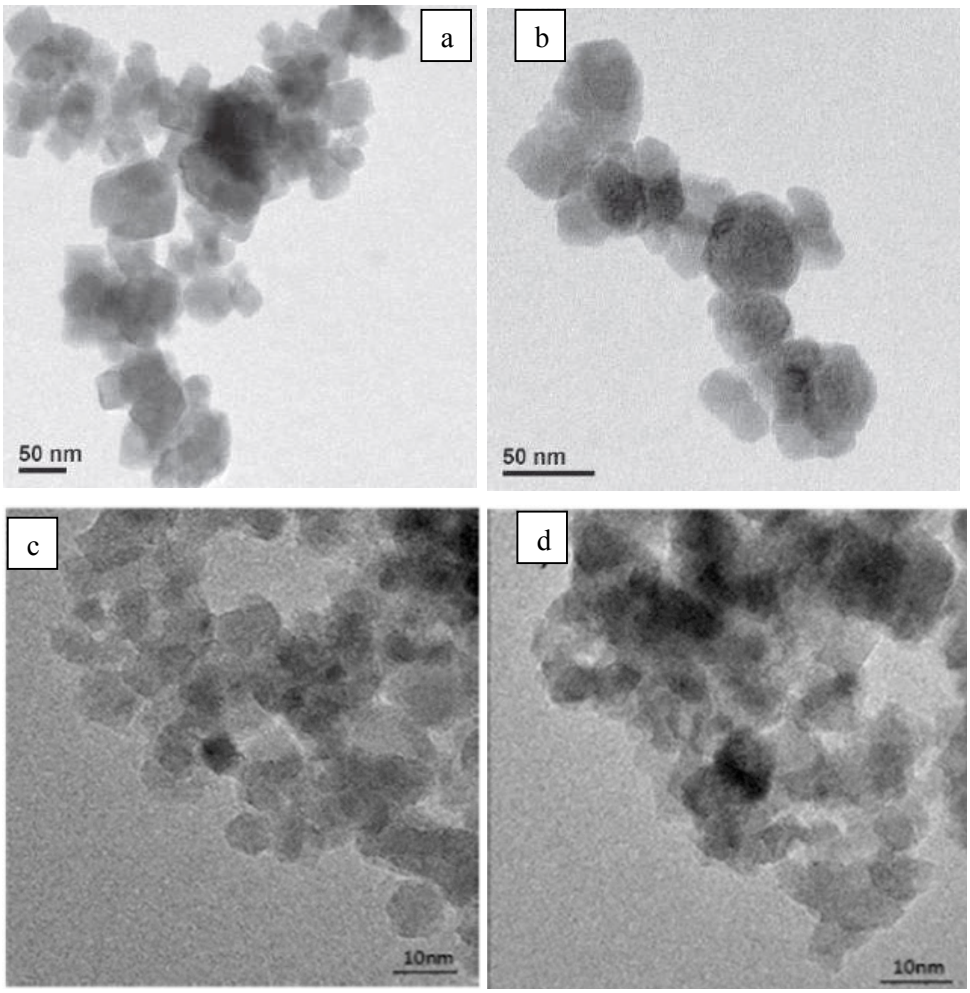

Figure 4. HR-TEM images of (a) magnetite obtained upon anaerobic reduction of lepidocrocite by *Shewanella putrefaciens*, (b) abiogenic magnetite produced from lepidocrocite, (c) stoichiometric magnetite produced from iron salts ($FeCl_2$ and $FeeCl_3$ by coprecipitation), and (d) maghemite nanoparticles produced from through the oxidation of the magnetite by adding 5 wt% of NaOCl. (a-b pictures are from (Carvallo et al., 2008) and c-d pictures are from (Demangeat et al., 2018).

Powder-X ray diffraction (XRD) is commonly used for crystallinity and unit cell parameters determination of minerals. XRD pattern of magnetite is typically characterized by several well-defined reflections. Figure 5 shows the eight peaks have been labeled with their crystallographic planes (hkl). Between stoichiometric magnetite (R=0.5), non-stoichiometric magnetite (R=0.25), and maghemite (R=0), similar crystal structure and unit-cell length are determined (8.394 Å, 8.366 Å, and 8.339 Å, respectively) as shown in Figure 5 (Gorski and Scherer, 2010), which makes the distinguishing between magnetite and maghemite nanoparticles from XRD quite difficult (Kim et al., 2012). However, relationships between cell parameters and stoichiometry have been evidenced (Gorski and Scherer, 2010; Pearce et al., 2012).

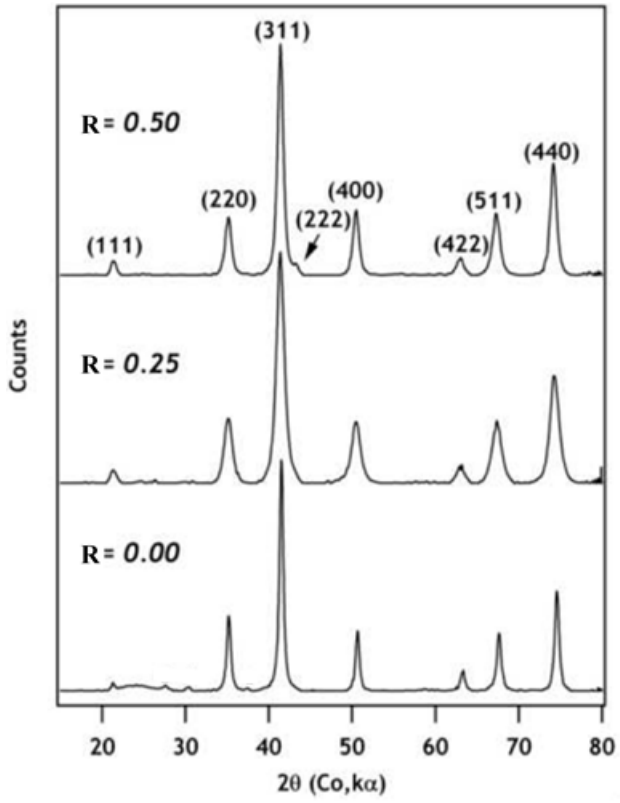

Figure 5. Powder-X ray diffraction (pXRD) of stoichiometric nanomagnetite (R=0.5), partially oxidized (R= 0.25), fully oxidized (R=0.00) (Gorski and Scherer, 2010).

X-ray absorption spectroscopy (XAS) and X-ray magnetic circular dichroism (XMCD) are commonly used synchrotron techniques to investigate the composition of iron oxide nanoparticles because it allows distinguishing between different oxidation states, and local geometry of iron ions and their local environment in the crystal lattice (Pellegrin et al., 1999; Signorini et al., 2006; Carvallo et al., 2008; Coker et al., 2008; Jiménez-Villacorta et al., 2011; Kuzmin and Chaboy, 2014; Peng et al., 2018; Stoerzinger et al., 2019). In the case of magnetite, investigations at the Fe L-edge, which corresponds to a dipole-allowed 2p → 3d transition, are particularly interesting. Owing to the longer core hole lifetimes at these energies, the particular spectral resolution is higher than that measured at the corresponding metal K-edge XAS (Pearce et al., 2012). Figures 6a show the XAS spectra at the Fe L-edge of nanomagnetite with different diameters (5, 9, 12, 16, and 22 nm) in the comparison of two references (both bulk γ-Fe_2O_3 and Fe_3O_4) (Park et al., 2004). The L-edge is split into the L_3 to L_2 edges, as a result of spin-orbit coupling because of the 2p core hole. Both edges provide the same information (see the insert in Figure 6a), although the L_3-edge is more intense. The Fe L_3-edge show two main contributions corresponding to Fe(II) on O_h sites, and Fe(III) on O_h and T_d sites, respectively. Magnetite spectrum also exhibits small pre-peaks visible in both L_3- and L_2-edges (arrows in Figure 6a). Accordingly, the Fe(II) signal disappears for maghemite. In the presently chosen example (Park et al., 2004), XAS spectra of nanomagnetite with different diameters (5, 9, 12, 16, and 22 nm) exhibit features of both magnetite and maghemite. Their stoichiometry can be determined by a linear combination fit using magnetite and maghemite reference spectra, when assuming a form of $(\gamma\text{-}Fe_2O_3)_{1-x}(Fe_3O_4)_x$. X-ray magnetic circular dichroism (XMCD), another synchrotron technique derived from XAS analysis, is a unique tools to distinguish the tetrahedral (T_d) and octahedral (O_h) iron and their oxidation state in magnetic compounds. XMCD originates from a coupling between the photon spin and the atomic

magnetic moment. In practice, the sample is placed in an external magnetic field and two XAS spectra are recorded by polarizing the incident photon beam parallel (ρ_+) or antiparallel (ρ_-) to the magnetic field (Signorini et al., 2006) (insert in Figure 6b). The XMCD spectrum is obtained by the difference between both XAS spectra ($\Delta\rho = \rho_+ - \rho_-$) and presents three main peaks at the L_3 edge (Figure 6b). The peak A corresponds to both Fe(II) and Fe(III) on O_h sites, but is dominated by Fe(II), the peak B corresponds to the contribution of Fe(III) in T_d sites while the peak C is attributed to Fe(III) on O_h sites. A and C are coupled antiparallel to B due to the ferromagnetic behavior of the inverse spinel structure of $Fe_{3-\delta}O_4$ nanoparticles. In the presently chosen example (Park et al., 2004), XAS, XMCD spectra of nanomagnetite with different diameters (5, 9, 12, 16, and 22 nm) exhibit features of both magnetite and maghemite as shown in Figure 6b. It allows the determination of magnetite composition according to the formula $[Fe_X^{2+}\ Fe_{(5-2X)/3}^{3+}\ \square_{(1-X)/3}]_{Oh}\ Fe_{Td}^{3+}O_4^{2-}$. Another advantage of XAS and XMCD analysis is that the total electron yield (TEY) used as detection mode is sensitive to the surface of the (nano)particles (~4-5 nm) (van der Laan and Figueroa, 2014). For this reason reasons, XAS and XMCD at the Fe $L_{2,3}$-edges were used in several studies to elucidate the structure and properties of magnetite surfaces (Pellegrin et al., 1999; Signorini et al., 2006; Carvallo et al., 2008; Coker et al., 2008; Jiménez-Villacorta et al., 2011; Kuzmin and Chaboy, 2014; Peng et al., 2018; Stoerzinger et al., 2019). For instance, when investigating the interaction of Fe^{2+} with magnetite in aqueous solution, redistribution of electron equivalents between bulk and the outermost surface of particles have been observed (Peng et al., 2018).

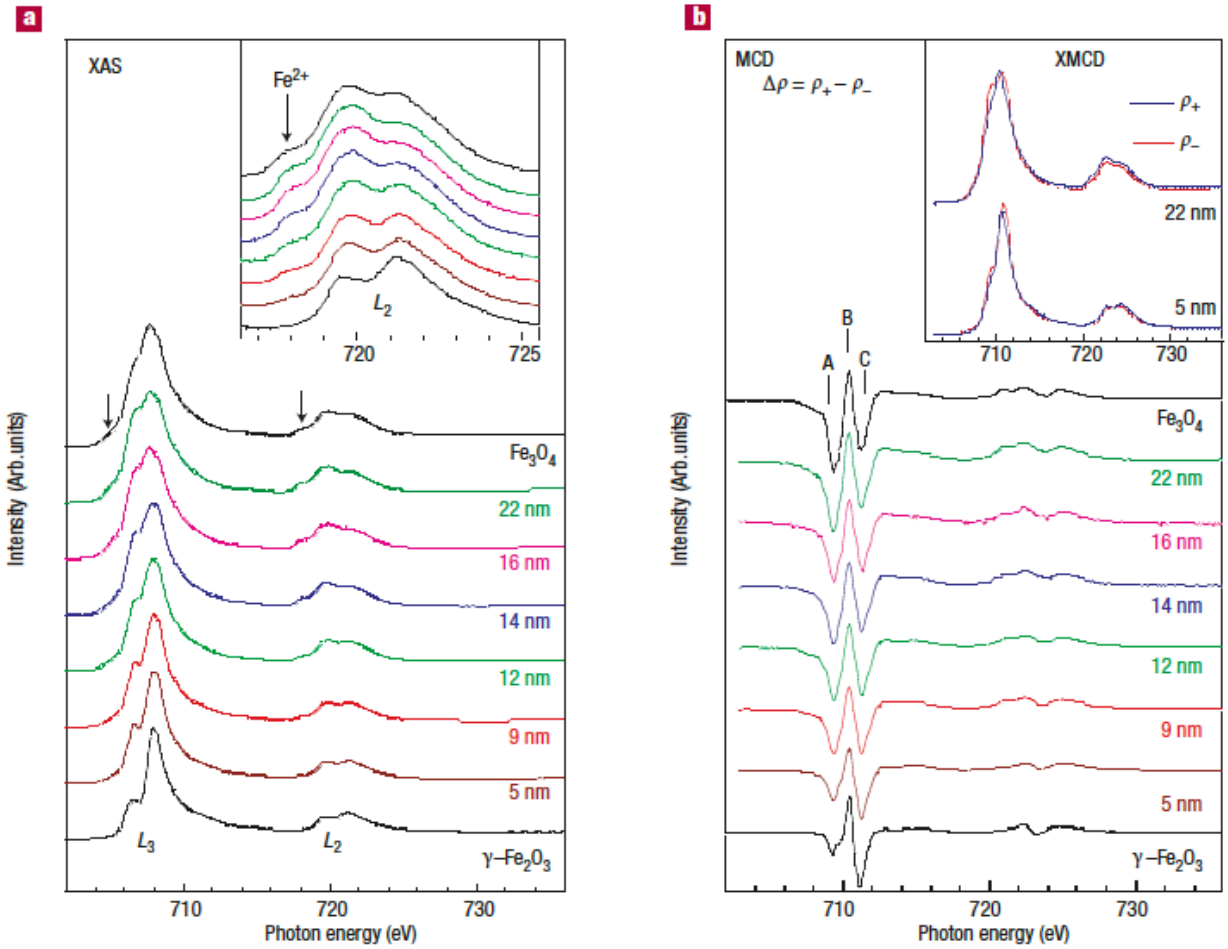

Figure 6. Characterization of magnetite and maghemite nanoparticles with different sizes (5 to 22 nm) by measuring (a) Fe $L_{2,3}$-edge XAS and (b) XMCD spectra of iron oxide nanoparticles in comparison with those of reference bulk materials (γ-Fe_2O_3 and Fe_3O_4). The insert pictures show (a) the magnified L_2 region XAS spectra and (b) $\rho+$ and $\rho-$ represent the absorption coefficients for the photon helicity vector parallel and antiparallel to the magnetization direction of these nanoparticles, respectively (adapted from (Park et al., 2004)).

1.5 Physicochemical surface properties

A link between composition, size, structure and morphology of metal oxide nanoparticles and the surface properties has been widely demonstrated (e.g. (Hiemstra and van Riemsdijk, 2007; Boily and Kozin, 2014). When the size decreases, the surface-to-volume ratio increases, which leads to a larger surface area. In addition, unique nanoscale features, which occur for diameters less than 20-30 nm (Carvallo et al., 2008; Gorski and Scherer, 2009, 2010; Auffan et al., 2009; Gorski et al., 2010), affect the interfacial reactivity and the intrinsic properties of nanoparticles (Usman et al., 2014). For instance, in the nano-size range, the interfacial properties of nanoparticles such as dissolution, oxidation, adsorption/desorption, electron transfer, redox cycles, Fenton reactions and surface acido-basicity can drastically differ from larger particles (Carvallo et al., 2008; Auffan et al., 2009; Gorski and Scherer, 2010; Weissleder et al., 2014; Nidheesh, 2015; Usman et al., 2018). Metal oxides can expose different crystallography planes to the solution, which exhibit different arrangements of atoms and, hence, different physico-chemical properties (Gaboriaud and Ehrhardt, 2003; Boily and Kozin, 2014). The morphology of the particle controls the proportion of the different exposed planes. Therefore, because magnetite nanoparticles exhibit different morphologies (Faivre et al., 2005), it may drastically affect its surface reactivity.

Besides the effect of size, structure and morphology on surface reactivity, which is observed of many metal oxides, the composition of magnetite nanoparticles, especially its stoichiometry (R = Fe(II)/Fe(III)) plays a crucial role both on its redox and adsorption properties. For instance, Figure 7 shows that the adsorption of organic contaminants, such as quinolone antibiotics, only depended on the pH for $R < 0.4$. However, Figure 7 shows that, at pH = 8, the percentage of nalidixic acid adsorbed to nanomagnetite increased from 0 to 100% when R varied from 0.4 to 0.5 (Cheng et al., 2018). This studysuggested that the magnetite surface is oxidized for

R < 0.4, hence exhibiting adsorption capacity independent to R, whereas surface enrichment in Fe(II) occurred when R increased above 0.4, which modified magnetite adsorption properties. The removal mechanism of uranium from solution in presence of magnetite depended on R (Figure 7). For R below ca. 0.3, U(VI) was found at the magnetite surface whereas, for larger R values, U(IV) reduction U(IV) occurred (Latta et al., 2012). The reduction rate constant of nitroaromatic compounds at pH = 7.2 also drastically increased with R (Gorski et al., 2010). For instance, the reduction rate constant of nitrobenzene to aniline was found to increase exponentially with R (Figure 7). Therefore, even if the surface is oxidized (e.g. R < 0.4), electron transfer from the bulk to the surface can occur.

The redox behavior of the magnetite remains relatively poorly understood. The measurement of redox potential in terms of the open circuit potential (E_{OCP}) of a variety of magnetite with different stoichiometry confirmed that stoichiometric magnetite (R=0.5) had the lowest redox potential, while the fully oxidized (R = 0) had the highest redox potential. However, prediction of the redox potential is still not possible probably because more than one redox-active species with different standard redox potentials might be present in magnetite at the same time which can lead to mixed potentials (Usman et al., 2018). In addition, the magnetite water interface is highly dynamic. Previous studies showed that partially oxidized magnetite can be converted into stoichiometric magnetite by dissolved Fe(II) amendment (Gorski and Scherer, 2009; Gorski et al., 2010; Cheng et al., 2018). Further complex surface reactions can take place when stoichiometric magnetite is equilibrated with dissolved Fe(II), such as rapid atomic exchange (Gorski et al., 2012), redistribution of electron equivalents between bulk and the outermost surface of particles (Peng et al., 2018), and surface-mediated electron transfer with redox-sensitive species in solution (Marsac et al., 2017). It is, therefore, necessary to thoroughly characterize both the bulk and surface of

magnetite to accurately evaluate the surface reactivity changes through oxidation-recharge processes. It is also necessary to develop numerical models able to predict the impact of magnetite and, in particular, its stoichiometry on the fate of contaminants in the environment.

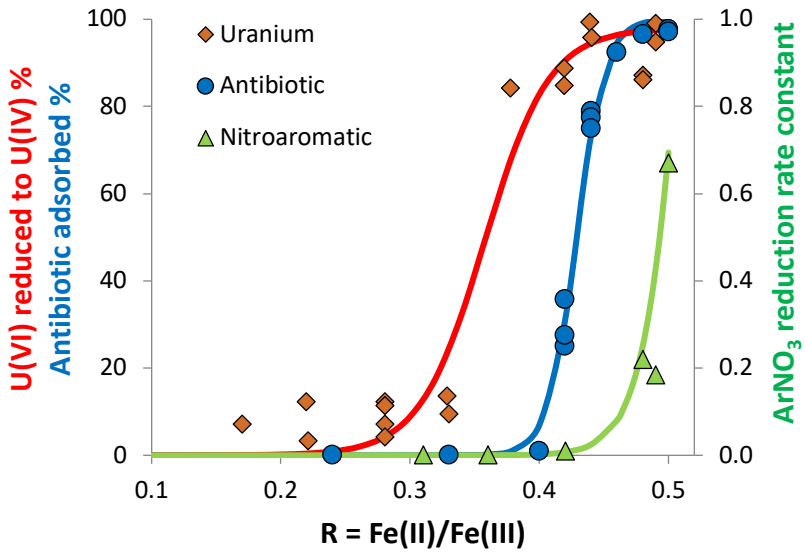

Figure 7. Percentage of (i) U(VI) reduced to U(IV) (Latta et al., 2012) and (ii) nalidixic acid (quinolone antibiotic) (Cheng et al., 2018) adsorbed at the surface of magnetite nanoparticles, and pseudo-first-order rate constant for the reduction of nitrobenzene ($C_6H_5NO_3$) to aniline ($C_6H_5NH_3$) (Gorski et al., 2010) by magnetite as a function of magnetite stoichiometry (R = Fe(II)/Fe(III)).

1.6 Environmental factors affecting magnetite stoichiometry

The oxidation of magnetite to maghemite is well documented and, in the presence of oxygen, can be formulated as:

$$4\ Fe_3O_{4(s)} + O_{2(g)} \rightleftharpoons 6\ Fe_2O_{3(s)} \quad (2)$$

This transformation is, however, not that straightforward because intermediate solid-solutions can form. Currently, no aqueous speciation models can predict the effect of the partial pressure of O_2, or the redox potential (E_h versus SHE) on magnetite stoichiometry. H^+-promoted dissolution of magnetite leads to the release of Fe^{2+} ions into the solution and leaves Fe^{3+} in the solid phase:

$$Fe_3O_{4(s)} + 2\ H^+_{(aq)} \rightleftharpoons Fe_2O_{3(s)} + Fe^{2+}_{(aq)} + H_2O_{(l)} \quad (3)$$

Despite the apparent importance of nano-magnetite stoichiometry concerning its reactivity, the transformation of nano-magnetite to non-stoichiometric nano-magnetite via Equation 3 has only been characterized in acidic solutions (e.g. pH < 3) (Jolivet and Tronc, 1988), with large magnetite particles (> 100 nm) (White et al., 1994), at high temperature (Sweeton and Baes, 1970) or in presence of O_2 (Ahmed and Maher, 2018). In addition, because of the very slow process observed, only the kinetic aspects of eq.2 were treated, and the experiments were rarely designed to observe a steady-state (Jolivet and Tronc, 1988; Sun et al., 1998). Therefore, even the effect of pH on magnetite stoichiometry is poorly characterized.

For practical use, to prevent the oxidation or agglomeration of magnetite nanoparticles, or to modify the surface properties, they are often modified by organic or inorganic molecules (Laurent et al., 2008). For instance, this is the case of citric acid used to modify the surface of iron oxide nanoparticles in a variety of syntheses (Hui et al., 2008; Liu et al., 2009; Jensen et al., 2014) and applications (Laurent et al., 2008) including wastewater purification (Baseri and Tizro, 2017),

NMR imaging (Fan et al., 2010; Mazarío et al., 2015; Lee et al., 2015), and biomolecule extraction(Nigam et al., 2011). These molecules are ligands that might adsorb to the surface by forming surface complexes, which is the desired process, but they might also complex Fe in solution by forming aqueous complexes. In natural systems, magnetite nanoparticles might interact with a large variety of ligands. For instance, in the rhizosphere, Low-Molecular-Weight Organic Acids (LMWOAs), including citric acid, and siderophores play an important role in metal tolerance and plant-microbe interactions operating at root and soil interface (López-Bucio et al., 2000). They can be used to solubilize Fe and increase its bioavailability. However, the impact of such ligand on magnetite solubility and stoichiometry has been largely overlooked.

1.7 Problematic, objectives, and thesis plan

Magnetite nanoparticles are not stable in presence of oxygen and acidic conditions, and some organic ligands in aqueous solutions might also affect its stoichiometry. Although most of the physico-chemical properties of magnetite, including its reactivity towards a large variety of contaminants, largely depend on its stoichiometry, the effect of pH and organic ligands on magnetite stoichiometry has been largely overlooked. Currently, no quantitative model can predict the effect of environmental factors such as pH, E_h, and the presence of ligands on magnetite stoichiometry. Therefore, the thesis focuses on the solubility of magnetite NPs in different pH conditions, in the presence of H_2O_2, dissolved Fe(II), and organic acids (acetate, lactate, citrate, and EDTA). It aims at providing a new predictive model of magnetite nanoparticles (10 nm) stoichiometry evolution with environmental conditions.

Chapter 2 aims to assess the physicochemical conditions (oxidation and recharge processes of nanomagnetite by using H_2O_2 and dissolved Fe(II), respectively) and to probe accurately the bulk and surface of magnetite nanoparticles by different techniques (wet chemistry, XRD, XAS, and XMCD). In particular, the impacts of recrystallization processes induced by H_2O_2 oxidation or Fe(II) amendment on spin canting were carefully addressed to determine the Fe(II)/Fe(III) ratio from XMCD data.

Chapter 3 aims to study the effect of oxidation and pH on magnetite solubility and stoichiometry in aqueous solutions. Long term kinetic studies were conducted in order to attest the establishment of a chemical equilibrium. A thermodynamic solid-solution model for the magnetite-maghemite system was develop to predict the combined effects of pH and E_h on magnetite stoichiometry.

Chapter 4 aims to characterize the effect of some organic ligands (acetate, lactate, citrate and EDTA) on magnetite stoichiometry. In order to deeply understand the determinant factors for the magnetite solubility, the effect of each organic molecule was investigated individually. The solubilities of magnetite with different stoichiometry in the absence and presence of the organic ligands as a function of pH were analyzed by the coupling of several methods (wet chemistry, XRD, XAS, and XMCD). The predictive capacity of the thermodynamic solid-solution model for the magnetite-maghemite system was verified in the presence of organic ligands.

For these reasons, the project investigated the behavior and surface of magnetite nanoparticles with different stoichiometries under various environmental conditions (pH, H_2O_2, dissolved Fe(II), and the presence of ligands (acetate, lactate, citrate, and EDTA) by experimentation using wet chemistry, XRD, XAS, and XMCD analysis, as well as geochemical speciation modeling. In addition, the outcomes of this thesis will assist to develop the decision support tools for strategies of soil remediation based on saving time and minimizing risks to the natural environments and human health.

Chapter 2 Probing the effects of redox conditions and dissolved Fe^{2+} on nanomagnetite stoichiometry by wet chemistry, XRD, XAS and XMCD

Phoomipat Jungcharoen[1], Mathieu Pédrot[1], Fadi Choueikani[2], Mathieu Pasturel[3], Khalil Hanna[4], Frank Heberling[5], Marawit Tesfa[1], Rémi Marsac[1]*

Abstract. Magnetite nanoparticles, commonly found in subsurface environments, are extensively used in various applications such as environmental remediation, catalysis, electronics and medicine. However, the oxidative transformation of magnetite (mixed-valent Fe-oxide) into maghemite (Fe(III)-oxide) that drastically affects magnetic, catalytic and redox properties of the mineral, is still poorly understood. In the present study, a thorough characterization of both particle core and surface of magnetite was performed to accurately assess the relationship between mineral composition and reactivity within the magnetite/maghemite core-shell structure. Previous work showed that X-ray absorption spectra (XAS) and X-ray magnetic circular dichroism (XMCD) can provide key insights into magnetite stoichiometry (R = Fe(II)/Fe(III)) of 10 nm sized particles, as compared to wet chemistry and X-ray diffraction (XRD). In the present study, XMCD signals have been used to further characterize the complex reactions involved in the magnetite/maghemite system upon oxidation and recharge processes, *e.g.* decreasing R from 0.5 to 0.1 using H_2O_2 or increasing from 0.1 to 0.5 through dissolved Fe^{2+} amendment. Indeed, surface recrystallization processes, induced by oxidation as well as Fe^{2+} diffusion into the solid phase and/or redistribution of electron equivalents between the aqueous solution and the magnetite bulk, led to decreased spin canting effects, altering XMCD signals. This study provides a fundamental understanding of the processes occurring in the magnetite/maghemite system upon the alteration of the redox conditions and offers a more accurate method for the determination of magnetite stoichiometry by XMCD.

Résumé. Les nanoparticules de magnétite, fréquemment présentes dans les environnements souterrains, sont largement utilisées pour diverses applications telles que la dépollution de l'environnement, la catalyse, l'électronique et la médecine. Cependant, la transformation de la magnétite (oxyde de Fe à valence mixte) en maghémite (oxyde de Fe(III)) par oxydation affecte considérablement les propriétés magnétiques, catalytiques et redox du minéral, mais est encore mal comprise. Dans cette étude, une caractérisation approfondie du cœur et de la surface de particules de magnétite a été réalisée pour évaluer avec précision la relation entre la composition du minérale et la réactivité de la structure cœur-coquille de magnétite/maghémite. Des travaux antérieurs ont montré que la spectroscopie d'absorption (XAS) et le dichroïsme magnétique circulaire des rayons X (XMCD) peuvent fournir des informations clés sur la stœchiométrie (R = Fe(II)/Fe(III)) de particules de magnétite de 10 nm, par rapport aux analyses chimiques en solution et à la diffraction des rayons X. Dans cette étude, les spectres XMCD ont été utilisés pour caractériser davantage les réactions complexes impliquées dans le système magnétite/maghémite lors des processus d'oxydation et de recharge, par exemple, en diminuant R de 0,5 à 0,1 par ajout de H_2O_2 ou en l'augmentant à nouveau de 0,1 à 0,5 par ajout de Fe^{2+} dissous. En effet, les processus de recristallisation de surface, induits par l'oxydation ainsi que la diffusion de Fe^{2+} dans la phase solide et/ou la redistribution d'équivalents d'électrons entre la solution aqueuse et le cœur de la magnétite, conduisent à une diminution des effets liés à l'inclinaison des spins (« spin canting », en anglais), altérant le signal XMCD. Cette étude fournit une compréhension des processus fondamentaux se produisant dans le système magnétite/maghémite lors de l'altération des conditions redox et offre une méthode plus précise pour la détermination de la stœchiométrie de la magnétite par XMCD.

2.1 Introduction

Magnetite nanoparticles have recently aroused great interest due to their large reactive surface area, good inherent magnetism, and redox properties (Usman et al., 2018). They have been evaluated as promising materials in various fields including, for instance, cancer diagnosis (Weissleder et al., 2014) and therapy (Li, 2014; Zanganeh et al., 2016), energy storage (Wang et al., 2010; Zhu et al., 2011), catalysis science (Rossi et al., 2014), and water treatment(Xu et al., 2012; Nidheesh, 2015). Furthermore, magnetite (Fe_3O_4) is a corrosion product of elemental iron and has recently been shown to control the surface properties and reactivity of nanosized zero-valent iron used for soil and groundwater remediation (Deng et al., 2020). Magnetite is ubiquitous in the earth's crust, soils, and sediments and exists under various particle sizes, morphologies, and stoichiometries (Cornell and Schwertmann, 2003; Lippert, 2008; Ahmed and Maher, 2018). It also plays an important role as electron source or sink for microorganisms (Byrne et al., 2015). The stoichiometry of the particles (R) is one of the most important factors in controlling the reactivity of magnetite*, e.g.* (i) reduction kinetics of nitroaromatic compounds (Gorski et al., 2010), (ii) adsorption capacity of organic compounds (Cheng et al., 2018), and (iii) sorption and redox speciation of inorganic contaminants (Latta et al., 2012). R can be defined as follows:

$$R = Fe(II)/Fe(III) \quad (1)$$

R equals 0.5 for a perfectly stoichiometric (Fe_3O_4) magnetite and 0 for maghemite (γ-Fe_2O_3), the fully oxidized form of magnetite, whose chemical formula can also be written $Fe_{8/3}O_4$ by analogy with that of magnetite. Partial oxidation of magnetite can lead to the formation of non-stoichiometric magnetite ($Fe_{3-\delta}O_4$) with $0 \leq R \leq 0.5$ ($0 \leq \delta \leq 1/3$). If non-stoichiometric magnetite is exposed to a source of dissolved Fe(II), perfectly stoichiometric magnetite (*i.e.* R = 0.5) can be

restored through oxidation of a Fe(II) ion adsorbed at the surface and reduction of underlying octahedral Fe(III) in the magnetite structure, as previously demonstrated using bulk characterization techniques such as Mössbauer spectroscopy, X-ray diffraction (XRD) or wet chemistry (Gorski and Scherer, 2009).

Heterogeneous redox reactions may occur at the magnetite-water interface with the potential formation of magnetite-maghemite core-shell structures (Ahmed and Maher, 2018). The surface properties of magnetite can be altered upon Fe(II)-recharge. Indeed, complex surface reactions can take place when stoichiometric magnetite is equilibrated with dissolved Fe(II), such as rapid atomic exchange (Gorski et al., 2012), redistribution of electron equivalents between bulk and the outermost surface of particles (Peng et al., 2018), and surface-mediated electron transfer with redox-sensitive species in solution (Marsac et al., 2017). It is, therefore, necessary to thoroughly characterize both the bulk and surface of magnetite to accurately evaluate the surface reactivity changes through oxidation-recharge processes, which cannot be done by Mossbauer, XRD or wet chemistry. Thanks to their chemical selectivity and valence state sensitivity, X-ray absorption spectroscopy (XAS) and X-ray magnetic circular dichroism (XMCD) are unique tools to separately probe the electronic properties of the *3d* transition element Fe. The total electron yield (TEY) used as detection mode is sensitive to the surface of the (nano)particles (~4-5 nm) (van der Laan and Figueroa, 2014). Isotropic XAS, i.e. obtained in the absence of a magnetic field, can be used to probe the Fe(II)/Fe(III) ratio of Fe-oxides but is not specific to spinel structures like magnetite. By contrast, XMCD enables to distinguish the tetrahedral (T_d) and octahedral (O_h) iron and their oxidation state in magnetic compounds. XMCD spectra of magnetite typically show two negative peaks due to Fe(II) and Fe(III) on a O_h site, and a positive one due to Fe(III) on a T_d site, whose relative intensities allow determining the magnetite stoichiometry. For these reasons, XAS

and XMCD at the Fe $L_{2,3}$-edges were used in several studies to elucidate the structure and properties of magnetite surfaces (Pellegrin et al., 1999; Signorini et al., 2006; Carvallo et al., 2008; Coker et al., 2008; Jiménez-Villacorta et al., 2011; Kuzmin and Chaboy, 2014; Peng et al., 2018; Stoerzinger et al., 2019).

The XMCD signal of nanostructured magnetically ordered materials is also sensitive to spin canting (Brice-Profeta et al., 2005; Signorini et al., 2006; Darbandi et al., 2012; Graf et al., 2015), which results from structural disorder, either in the interior or at the surface, giving rise to the misalignment of atomic magnetic moments. The spin canting effect is visualized in XMCD spectra through the decrease in the intensity of the peaks of $Fe(II)_{Oh}$ and $Fe(III)_{Oh}$ relative to that of $Fe(III)_{Td}$ (Brice-Profeta et al., 2005; Signorini et al., 2006; Graf et al., 2015). The fact that the XMCD signal is not only sensitive to the Fe oxidation state but also to spin canting may hamper the determination of magnetite surface stoichiometry. Because spin canting globally minors the signal of Fe(II) relative to that of Fe(III), its effect might be wrongly attributed to partial oxidation of magnetite. Conversely, in a recent study, (Peng et al., 2018) the Fe(II) signal of a stoichiometric magnetite in aqueous suspension was shown to increase upon addition of dissolved Fe^{2+}, which suggested the formation of hyperstoichiometric or "cation-excess" magnetite. However, because recrystallization processes can decrease spin canting at the magnetite surface, (Signorini et al., 2006; Graf et al., 2015) an alternative interpretation to the formation of hyperstoichiometric magnetite (Peng et al., 2018) might be the decrease in spin canting effect upon Fe^{2+}-induced recrystallization at the magnetite surface. Therefore, the latter hypothesis deserves further investigation.

The aim of this study is to assess the oxidation and recharge processes of nanosized magnetite (~ 10 nm), using H_2O_2 and dissolved Fe(II), respectively, as well as the impact of the presence of

a dissolved Fe(II) excess on the magnetite surface and bulk structure using a combination of techniques: wet chemistry, XRD, XAS, and XMCD. In particular, the impacts of recrystallization processes induced by H_2O_2 oxidation or Fe(II) amendment on spin canting were carefully addressed to determine the Fe(II)/Fe(III) ratio from XMCD data. This study provides a comprehensive understanding of the behavior and reactivity of magnetite nanoparticles and paves the way for developing more accurate methods to determine magnetite stoichiometry in aqueous solution. As a result, these findings will have strong implications in various research fields including medicine, catalysis, electrochemistry, and environmental research and applications.

2.2 Materials and methods

2.2.1 Materials

All chemicals were of analytical grade or better and were purchased from Sigma-Aldrich. The sample solutions were prepared with ultrapure "MilliQ" water (specific resistivity 18.2 MΩ cm). All experiments were carried out in an anaerobic chamber (N_2-glovebox, JACOMEX, $O_{2(g)}$ < 1 ppm), and all solutions were purged with $N_{2(g)}$ for at least 12 h inside the glovebox before use.

2.2.2 Synthesis of magnetites with various stoichiometries

Stoichiometric magnetite (R0.5) has been synthesized in an N_2-glovebox following a well-known room temperature aqueous precipitation method, which produces ~10 nm particles (Massart, 1981; Demangeat et al., 2018). A 0.5 M HCl solution (40 mL) containing a 0.5 M $FeCl_2$ and 1 M $FeCl_3$ (1:2 molar ratio) was added dropwise into a 0.5 M NaOH solution (250 mL) while continuously stirring, leading to instantaneous precipitation of magnetite particles. After the synthesis, the pH of the suspension was adjusted to pH 8.5. Then, the solid phase was washed three times with ultrapure water, pH 8.5 (adjusted using NaOH) to avoid the release of Fe^{2+}, as observed in previous work (Marsac et al., 2017; Cheng et al., 2018), and thus, to guarantee a stoichiometry of R0.5. Specific stoichiometric amounts of H_2O_2 were added to R0.5 to produce different sets of partly oxidized non-stoichiometric magnetites (R0.1, R0.2, R0.3, R0.4) (Gorski and Scherer, 2010; Cheng et al., 2018). The non-stoichiometric magnetites were washed with ultrapure water (at pH = 8.5) to remove residual H_2O_2.

Effective Fe(II)/Fe(III) ratios (R_{eff}) of all magnetites (R0.1, R0.2, R0.3, R0.4, and R0.5) were determined by acid digestion of magnetites in 0.6 M HCl during 3 days, followed by

spectrophotometric determination of dissolved [Fe(II)] and total [Fe] (= [Fe(III)] + [Fe(II)]) using the 1-10 phenanthroline colorimetric method (Fortune and Mellon, 1938). Results were in excellent agreement with values expected from the amount of added H_2O_2, as in previous studies (Gorski and Scherer, 2009, 2010; Cheng et al., 2018). Repetition of acid digestion followed by spectrophotometry led to an error of ±0.01 on the determination of R_{eff}.

2.2.3 Batch studies

All magnetite aqueous suspensions were prepared for a total Fe concentration of 6.5 mM (~0.5 g L^{-1} of magnetite) in 10 mM NaCl solutions, in 15 mL polypropylene tubes containing 10 mL of solution. HCl and NaOH were used to adjust pH to a final value of 8.5 (no buffer was used). The impact of dissolved Fe(II) addition on the recharge of R0.1 to R0.2, R0.3, R0.4 or R0.5 was investigated by adding small amounts of a 100 mM $FeCl_2$ solution. The impact of the presence of an excess of Fe(II) on R0.5 was investigated by adding 250, 500, 1000, and 2500 µM Fe^{2+} to R0.5. Although magnetite interaction with Fe^{2+} proceeds within less than one day at pH > 7 (Gorski and Scherer, 2009; Cheng et al., 2018), a reaction time of 20 days was applied to ensure chemical equilibrium. pH was controlled and adjusted regularly if needed. After 20 days, a fraction of the solid phase was separated from the solution using a magnet to determine R_{eff} by acid digestion followed by spectrophotometry. An aliquot of the suspension was filtered using 0.2 µm cellulose acetate filters (Sartorius Minisart). The absence of Fe nanoparticles in the filtrate was checked by dynamic light scattering (VASCO Flex). Dissolved [Fe(II)] was measured by spectrophotometry (dissolved Fe(III) was never detected). The error on [Fe] determination was assumed equal to 5 %. Knowing the total [Fe(II)] and [Fe(III)] in the initial suspension (*i.e.* solid and solution) and dissolved $[Fe(II)]_{aq}$ after filtration, R_{eff} could be calculated according to the following equation:

$$R_{eff} = ([Fe(II)]_{Total} - [Fe(II)]_{aq})/([Fe(III)]_{Total}) \quad (2)$$

R_{eff} determined by acid digestion or by measurement of $[Fe(II)]_{aq}$ using eq. 2 were in excellent agreement.

All syntheses were carried out at Geosciences Rennes. A fraction of samples was transported to the SOLEIL Synchrotron facility at the DEIMOS beamline (Ohresser et al., 2014) in 1 mL tubes, placed in airtight bottles that had been closed in the N_2-glovebox. At SOLEIL, samples were handled in an Ar-glovebox connected to the end station of DEIMOS. To ensure that no sample oxidation occurred during transport, the samples were brought back to Geosciences Rennes after analysis at the DEIMOS beamline, and the Fe(II)/Fe(III) ratio of the suspension was checked by acid digestion.

2.2.4 Characterization

Transmission electron microscopy (TEM; Jeol JEM 1230 microscope) was used for magnetite nanoparticles characterization. A small aliquot of magnetite suspension was diluted with ultrapure water (at pH = 8.5) and sonicated for 20 min. A droplet of the diluted suspension was deposited on a carbon-coated 200 mesh copper grid and dried inside the anaerobic chamber. Samples were transported to the microscope under an N_2 atmosphere using a hermetic holder and the samples were analyzed at an acceleration voltage of 200 kV. Average particle diameters were determined by measuring 100 particles.

Powder X-ray diffraction (XRD) was performed on a Bruker D8 Advance diffractometer working with a monochromatized Cu $K_{\alpha 1}$ radiation (λ = 1.5406 Å) and equipped with a LynxEye fast detector enabling a photon energy selection and thus the removal of Fe-fluorescence background signal. Magnetite suspension was placed on a misoriented Si single crystal holder and dried for 2 h in an anaerobic chamber. To avoid the oxidation of magnetite during the XRD

analysis, the dried samples were covered by a drop of glycerol. The samples were scanned in the 2θ range from 20° to 120° with steps of 0.02° and an integration time of 716 s per step. Rietveld refinement of the XRD patterns, using the FullProf software (Rodríguez-Carvajal, 1993), enabled to determine (i) the cell parameters of the phase and (ii) the average crystallite size by fitting the Lorentzian broadening of the peaks compared to a standard corundum sample and deconvoluting the instrumental contribution from the total FWHM using a Thompson-Cox-Hastings profile function (Rodríquez-Carvajal and Roisnel, 2004).

XAS and XMCD signals were recorded at the Fe $L_{2,3}$ edges (700 – 730 eV) on the DEIMOS beamline at the synchrotron light source SOLEIL (Ohresser et al., 2014). The measurement protocol was detailed in previous studies(Daffé et al., 2018; Sartori et al., 2019). Colloidal suspensions of nanoparticles were drop-casted on silicon substrates and dried at room temperature, in the Ar-glove box ($O_{2(g)}$ < 1 ppm) connected to the end station. The silicon substrates were fixed on a sample holder and transferred into the cryomagnet, under ultra-high vacuum (UHV-10^{-10} mbar). All spectra were measured in Total Electron Yield mode (TEY) at 4.2 K under UHV conditions and an applied magnetic field H (H^+ = +6 Tesla and H^- = -6 Tesla). The beam size was 800*800 μm^2 and the resolution was 100 meV. XAS and XMCD spectra were plotted by considering the absorption cross-section measured with left (σ_L) and right (σ_R) circularly polarized X-rays. Isotropic XAS were plotted as $\sigma_{XAS}= (\sigma_+ + \sigma_-)/2$ and XMCD spectra were plotted as $\sigma_{XMCD}= (\sigma_+ - \sigma_-)$ where $\sigma_+ = [\sigma_L(H^+) + \sigma_R(H^-)]/2$ and $\sigma_- = [\sigma_L(H^-) + \sigma_R(H^+)]/2$. The circularly polarized X-rays are provided by an Apple-II HU-52 helical undulator for both XAS and XMCD measurements and by sweeping the magnetic field from +6T to -6T. Both isotropic XAS and XMCD signals were normalized by dividing the raw signal by the edge jump of the isotropic XAS.

2.3 Results and discussion

2.3.1 Effects of oxidation on magnetite characteristics

The individual sizes and shapes of magnetite nanoparticles were measured by TEM imaging (Figure S1). The synthesized magnetite and oxidation products displayed nearly spherical shapes and similar sizes with diameters of ca. 10 nm (i.e. between 8.9 ± 2.1 and 11.5 ± 1.5 nm; Table S1). This agrees with previous work (Demangeat et al., 2018) where the oxidation of iron nanoparticles (magnetite to maghemite) did not affect much the magnetite particle size. The XRD patterns of magnetite nanoparticles have previously been shown to depend on the stoichiometry of the nanoparticles (Gorski and Scherer, 2010). Cell parameters of stoichiometric magnetite range from 8.39 to 8.40 Å (Cornell and Schwertmann, 2003; Gotić et al., 2009). XRD analysis confirmed the purity of R0.5 (8.3976 Å; Table S1 and Figure. S2). Oxidation of R0.5 leads to non-stoichiometric magnetite with smaller cell parameters (*e.g.* 8.3685 Å for R0.1; Table S1 and Figure. S2) (Yang et al., 2004; Gorski and Scherer, 2010; Pearce et al., 2012). Cell parameters of these samples fall between that of magnetite and maghemite (8.34 Å)(Cornell and Schwertmann, 2003) which confirms that these samples are magnetite-maghemite solid-solutions. It is interesting to note that R does not seem to evolve linearly with the cell parameter in the present work, by contrast with Gorki et al.'s findings (Gorski and Scherer, 2010) but in agreement with (Pearce et al., 2012) (Figure S3). However, given the small discrepancies between all these studies, results might be considered in relatively good agreement (Gorski and Scherer, 2010; Pearce et al., 2012). Bragg peaks enlargement observed on XRD patterns (Figure S2) was treated during Rietveld refinements as "crystallite size" effect. This led to ca. 6.3-9.4 nm crystallites, in relatively good agreement with TEM when keeping in mind that differentiating between size effect,

crystallographic defects or internal strains by XRD is difficult for nanoparticles (Balzar et al., 2004).

Figure 1a shows the isotropic XAS spectra at $L_{2,3}$ edges of stoichiometric nanomagnetite (R0.5) and oxidation products (R0.1 to R0.4) at pH 8. They are typical spectra of ferrite spinel structures (Pellegrin et al., 1999; Signorini et al., 2006; Carvallo et al., 2008; Coker et al., 2008; Jiménez-Villacorta et al., 2011; Kuzmin and Chaboy, 2014; Peng et al., 2018). The Fe L_3-edge show two main contributions at 706.9 eV (I_1) and 707.2 eV (I_2) that correspond to Fe(II) on O_h sites (I_1), and Fe(III) on O_h and T_d sites at 707.2 eV (I_2), respectively. The evolution of the I_1/I_2 ratio versus the R provides information about the amount of Fe(II) at the surface of the nanoparticles. In addition, the series of pre-edge-peaks between 703 and 705 eV, increased with increasing R, which is attributed to the increase in the amount of Fe(II) in the near-surface region of the nanoparticles from R0.1 to R0.5. Corresponding XMCD spectra, illustrated in Figure 1b, present three main peaks at the L_3 edge. The peak S_1 corresponds to both Fe(II) and Fe(III) on O_h sites, but is dominated by Fe(II), the peak S_2 corresponds to the contribution of Fe(III) in T_d sites while the peak S_3 is attributed to Fe(III) on O_h sites. S_1 and S_3 are coupled antiparallel to S_2 due to the ferromagnetic behavior of the inverse spinel structure of $Fe_{3-\delta}O_4$ nanoparticles. A very low intensity of S_1 (R0.1) with an oscillation between S_1 and S_2 corresponds to an iron oxide spinel structure with deficiency in Fe(II) atoms, that is, a structure very close to maghemite (Pellegrin et al., 1999; Park et al., 2004; Kuzmin and Chaboy, 2014). However, the XMCD of R0.1 also shows characteristic features of magnetite such as pre-peaks between 703 and 705 eV, which confirms the presence of Fe(II) in the structure (Pellegrin et al., 1999). The increase of S_1 versus R indicates the increase of the amount Fe(II) in the structure.

The decrease in S_1 intensity with constant S_3 intensity explains the decreasing Fe(II) content from R0.4 to R0.1. However, the intensities of both negative peaks S_1 and S_3 are smaller for R0.5 than for R0.4 (inset to Figure 1). This is consistent with previous investigations, which have ascribed this phenomenon to surface spin canting effects with increased spin disorder occurring preferentially at the octahedral sites (Signorini et al., 2006; Graf et al., 2015). The growth process of maghemite is mediated by Fe^{2+} cations and vacancy diffusion that can give rise to structural reorganization and a lower degree of structural disorder. This mechanism could thus result in a smaller spin canting of partially oxidized magnetite compared to the pristine stoichiometric magnetite (Signorini et al., 2006).

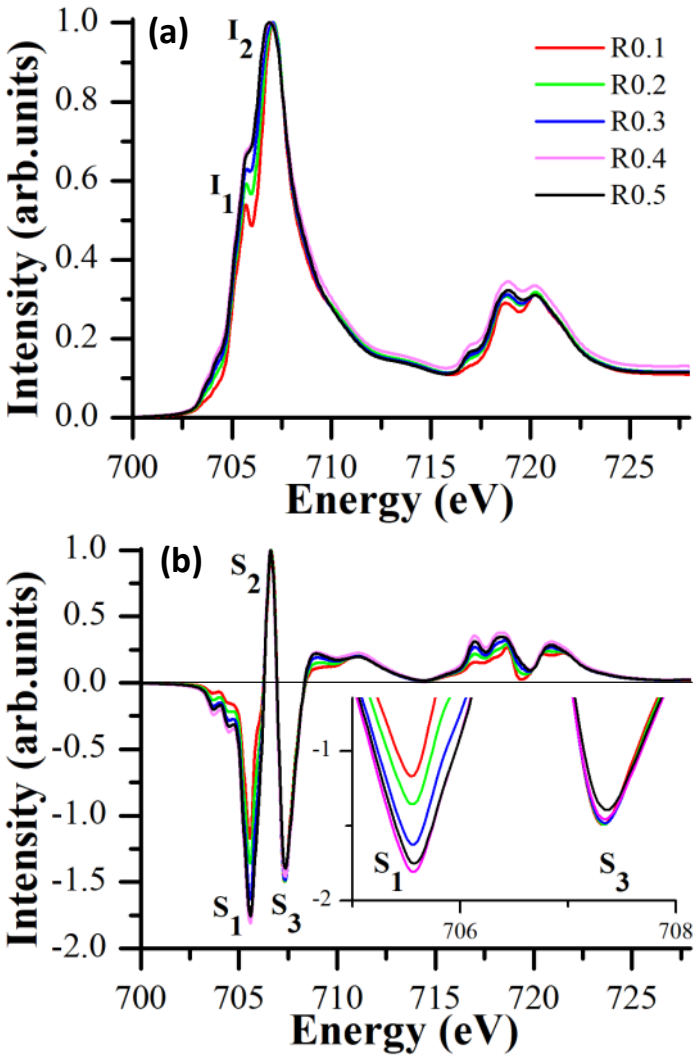

Figure 1. (a) Isotropic XAS and (b) normalized XMCD spectra of stoichiometric magnetite (R0.5) and its oxidation products (R0.1, R0.2, R0.3, and R0.4). XAS was normalized to the jump of edge and XMCD was normalized to the peak S_2.

2.3.2 Impact of an oxidation-recharge cycle on the magnetite surface structure

Previous studies showed that partially oxidized magnetite can be converted into stoichiometric magnetite by dissolved Fe(II) amendment (Gorski and Scherer, 2009; Gorski et al., 2010; Cheng et al., 2018). Accordingly, a complete uptake of dissolved Fe(II) by R0.1 was observed when appropriate amounts of Fe(II) were added to reach R_{eff} = 0.2, 0.3, 0.4, and 0.5, at pH = 8.5. XRD and XAS analyses revealed, that the cell parameter and I_1/I_2 ratio of the magnetite with R_{eff} = 0.5 produced by the addition of Fe(II) to R0.1 was similar to that of the pristine stoichiometric magnetite (Table S1, Figures S2 and S4), and TEM evidenced no significant size or morphological evolution of the nanoparticles upon recharge (Figure S1). The XMCD spectra of samples obtained by the recharge of R0.1 were very similar to those obtained for the corresponding magnetites produced by oxidation of R0.5 (Figure 2). However, the S_1 and S_3 peak intensities in the XMCD spectrum of the recharged R0.1 to R0.5 are larger than those of stoichiometric magnetite (R0.5). This might be attributed to decreased spin canting after the oxidation-recharge cycle. Indeed, two mechanisms could explain the recharge of partially oxidized magnetite into stoichiometric magnetite. Firstly, Mössbauer spectroscopy investigations showed that adsorption of Fe(II) is followed by an electron transfer, leading to the reduction of the octahedral Fe^{3+} atoms in the underlying magnetite to octahedral Fe^{2+} atoms (Gorski and Scherer, 2009). Secondly, isotopic exchange experiments suggested a fast Fe atom exchange between magnetite and the aqueous solution (Gorski et al., 2012). Both Fe^{2+} cations diffusing into the solid phase and/or the redistribution of electron equivalents between the aqueous solution and the interior of magnetite may involve recrystallization, as previously shown (Hansel et al., 2005; Handler et al., 2009; Jones et al., 2009; Yang et al., 2010). This scenario is supported by the Bragg peaks enlargement observed on XRD patterns (Figure S2). The determined apparent crystallite size by Rietveld

refinements, whose determination is affected by crystallographic defects or internal strains for nanoparticles (Balzar et al., 2004), increases from 6.3 nm to 9 nm after recharging R0.1 up to R = 0.5. In fact, because the size of the particles hardly changes during the oxidation/recharge process (9.6 ± 2.3 nm for R0.1, 11.3 ± 2.0 nm for the recharged sample; Figure S1; Table S1), narrower peaks (and apparently larger crystallite size) after the recharge process indicate a higher crystallinity compared to the initial material. Because surface spin canting affects the XMCD signal of poorly-crystalline magnetite nanoparticles (Brice-Profeta et al., 2005; Darbandi et al., 2012), our data suggest that the recrystallization processes induced by the oxidation-recharge cycle lead to decreased spin canting *i.e.* decreased structural disorder.

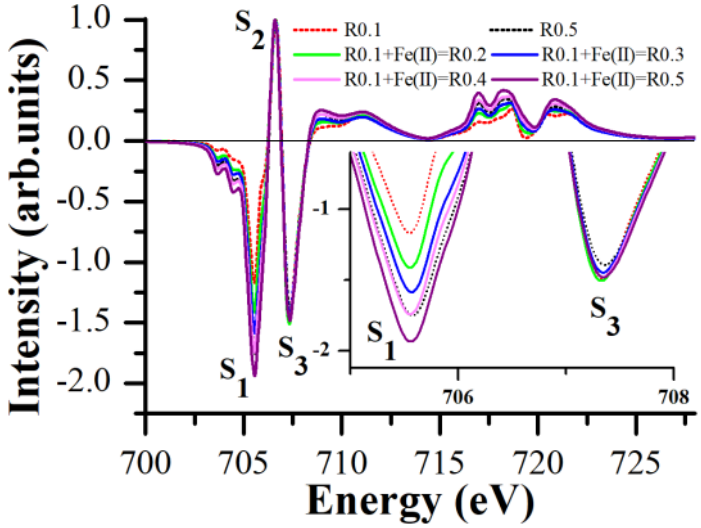

Figure 2. Normalized XMCD spectra of non-stoichiometric magnetite (R0.1) amended with dissolved Fe^{2+} to increase R_{eff}. Data are compared with pristine stoichiometric magnetite (R0.5).

2.3.3 Effects of Fe^{2+}excess on magnetite surface properties

Fe atom exchange and redistribution of electron equivalents between the aqueous solution and the interior of magnetite may not only occur during the recharge of partially oxidized magnetite but also the reaction of pristine stoichiometric magnetite with an excess of aqueous Fe(II) (Gorski et al., 2012; Peng et al., 2018). Therefore, "overloading" stoichiometric magnetite with dissolved Fe(II) may also affect the surface atomic ordering and related spin canting. To test this hypothesis, R0.5 was reacted with 250-2500 μM Fe(II) at pH 8.5. Complete uptake of Fe(II) by R0.5 was observed by spectrophotometric analysis, which leads to an apparent increase of R_{eff} with increasing added $[Fe(II)]_{aq}$ (Table S1). Accordingly, XAS spectra exhibited an increase in I_1 compared to that of R0.5 (Figure 3a). This peak became predominant for [Fe(II)] = 2500 μM (Figure 3a), where the solid phase exhibits an R_{eff} = 0.93. Such a very intense I_1 peak suggests precipitation of a Fe(II)-solid phase. In the normalized XMCD spectra (Figure 3b), both the intensity of S_1 and S_3 increased with an increasing amount of added Fe(II) up to 1000 μM. Thus, spin canting effects decreased, allowing an increase of the magnetic properties. However, a large excess of Fe(II) (2500 μM) did not further affect the normalized XMCD signal, which confirms the formation of magnetically silent Fe(II)-solid phase at the magnetite surface. A comparable process was observed during the synthesis of titanomagnetites nanoparticles at large Fe(II) concentrations, when Fe(II) could not enter the titanomagnetite structure (Pearce et al., 2012). We suspect that, given our experimental conditions, that Fe(II) oxide or hydroxide formed. The cell parameter determined by XRD analysis did not significantly differ between the overloaded magnetite (2500 μM) and the pristine R0.5 (Table S1), probably because of the amorphous structure of the Fe(II)-containing layer. TEM confirmed the formation of an amorphous layer at the magnetite surface (Figure S1). The presence of this Fe(II)-containing precipitate onto the

magnetite surface explains the strong increase of I_1, while the normalized XMCD spectrum remained unchanged (Figure 3b).

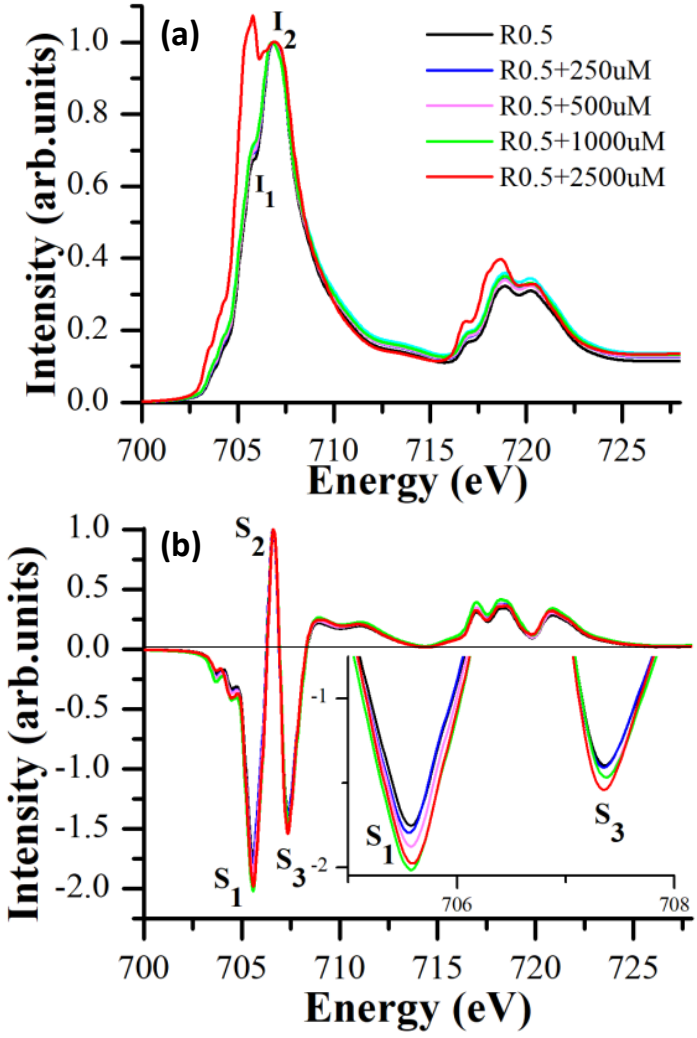

Figure 3. (a) Isotropic XAS and (b) normalized XMCD spectra of stoichiometric magnetite reacted with an excess of dissolved Fe^{2+} (250-2500µM).

2.3.4 Determination of nanomagnetite stoichiometry using XMCD

The determination of the magnetite stoichiometry - or the mole fraction (X) of magnetite in the magnetite (Fe_3O_4)/maghemite ($Fe_{8/3}O_4$) solid solution - by XMCD is often based on linear combination fits (LCF) involving maghemite and stoichiometric magnetite references:

$$Int(Sample) = X \times Int(Magnetite) + (1-X) \times Int(Maghemite) \quad (3)$$

where "Int" is the XMCD signal intensity of the sample or a reference at a given energy, and the relationship between X and R_{eff} being given by the following equation where "n" refers to quantities of matter (moles):

$$X = n(Fe_3O_4)/(n(Fe_3O_4)+n(Fe_{8/3}O_4)) = 8R_{eff}/(3+2R_{eff}) \quad (4)$$

However, the present results show that the XMCD signal of nanomagnetite does not only depend on its stoichiometry but it can also be affected by the crystallinity at the nanoparticle surface and related spin canting effects. Hence, the XMCD signal depends on the alternation of redox conditions, because oxidation and reaction with Fe(II) lead to recrystallization at the nanoparticle surface. This may hamper the determination of magnetite stoichiometry by XMCD.

Given the size (around 10 nm) of the presently studied $Fe_{3-\square}O_4$ nanoparticles, the TEY used as surface detection mode, is also sensitive to the core of the nanoparticles. By making the approximation that the TEY probes the entire particle, although more sensitive to the surface, it is possible to use experimental values of R_{eff} measured by spectrophotometry (eq. 2) to estimate the respective XMCD signals of magnetite and maghemite by a least-square fit. Normalized XMCD spectra and R_{eff} of the four non-stoichiometric magnetites produced by oxidation of R0.5 were used for this purpose. The calculated spectrum of maghemite (R0) is qualitatively consistent with literature data (Pellegrin et al., 1999; Park et al., 2004; Kuzmin and Chaboy, 2014) and the intensity

of peak S_3 is similar to that of the calculated spectrum of magnetite (R0.5), as expected in the absence of spin canting effects (Figure 4). Interestingly, if the XMCD spectrum of the pristine stoichiometric magnetite R0.5 is affected by spin canting, the oxidation-recharge cycle or the overloading with 1000 μM Fe(II) improved the XMCD signal and lead to similar spectra as the calculated one (Figure 4). This comparison suggests that this spectrum corresponds to the spin canting-free stoichiometric magnetite nanoparticles (~10nm), and then can be used as a good reference to determine magnetite stoichiometry by LCF of XMCD data.

Conversely, when neglecting spin canting effects, attempts to re-evaluate R_{eff} of the stoichiometric magnetite subjected to a complete oxidation-recharge cycle using the XMCD spectrum of the pristine stoichiometric magnetite, can be made with equations 3-4 and a least-square fit, in which the maghemite term is set to 0. The fitted spectrum over the energy range 700-715eV (Figure 4b) accurately predicts the intensity of the $Fe(II)_{Oh}$ peak while only slightly overestimating that of the $Fe(III)_{Oh}$ and $Fe(III)_{Td}$ peaks, respectively, hence providing a reasonable estimate for the present purpose. The corresponding value of R_{eff} equals 0.57. Repeating the same exercise for the overloaded stoichiometric magnetite with 1000 μM Fe(II) leads to $R_{eff} = 0.61$ (not shown). These larger values than 0.5 might suggest the formation of hyperstoichiometric or "cation-excess" magnetite, as previously suggested (Peng et al., 2018). Therefore, although the presently observed spin canting effect is relatively small, this demonstrates that its omission has important consequence for the determination of the magnetite stoichiometry.

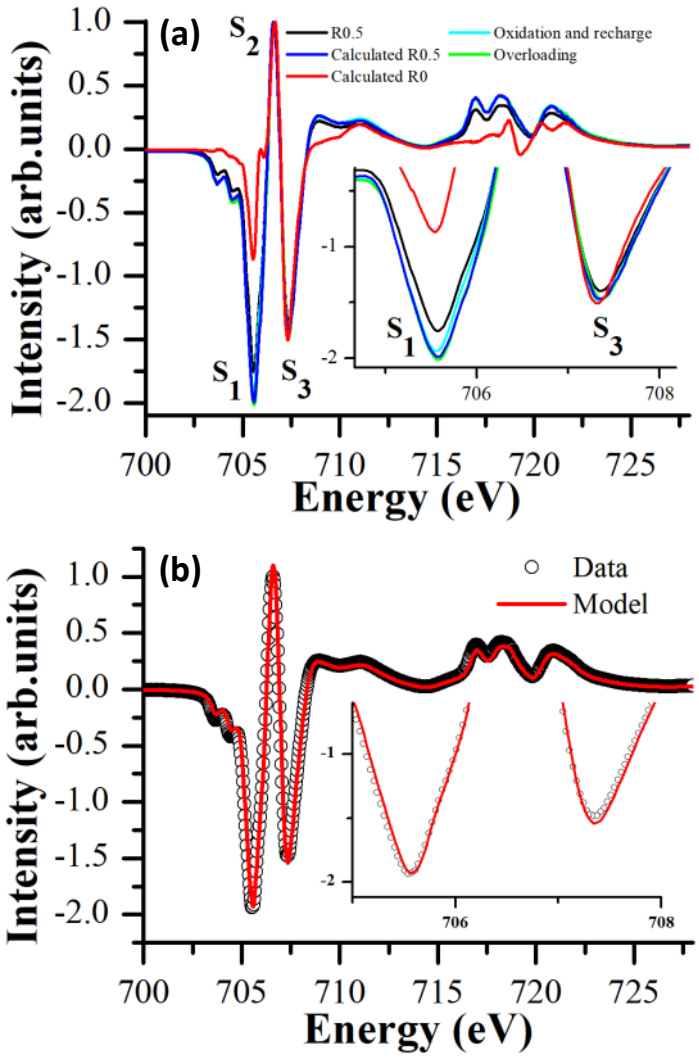

Figure 4. (a) Normalized XMCD spectra of pristine stoichiometric magnetite (R0.5), amended R0.1 with Fe(II) ("oxidation and recharge"), amended R0.5 with 1000 µM Fe(II) ("overloading"), and comparison with the calculated spectra of maghemite and stoichiometric magnetite ("calculated" R0 and R0.5, respectively). (b) Normalized XMCD spectrum of the stoichiometric magnetite subjected to a complete oxidation-recharge cycle (data) fitted using equations 3-4 and the XMCD spectrum of the pristine stoichiometric magnetite (model).

Another approach can be used to estimate magnetite stoichiometry. An indicator (S) was defined in order to follow the evolution of peak intensities versus stoichiometry (Brice-Profeta et al., 2005):

$$S = (S_1 + S_2)/ (S_2 + S_3) \quad (5)$$

This approach can also be used to compare our results with literature data. The value of S is plotted against X determined by acid digestion in Figure 5 for $X \leq 1$ (other data are given in Table S1). An error of 5% is assumed on the determination of S. Measured values (Pellegrin et al., 1999) or presently estimated ones for maghemite (X = 0) agree relatively well (S = 0.69 and 0.75, respectively). The presently synthesized pristine stoichiometric magnetite exhibits S approximately equal to 1.15, in excellent agreement with about 10 nm stoichiometric magnetite particles synthesized by coprecipitation(Peng et al., 2018) or with few nanometer thin films (Pellegrin et al., 1999). Spectra recorded after an oxidation-recharge cycle, in the presence of excess Fe(II) and the calculated spectrum of R0.5 lead to S = 1.22, in agreement with the experimental study (Peng et al., 2018) which contained stoichiometric magnetite with 1000µM Fe(II) (S = 1.25). The following relationship was graphically found to estimate X (± 0.05 X units) from the S value:

$$X = (S - 0.737) / 0.446 \quad (6)$$

However, it appears that very different XMCD spectra were published for stoichiometric magnetite, leading to a broad range of S values, from 1.15 to 1.46 (Table S2) (Pellegrin et al., 1999; Signorini et al., 2006; Carvallo et al., 2008; Coker et al., 2008; Jiménez-Villacorta et al., 2011; Kuzmin and Chaboy, 2014; Peng et al., 2018). Such a large variation cannot be attributed to a variable Fe(II) content between the studied magnetites. Instead, we suspect that the synthesis

procedures can affect the morphology and surface characteristics of stoichiometric magnetite (Ravikumar and Bandyopadhyaya, 2011; Unni et al., 2017). For instance, biogenic magnetite nanoparticles (20-30 nm) are more crystalline than abiotic ones (Carvallo et al., 2008; Coker et al., 2008), and produce larger S values (1.30), while magnetite nanoparticles synthesized by thermal decomposition (5-22 nm) are also well crystallized with large S values (Park et al., 2004; Kuzmin and Chaboy, 2014) (Table S2). Therefore, the determined reference stoichiometric magnetite XMCD spectrum (eq. 3) and the present calibration using X versus S (eq. 6) might be only used to determine the stoichiometry of about 10 nm-sized precipitated particles. Further studies are required to quantify the combined effects of magnetite stoichiometry, particle size, and crystallinity on the XMCD spectra.

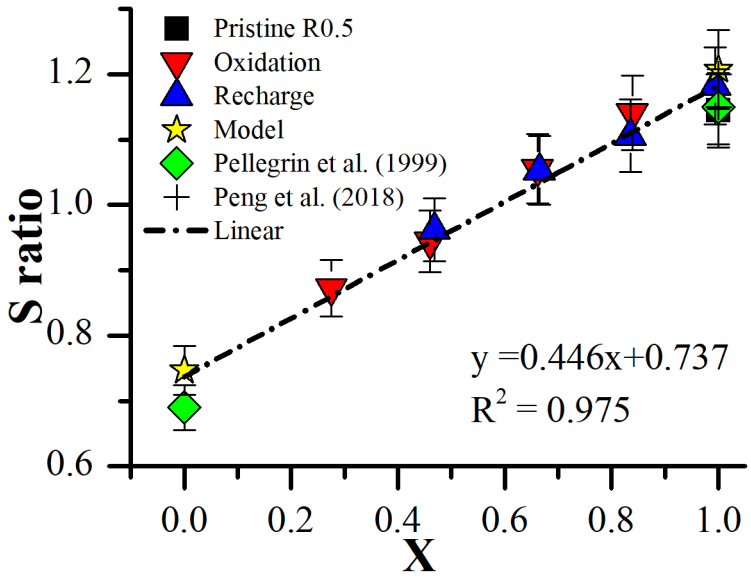

Figure 5. S ratio (eq. 5) versus the mole fraction of magnetite (X) for all samples presently analyzed by XMCD. S values are compared with that obtained from previous studies (Pellegrin et al., 1999; Peng et al., 2018) and presently calculated spectra of R0 and R0.5 (eq. 3).

2.4 Conclusions

Magnetite nanoparticles have broad implications in geochemistry, environmental science, and materials science, due to their large reactivity, good inherent magnetism, and redox properties. Although the surface reactivity of $Fe_{3-\delta}O_4$ nanoparticles is extensively investigated, knowledge regarding the transformation of magnetite into maghemite, and *vice versa*, is limited. In the present study, magnetite stoichiometry was tuned in aqueous suspension by adding appropriate amounts of H_2O_2 or dissolved Fe^{2+}. The experimental dataset presented in this work confirmed that XMCD analysis may be used to follow the Fe(II)/Fe(III) ratio (Pellegrin et al., 1999; Carvallo et al., 2008; Pearce et al., 2012; Peng et al., 2018) but caution with respect to spin canting or the degree of structural order of the minerals is required (Signorini et al., 2006; Graf et al., 2015). Indeed, oxidation as well as Fe^{2+} diffusion into the solid phase and/or redistribution of electron equivalents between the aqueous solution and the magnetite bulk implied surface recrystallization processes, thereby affecting XMCD signals. This was evidenced through an oxidation-recharge cycle of the pristine magnetite and by adding an excess of dissolved Fe(II) to a stoichiometric magnetite suspension. The implication of the present work is twofold. First, it provides a more comprehensive examination of the dynamic behavior of the magnetite-maghemite system in aqueous solutions. Second, these results uncover a more accurate method for the determination of the stoichiometry of nanosized magnetite particles (~ 10 nm) by XMCD. Therefore, for future studies, the present results might be useful to further elucidate, for instance, the impact of magnetite stoichiometry on the redox transformation of various organic and inorganic pollutants or the role of microorganisms for magnetite stoichiometry.

Appendix

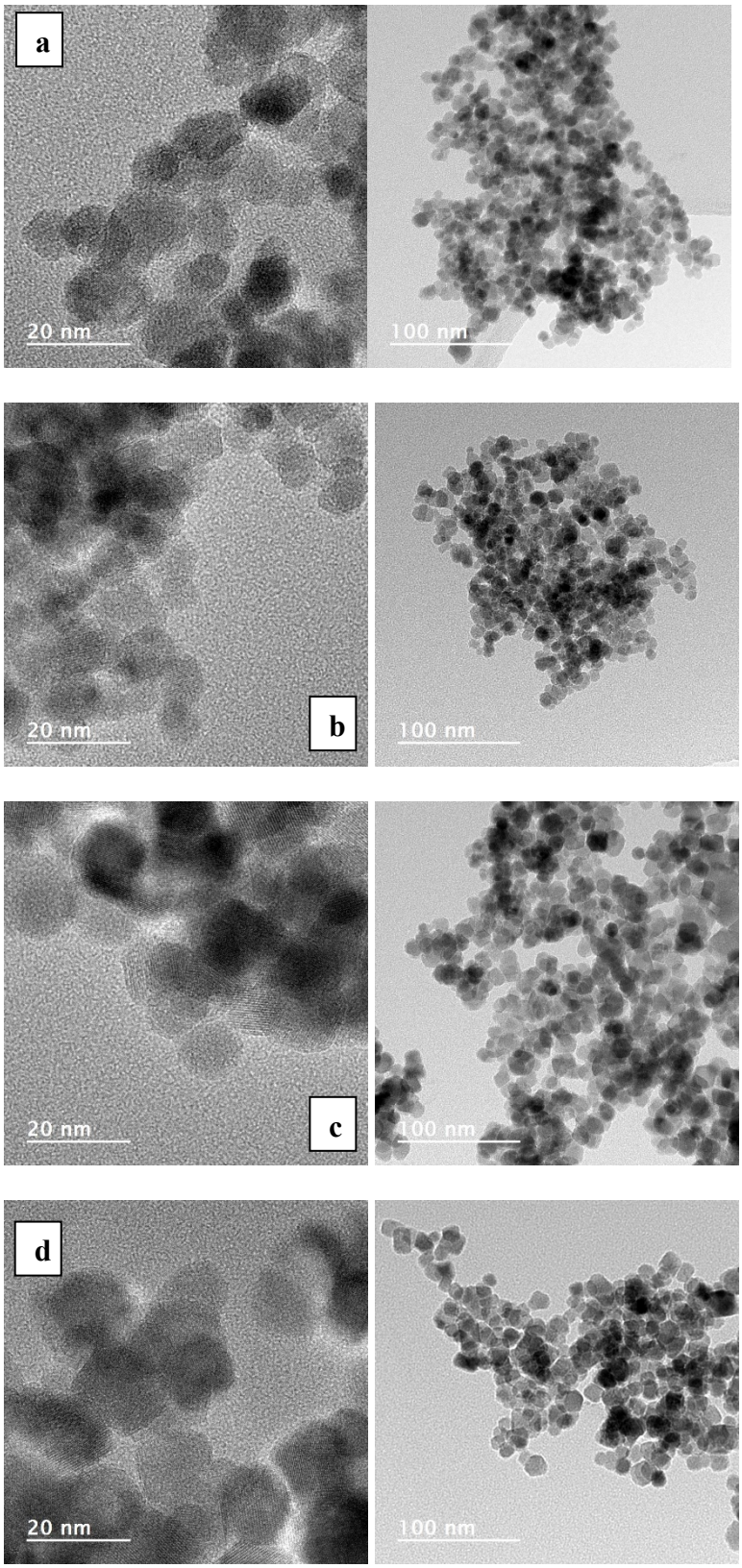

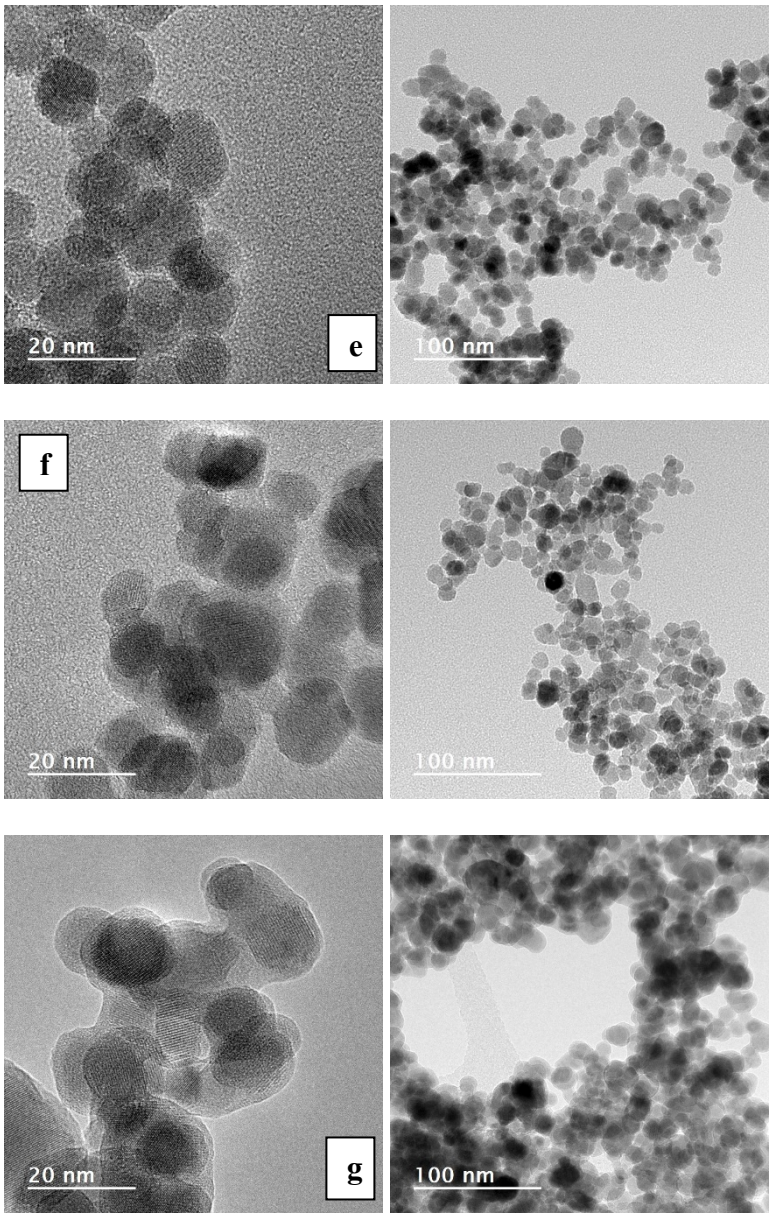

Figure S1. TEM images of synthetic magnetite nanoparticles with various stoichiometries ((a) R0.1, (b) R0.2, (c) R0.3, (d) R0.4, (e) R0.5), (f) the addition of Fe(II) to R0.1 to reach R = 0.5, and (g) overloading of R0.5 with 2500 μM Fe(II).

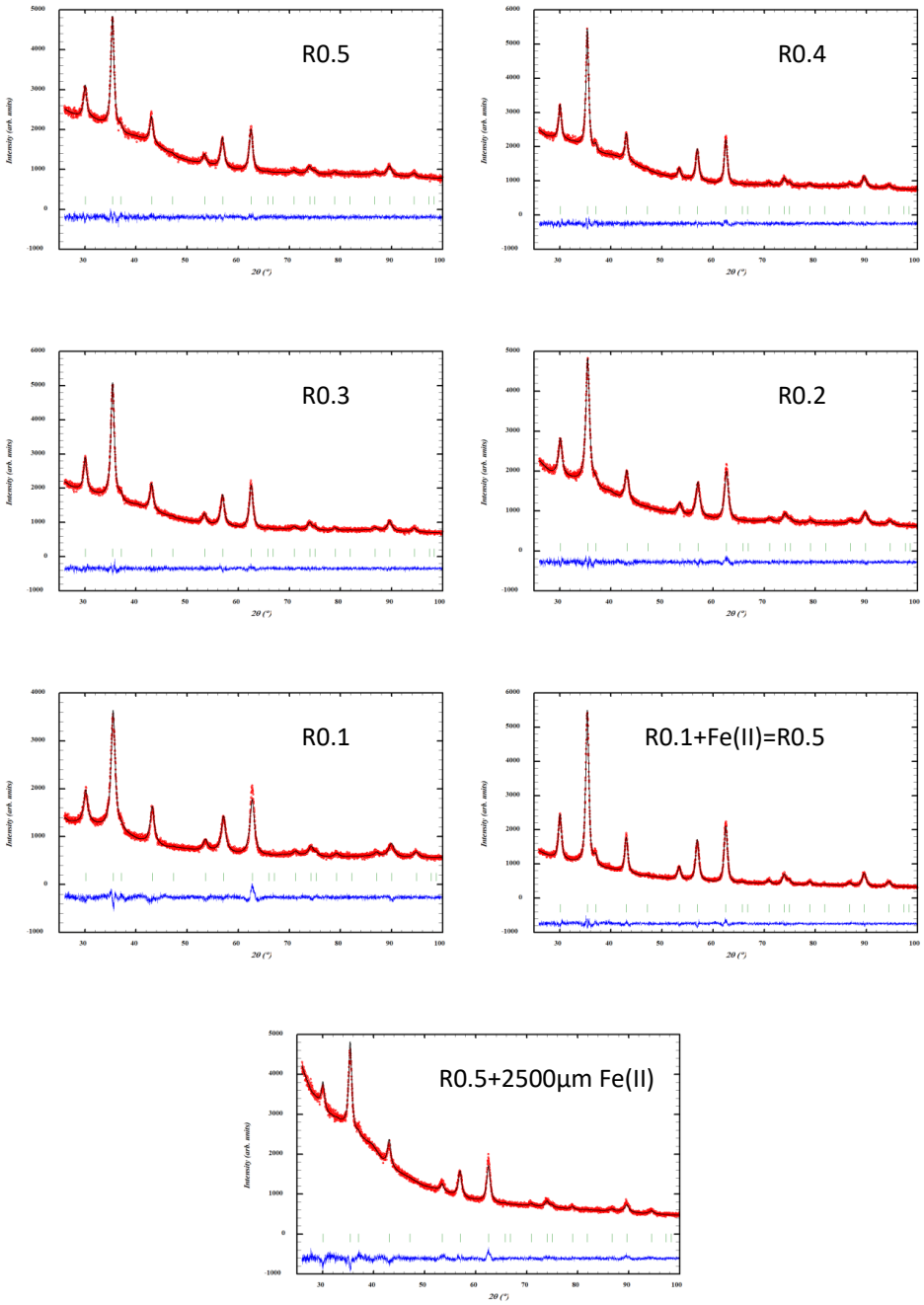

Figure S2. Selected angular domain of the Rietveld refined XRD patterns of the different magnetite samples presented in Table S1. The experimental diffractograms are plotted in red symbols, the calculated pattern in black line, and the difference between them as lower blue line. The vertical ticks indicate the Bragg peak positions for the cubic magnetite structure. The strong

background observed below 60° is due to the glycerol used to protect the powders against oxidation in air.

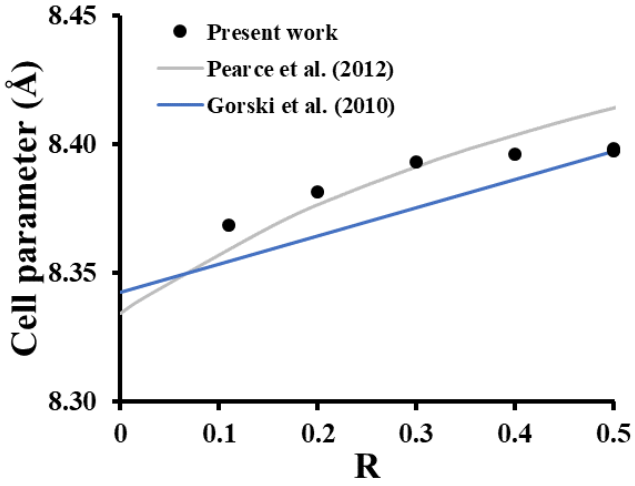

Figure S3. Cell parameter versus magnetite stoichiometry (R). Presently measure values are compared with calculated ones in previous studies (Gorski and Scherer, 2010; Pearce et al., 2012).

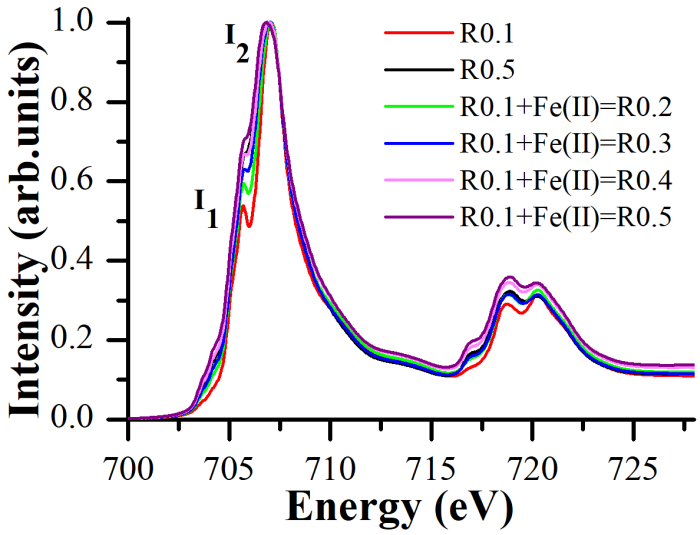

Figure S4. Isotropic XAS of the dissolved Fe^{2+} addition on non-stoichiometric magnetite (R0.1) to increase the stoichiometry at pH 8, and measured at B= 6 T and T=4 K at the Fe-$L_{2,3}$-edge.

Table S1. Effective Fe(II)/Fe(III) ratio R_{eff} obtained from chemical analysis, cell parameter and Crystallite size from XRD pattern refinements, average particle size by TEM and determined S value by XMCD for stoichiometric nanomagnetite (R0.5), oxidized products (R0.1 to R0.4), recharged sample (R0.1 + Fe(II) = R0.5) and overloaded samples (R0.5 + 250-2500 µM Fe(II)). "nd" means "non-determined".

Sample	**R_{eff} in solid phase**	**Cell parameter (Å)**	**Crystallite size by XRD (nm)**	**Particle size by TEM (nm)**	**S value**
R0.1	0.11	8.3685(4)	6.3	9.6±2.3	0.87
R0.2	0.20	8.3814(3)	7.1	8.9±2.1	0.95
R0.3	0.30	8.3932(3)	7.7	10.6±2.3	1.06
R0.4	0.40	8.3964(3)	9.4	11.1±2.0	1.14
R0.5	0.50	8.3976(4)	8.0	11.5±1.5	1.15
R0.1+Fe(II)=R0.5	0.50	8.3983(2)	9.0	11.3±2.0	1.19
R0.5+250 µM Fe(II)	0.54	nd	nd	nd	1.16
R0.5+500 µM Fe(II)	0.58	nd	nd	nd	1.17
R0.5+1000 µM Fe(II)	0.65	nd	nd	nd	1.22
R0.5+2500µM Fe(II)	0.932	8.3951(5)	8.3	12.9±1.8	1.17

Table S2. Literature values of the S ratio of magnetite and maghemite nanoparticles and methods of syntheses.

References	$S_{magnetite}$	$S_{maghemite}$	**Sizes and methods of synthesis**
This study	1.15	-	10 nm. Co-precipitation in NaOH
(Pellegrin et al., 1999)	1.15	0.69	4 nm. Thin film
(Peng et al., 2018)	1.15	-	10 nm. Co-precipitation in NH_4OH. Sample at pH8
(Park et al., 2004)	1.30	0.65	5-22 nm. Thermal decomposition
(Kuzmin and Chaboy, 2014)	1.30	0.68	9 nm. Thermal decomposition
(Carvallo et al., 2008)	1.30	-	31 ± 7.2 nm. Biogenic magnetite
(Coker et al., 2008)	1.35	-	20-30 nm. Biogenic magnetite
(Signorini et al., 2006)	1.46	0.76	5-13 nm. Iron/iron oxide granular nanostructures obtained by cold compacting core-shell nanoparticles
(Jiménez-Villacorta et al., 2011)	1.42	0.75	12 nm. Iron-iron oxide nanostructured under frozen state at low temperature

Chapter 3 How stable are stoichiometric magnetite nanoparticles in aqueous solutions?

Abstract. Magnetite ($Fe(III)_2Fe(II)O_4$) is a fascinating mineral in many scientific disciplines. The most interesting properties (magnetic, electronic, catalytic, redox, etc) of magnetite nanoparticles do not only arise from the "nano-effect" but also from the Fe^{2+} ion in its structure. Although the stability of these nanosized particles is often touted as a key technological advantage, here, we show that 10 nm-sized stoichiometric magnetite particles (Fe(II)/Fe(III) = 0.5) are not stable in aqueous solutions under a biologically or environmentally relevant pH range. In the absence of O_2, the H^+-promoted dissolution process was responsible for the preferential release of Fe(II) over Fe(III) to the solution, which led to the partial transformation of magnetite into maghemite. If a small magnetite core is hardly affected over a few years in acidic conditions (pH < 5), a thin shell at the surface can be formed even at circumneutral pH and rapidly equilibrates with the aqueous solution. Finally, we propose a thermodynamic model for the magnetite-maghemite solid-solution capable of predicting the stability and redox-reactivity of nano-magnetite. These results call for the reconsideration of how to assess the properties of magnetite nanoparticles before nanotechnological applications in water.

Résumé. La magnétite ($Fe(III)_2Fe(II)O_4$) est un minéral fascinant dans de nombreuses disciplines scientifiques. Les propriétés les plus intéressantes (magnétiques, électroniques, catalytiques, redox, etc…) des nanoparticules de magnétite ne sont pas seulement liées à « l'effet nano » mais également à la présence d'ion Fe^{2+} dans leur structure. Bien que la stabilité de ces particules nanométriques soit souvent présentée comme un avantage technologique clé, nous montrons ici que les particules de magnétite stœchiométriques (Fe(II)/Fe(III) = 0,5) de 10 nm ne sont pas stables dans des solutions aqueuses sur une gamme de pH couramment rencontrée dans l'environnement. En l'absence d'O_2, le processus de dissolution, favorisé par la présence de H^+, est responsable de

la libération préférentielle du Fe(II) par rapport au Fe(III) dans la solution, ce qui conduit à la transformation partielle de la magnétite en maghémite. Si un cœur de magnétite peut persister pendant plusieurs années dans des conditions acides (pH < 5), une couche de maghémite peut se former à la surface en s'équilibrant rapidement avec la solution aqueuse même à pH neutre. Finalement, nous proposons un modèle thermodynamique pour la solution-solide magnétite-maghémite capable de prédire la stabilité et la réactivité redox de nano-magnétites. Ces résultats appellent à reconsidérer la manière d'évaluer les propriétés des nanoparticules de magnétite en phase aqueuse pour des applications en nanotechnologie.

3.1 Introduction

Magnetite is a mixed-valence iron oxide with an inverse spinel structure. Its formula is Fe_3O_4, or $[Fe^{2+}\ Fe^{3+}]_{Oh}\ Fe^{3+}_{Td}O^{2-}_4$, where high spin Fe^{2+} and Fe^{3+} can be found in octahedral (Oh) and tetrahedral (Td) coordination. Fast electron hopping between Fe ions on Oh sites leads to the high bulk electron conductivity of magnetite. Special magnetic properties are due to the Fe^{2+}_{Oh} because the magnetic moments of both types of Fe^{3+} ions cancel each other (Cornell and Schwertmann, 2003). Magnetite can be useful for the reduction and oxidation of chemical compounds (Peterson et al., 1997; Gorski et al., 2010; Latta et al., 2012; Liu et al., 2015; Usman et al., 2018; Pan et al., 2020). Electrons, released during Fe^{2+}-Fe^{3+} transformation may reduce other chemical species. Conversely, Fe^{2+} in magnetite can catalyze the formation of highly oxidative radicals in presence of O_2 or H_2O_2 leading to the oxidation of other chemical compounds (e.g. Fenton-like reactions (Gao et al., 2007). The redox properties make magnetite an excellent "battery" for humans activities(Lininger et al., 2018) and microorganisms (Byrne et al., 2015).

Most of the interesting properties (magnetic, redox, electronic, catalytic, medical, environmental, etc.) of magnetite are due to the presence of Fe^{2+} ions in the magnetite structure. Oxidation reactions transform magnetite into maghemite (Fe_2O_3 or $[Fe^{3+}_{5/3}\square_{1/3}]_{Oh}Fe^{3+}_{Td}\ \ O^{2-}_4$). Maghemite is isostructural to magnetite but contains vacant Oh sites (□) instead of Fe^{2+}. Partial oxidation largely affects magnetite properties, such as its reduction capacity for heavy metals and radionuclides (e.g. U(VI) to U(IV)) (Latta et al., 2012; Pan et al., 2020), reduction rates of organic compounds (e.g. nitrobenzene) (Gorski et al., 2010) or adsorption of organic molecules (e.g. quinolone antibiotics), (Cheng et al., 2018) as illustrated in Figure 1. The oxidation of magnetite to maghemite is well documented and, in the presence of oxygen, can be formulated as:

$$4\ Fe_3O_{4(s)} + O_{2(g)} \rightleftharpoons 6\ Fe_2O_{3(s)} \quad (1)$$

This transformation is, however, not that straightforward because intermediate solid-solutions form, so-called non-stoichiometric magnetites, $[Fe_X^{2+}\ Fe_{(5-2X)/3}^{3+}\ \square_{(1-X)/3}]_{Oh}\ Fe_{Td}^{3+}O_4^{2-}$, where X is the mole fraction of magnetite in the solid ($0 \leq X \leq 1$). Note that magnetite stoichiometry is often characterized by the ratio R = Fe(II)/Fe(III), which ranges from R = 0 (pure maghemite) to R = 0.5 (pure magnetite) (Cornell and Schwertmann, 2003; Lilova et al., 2012; Usman et al., 2018). In addition, many applications of magnetite nanoparticles involve their suspension in aqueous solution (medicine (Stephen et al., 2011; Revia and Zhang, 2016), biology (Faivre and Godec, 2015; Byrne et al., 2015), chemistry (Laurent et al., 2008; Polshettiwar et al., 2011), environment (Ahmed and Maher, 2018; Kobayashi et al., 2018), etc). H^+-promoted dissolution of magnetite leads to the release of Fe^{2+} ions into the solution and leaves Fe^{3+} in the solid phase:

$$Fe_3O_{4(s)} + 2\ H^+_{(aq)} \rightleftharpoons Fe_2O_{3(s)} + Fe^{2+}_{(aq)} + H_2O_{(l)} \quad (2)$$

Despite the apparent importance of nano-magnetite stoichiometry concerning its reactivity, the transformation of nano-magnetite to non-stoichiometric nano-magnetite via eq.2 has only been characterized in acidic solutions (e.g. pH < 3), (Jolivet and Tronc, 1988) with large magnetite particles (> 100 nm),(White et al., 1994) at high temperature, (Sweeton and Baes, 1970) or in presence of O_2. (Ahmed and Maher, 2018) In addition, because of the very slow process observed, only the kinetic aspects of eq.2 were treated, and the experiments were rarely designed to observe a steady-state (Jolivet and Tronc, 1988; Sun et al., 1998). By contrast, environmental or biological conditions in which magnetite may be found or used are characterized by low O_2 content and circumneutral pH. Because magnetite often occurs in environmental systems experiencing fluctuating pH and redox conditions, knowledge of the sign and magnitude of the free energy change is required to judge which direction eqns. 1-2 would take. Because of the lack of knowledge

on the chemical behavior of magnetite nanoparticles in water, experiments under inert ("O_2-free") atmosphere are often limited to neutral and alkaline conditions, to limit Fe^{2+} release to the solution (e.g. (Peterson et al., 1997; Gorski et al., 2010; Latta et al., 2012; Marshall et al., 2014; Cheng et al., 2018; Morelová et al., 2020)). Alternatively, the impact of eq.1 is simply neglected and magnetite nanoparticles subjected to different pH values are considered to remain "as prepared" (e.g. (Gao et al., 2007; Liu et al., 2015; Schwaminger et al., 2015; Gumpelmayer et al., 2018)). Unwanted or unexpected chemical transformation of magnetite may potentially explain contradictions between different studies, such as in the case of the Fenton-like (discussed as peroxidase-like) activity of nano-magnetites at pH = 3.5 (Gao et al., 2007; Gumpelmayer et al., 2018). Given the extensive use of magnetite nanoparticles and their importance in many biological and environmental context, it become urgent to fully characterize the impact of physico-chemical conditions, and especially the pH on magnetite stoichiometry, and the consequences on magnetite redox and surface reactivity in aqueous systems.

Here an extensive dataset on the solubility of magnetite nanoparticles in aqueous suspension is presented, in which long-term kinetic investigations (560 days) shed light on overlooked aspects of the dissolution processes and allowed to determine physico-chemical conditions in which a chemical equilibrium was reached. Based on these data we develop the first chemical thermodynamic model for nano-magnetite stoichiometry in aqueous solutions, capable of predicting the composition of nano-magnetite as a function of aqueous solution characteristics (especially dissolved Fe^{2+} concentration, pH, and redox potential, cf. eqns.1-2). These findings will help predicting or tuning the redox and surface reactivity of magnetite nanoparticles.

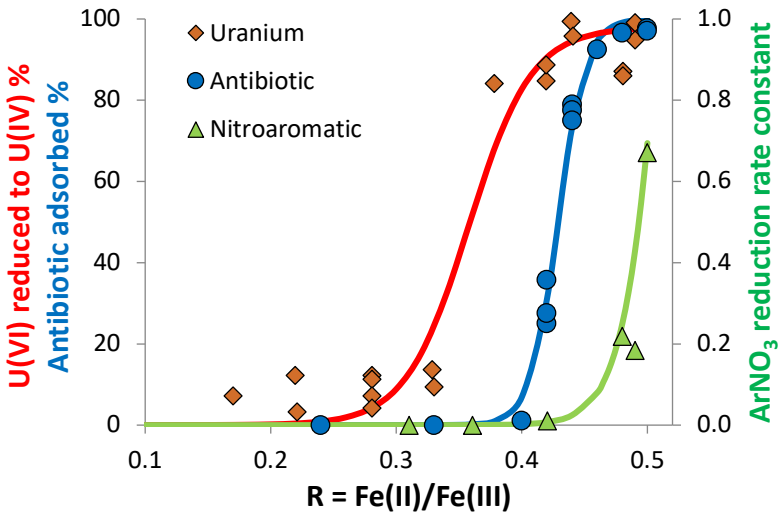

Figure 1. Percentage of (i) U(VI) reduced to U(IV) (Latta et al., 2012) and (ii) nalidixic acid (quinolone antibiotic) (Cheng et al., 2018) adsorbed at the surface of magnetite nanoparticles, and pseudo-first-order rate constant for the reduction of nitrobenzene ($C_6H_5NO_3$) to aniline ($C_6H_5NH_3$) (Gorski et al., 2010) by magnetite as a function of magnetite stoichiometry (R = Fe(II)/Fe(III)). Lines are just to guide the eye.

3.2 Materials and methods

3.2.1 Chemicals

Iron(III) chloride hexahydrate ($FeCl_3 \cdot 6H_2O$) and Iron(II) chloride tetrahydrate ($FeCl_2 \cdot 4H_2O$) were purchased from AnalaR NORMAPUR. Hydrogen peroxide (H_2O_2), hydrochloric acid (HCl), and sodium hydroxide (NaOH) were obtained from Sigma-Aldrich. The sample solutions were prepared with ultrapure "MilliQ" water (specific resistivity which is 18.2 $M\Omega cm^{-1}$). All experiments were carried out in an anaerobic chamber (N_2-glovebox, JACOMEX) and all solutions were purged from $O_{2(g)}$ prior to use. All samples were also adjusted pH by HCl and NaOH (no buffer was used).

3.2.2 Synthesis of magnetites with various stoichiometries

Magnetite nanoparticles (10 nm) preparation was described in Chapter 2 of this thesis (Jungcharoen et al., 2021). Samples used in the present chapter come from the same batch. The synthesis procedure is repeated for clarity. The procedure involves a room temperature aqueous precipitation and following the method of (Chapter 2) (Massart, 1981; Demangeat et al., 2018; Jungcharoen et al., 2021). Briefly, a 0.5 M HCl solution (40 mL) containing a 0.5 M $FeCl_2$ and 1 M $FeCl_3$ (1:2 molar ratio) was added dropwise into a 0.5 M NaOH solution (250 mL) with continuous stirring, leading to instantaneous precipitation of magnetite particles. After the synthesis, the solid phase was washed three times with ultrapure water whose pH was adjusted to 8.5 (using NaOH) to avoid the release of Fe^{2+}, as observed in previous work (Marsac et al., 2017; Cheng et al., 2018), and thus, to guarantee the stoichiometry of 0.5. Known amounts of H_2O_2 were added to R0.5 to produce different sets of non-stoichiometric magnetites (R0.1, R0.2, R0.3, R0.4) (Gorski and Scherer, 2010; Cheng et al., 2018). Then, mother solutions were washed with ultrapure

water (at pH = 8.5) in order to remove residual H_2O_2. Initial Fe(II)/Fe(III) ratios (R_{ini}) of these (non-)stoichiometric magnetites were determined by acid digestion in 0.6 M HCl during 3 days, followed by spectrophotometric determination of dissolved [Fe(II)] and total [Fe] (= [Fe(III)] + [Fe(II)]) using the 1-10 phenantroline colorimetric method (AFNOR NF T90-017), (Fortune and Mellon, 1938) as well as by X-ray Magnetic circular dichroism (XMCD, Chapter 2) (Jungcharoen et al., 2021). Repetition of acid digestion followed by spectrophotometry led to an error of ±0.01 on the determination of R_{eff}. Results were in excellent agreement with expected values from the amount of H_2O_2 added, as expected from previous studies (Gorski and Scherer, 2009, 2010; Cheng et al., 2018).

3.2.3 Batch studies

All experiments were conducted with 10 mM NaCl as background electrolyte. Fe dissolution kinetic studies were at pH 4, 5.5 and 8 for R_{ini} = 0.5, and at pH 4 for R_{ini} = 0.1 and 0.3. Iron total concentration in the suspension was 6.5 mM, corresponding to ~0.5 g L^{-1} of magnetite, in 100 mL suspension in 250 mL HDPE bottle. pH was controlled and adjusted regularly over a 560-days period using HCl and NaOH. Equilibrium studies were conducted in 10 mM NaCl solutions and in 15mL polypropylene tubes containing 10 mL of solution. Reaction time was 20 days (for R_{ini} = 0.5), 60 days (R_{ini} = 0.3, 0.4) or 320 days (R_{ini} = 0.1, 0.2). The impact of dissolved Fe(II) addition on the recharge of R0.1 was investigated by adding small amounts of a 100 mM $FeCl_2$ solution. The impact of the presence of an excess of Fe(II) on R0.5 was investigated by adding 0.25, 0.5 or 1 mM Fe^{2+} to R0.5.

After a given reaction time, pH and ORP were measured and the suspension was passed through a 0.2 μm cellulose acetate filter (Sartorius Minisart), followed by dissolved [Fe(II)] and

[Fe(III)] determination by spectrophotometry. The error on [Fe] determination was assumed equal to 5 %. The absence of Fe nanoparticles in the filtrate was checked by dynamic light scattering (VASCO Flex). pH and redox potential (Eh) were recorded in both magnetite and Fe(II)-amended magnetite suspensions using a portable multiparameter electrode (pH, Eh and T; Hach, sensION+5045). The pH electrode was calibrated with 3 standard buffers (pH 4, 7, and 10). The Pt electrode combined with a Ag/AgCl reference electrode, used for redox potential measurements, was calibrated using a commercial redox buffer (220 mV vs Ag/AgCl). Raw data were converted into Eh vs standard hydrogen electrode (SHE) by correcting for the potential of the reference electrode. An equilibrium time of 15 minutes was applied for all E_h measurements (Marsac et al., 2015). The suspension was stirred prior to the E_h measurements. The electrode surface was periodically cleaned by exposing it to 0.1 M HCl for 1 h. (Teasdale et al., 1998).

3.2.4 Characterization by TEM and XMCD

Transmission electron microscopy (TEM; Jeol JEM 1230 microscope) was used for magnetite nanoparticles characterization. Briefly, A small aliquot of magnetite suspension was diluted with ultrapure water and sonicated for 20 min. A droplet of the diluted suspension was deposited on a carbon-coated 200 mesh copper grid and dried inside the anaerobic chamber. Samples were transported to the microscope under an N_2 atmosphere using a hermetic holder and the samples were analyzed at an acceleration voltage of 200 kV. Average particle diameters were determined by measuring 100 particles.

XMCD signals were recorded at the Fe $L_{2,3}$ edges (700 – 730 eV) on the DEIMOS beamline at the synchrotron light source SOLEIL as previously described (Chapter 2) (Daffé et al., 2018; Sartori et al., 2019; Jungcharoen et al., 2021). Briefly, samples were transported to the SOLEIL

Synchrotron facility at the DEIMOS beamline (Ohresser et al., 2014) in 1 mL tubes, placed in airtight bottles that had been closed in the N_2-glovebox. Colloidal suspensions of nanoparticles were drop-casted on silicon substrates and dried at room temperature, in an Ar-glove box ($O_{2(g)}$ < 1 ppm) connected to the end station. The silicon substrates were fixed on a sample holder and transferred into the cryomagnet, under ultra-high vacuum (UHV-10^{-10} mbar). All spectra were measured in Total Electron Yield mode (TEY) at 4.2 K under UHV conditions and an applied magnetic field H (H^+ = +6 Tesla and H^- = -6 Tesla). The beam size was 800*800 μm^2 and the resolution was 100 meV. XMCD spectra were plotted by considering the absorption cross-section measured with left (σ_L) and right (σ_R) circularly polarized X-rays. XMCD spectra were plotted as $\sigma_{XMCD}= (\sigma_+ - \sigma_-)$ where $\sigma_+ = [\sigma_L(H^+) + \sigma_R(H^-)]/2$ and $\sigma_- = [\sigma_L(H^-) + \sigma_R(H^+)]/2$. The circularly polarized X-rays are provided by an Apple-II HU-52 helical undulator for XMCD measurements and by sweeping the magnetic field from +6T to -6T. XMCD signals were normalized by dividing the raw signal by the height of the maximum.

3.3 Results and discussion

3.3.1 Fast and slow Fe2+ release processes from magnetite

When maintaining stoichiometric magnetite nanoparticles (0.5 g L^{-1}) at pH = 8 in 10 mM NaCl solution, a marginal release of Fe into solution is observed, evidencing the stability of magnetite at these conditions. In contrast, at pH = 5.5, a fast release of Fe^{2+} occurred after 1 day (aqueous Fe^{3+} below detection limit). This incongruent dissolution process impacts the effective magnetite stoichiometry (R_{eff}; Fig. 2a), which may be calculated from the initial stoichiometry (R_{ini}, here equal to 0.5), the total concentration of Fe(III) in both the aqueous and solid phases ($[Fe(III)]_{tot}$) and the measured aqueous Fe^{2+} concentration ($[Fe^{2+}]_{aq}$):

$$R_{eff} = R_{ini} - [Fe^{2+}]_{aq}/[Fe(III)]_{tot} \quad (3)$$

Accordingly, R_{eff} drops from 0.5 to 0.36 within 1 day. At this value, R_{eff} remains constant over time, suggesting chemical equilibrium.

Exposing magnetite to a pH 4 solution leads to a rapid release of Fe^{2+} within the first two days, which progressively slows down after this initial step. Concomitantly, R_{eff} dropped from 0.5 to 0.2 within two days. The decrease of R_{eff} slowed down when approaching 0.1, but seems to tend to 0 over longer time scales (Fig. 2a). To confirm that at least two processes were involved when R_{eff} was above or below 0.1, nano-magnetites of defined stoichiometries (R_{ini} = 0.1, 0.3 and 0.5) were prepared from the stoichiometric magnetite sample, by addition of H_2O_2, to study their transformation kinetics at pH 4 (Fig. 2b). As expected, a fast initial Fe^{2+} release was observed for R_{ini} = 0.3 then the reaction slows down when R_{eff} approaches 0.1, whereas the process is slow from the beginning for R_{ini} = 0.1. As previously suggested, (Jolivet et al., 2004) the initial release of Fe(II) from the near surface region may be fast due to electron transfer from the interior of the

particle to the surface. This, however, causes a charge imbalance inside the particle, which must be compensated by the movement of Fe-ions and concomitant generation of Oh vacancies. Recent diffraction investigations (Yuan et al., 2019) demonstrated oxidation-induced strain in magnetite particles, an effect that may likely correlate with these interpretations. This process is likely much slower, and may even slow down further as the Fe(II)-depleted outer rim grows thicker while the core shrinks (White et al., 1994; Ahmed and Maher, 2018). When applying a shrinking-core model to the data obtained for $R_{ini} = 0.1$ at pH = 4 (Fig. 2b) – conditions where only the slow process was observed – a complete release of Fe(II) (or $R_{eff} < 0.01$) is expected after around 1800 days (~5 years).

3.3.2 Reaction products of magnetite with H^+, H_2O_2 or Fe^{2+}

No significant evolution of the particle size and shape was observed between the pristine stoichiometric magnetite at pH = 8 ($R_{ini} = 0.5$; Fig. 2c), after acid treatment at pH = 4 ($R_{eff} = 0.13$; Fig. 2d), oxidation by H_2O_2 (e.g. $R_{ini} = 0.1$; Fig. 2e) and subsequent recharge with dissolved Fe^{2+} (Fig. 2f). The structure of these magnetites were probed by synchrotron X-ray magnetic circular dichroism (XMCD) spectroscopy, which enables to distinguish Fe^{2+}_{Oh}, Fe^{3+}_{Td} and Fe^{3+}_{Oh} according to their distinct characteristic peaks (Fig. 2g) (Pellegrin et al., 1999). The intensity of the Fe^{2+}_{Oh} peak relative to that of Fe^{3+}_{Td} and Fe^{3+}_{Oh} decrease with decreasing pH or after oxidation of the pristine magnetite with H_2O_2 at pH 8. XMCD spectra of magnetite exposed to H_2O_2 and showing $R_{ini} = 0.1$ and 0.3 were quite similar to those of stoichiometric magnetite equilibrated at pH 4 and 5.5 during 300 days. As observed in previous studies, a complete Fe^{2+} uptake proceeded within 1 day when equilibrating a non-stoichiometric magnetite ($R_{ini} = 0.1$) at pH = 7 with an appropriate amount of dissolved Fe^{2+} to fully restore $R_{eff} = 0.5$ (Gorski and Scherer, 2009; Gorski et al., 2010;

Cheng et al., 2018). Although Fe^{2+} uptake by oxidized magnetite led to surface recrystallization (Chapter 2) (Jungcharoen et al., 2021), similar reactivity of the pristine magnetite and the oxidized then recharge one concerning contaminants reduction (Gorski et al., 2010) and surface complexation support the assumption of a reversible process (Cheng et al., 2018).

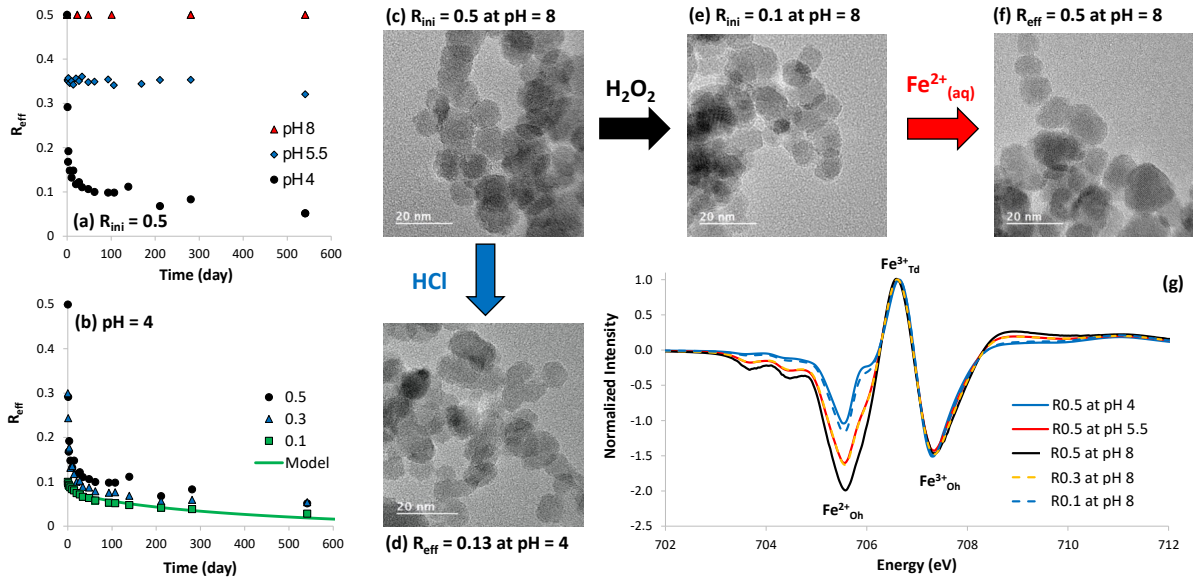

Figure 2. (a) Transformation kinetics of stoichiometric magnetite (R_{ini} = 0.5) at different pH values (4, 5.5 and 8). Closed and open symbols refer to R_{eff} calculated using eq.3 and measured after acid dissolution, respectively. (b) Dissolution kinetics of different magnetites (R_{ini} = 0.1, 0.3 and 0.5) at pH 4. The line represents calculations using the shrinking-core model. (c,d,e,f) HRTEM images of the pristine magnetite (R_{ini} = 0.5; c), equilibrated at pH = 4 (R_{eff} = 0.13; d), or oxidized with H_2O_2 (R_{ini} = 0.1; e) followed by the addition of $Fe^{2+}_{(aq)}$ (R_{eff} = 0.5; f). (g) Normalized XMCD spectra of stoichiometric magnetite (R0.5) equilibrated at different pH values (4, 5.5 and 8) compared with those of stoichiometric maghemite oxidized by H_2O_2 (R0.1 and R0.3) at pH 8.

3.3.3 Impact of pH and partial oxidation on magnetite stoichiometry

The apparent establishment of an equilibrium at pH ≥ 5.5 after one day, which might be extended to pH ≥ 5 after 20 days, (Sun et al., 1998) and the similar reaction products of magnetite with H^+, H_2O_2 or Fe^{2+} further motivated investigation of magnetite solubility at chemical equilibrium. Stoichiometric magnetite suspensions (0.5 g L^{-1}) were equilibrated at different pH values during 20 days (Fig. 3a, in black). Samples at pH < 5 ($R_{eff} \leq 0.1$) did not reach equilibrium during the experimental time-frame, but are also shown (Fig. 3a). A linear combination fit involving magnetite and maghemite references (Chapter 2) (Jungcharoen et al., 2021) was used to calculated R_{eff} from the XMCD results, which were found in excellent agreement with wet chemical analysis (large diamonds in Fig. 3a). In agreement with eq.2, $[Fe(II)]_{aq}$ increases with decreasing pH, and R_{eff} decreases from 0.5 at pH = 7 to 0.18 at pH = 5.5. These results show that the studied magnetite nanoparticles cannot be considered as stoichiometric after contact with aqueous solution under mildly acidic conditions (pH < 7). Attempts to maintain magnetite stoichiometry by supersaturating the system failed: (i) by working with 5 times more concentrated magnetite suspensions (2.5 g L^{-1}), similar R_{eff} values were obtained although about 5 times larger $[Fe(II)]_{aq}$ were measured (Fig. 3a, in red), and (ii) addition of dissolved Fe(II) excess (0.25-1 mM) to a stoichiometric magnetite did not significantly affect R_{eff} at pH < 7 (Fig. S1). In fact, in all the experiments at pH < 7, suspensions were composed of non-stoichiometric magnetites with aqueous Fe(II).

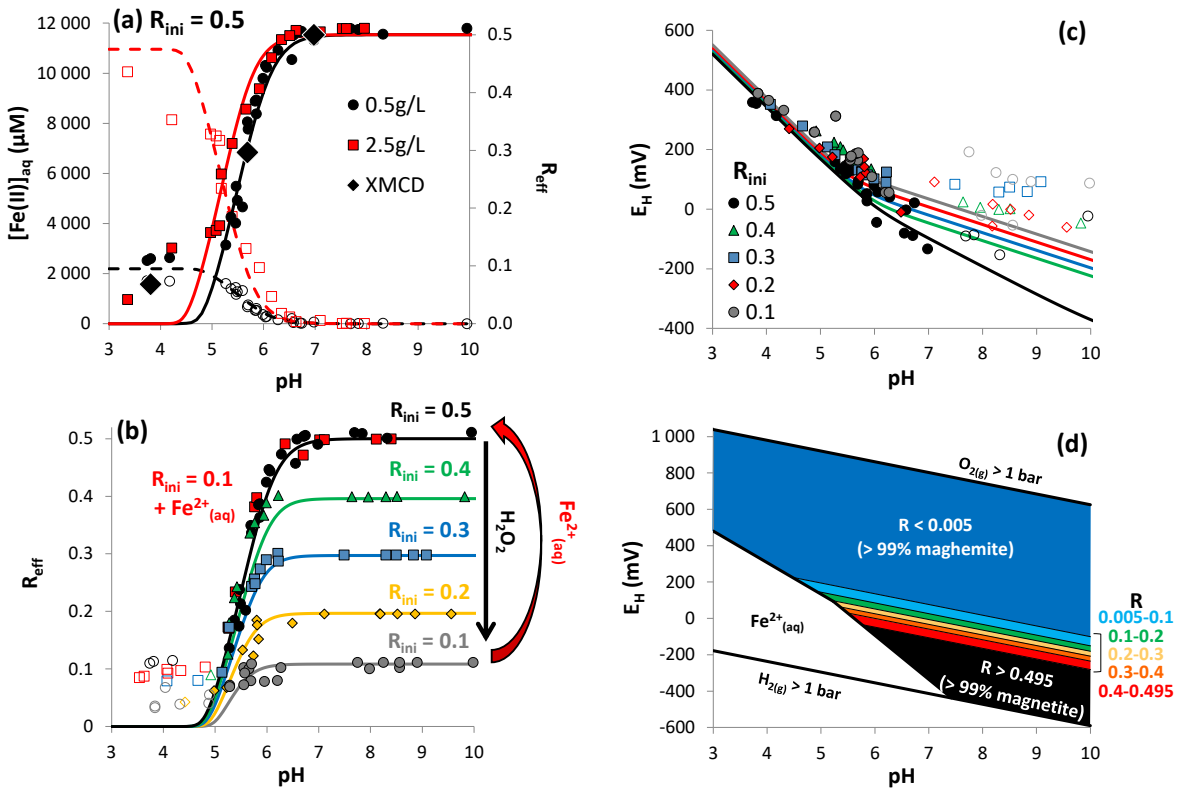

Figure 3. (a) Effect of pH (3-10) and magnetite concentration (0.5 and 2.5 g L^{-1}) on Fe(II) solubility (open symbols) and corresponding magnetite effective stoichiometry (for R_{ini} = 0.5; full symbols). Large diamonds correspond to R_{eff} determined by X-ray magnetism circular dichroism (XMCD). (b) Effect of pH on R_{eff} of magnetites exhibiting different initial stoichiometries ($0.1 \leq R_{ini} \leq 0.5$), and of a non-stoichiometric magnetite (R_{ini} = 0.1) to which dissolved Fe(II) was added in order to reach an overall (solid+solution) Fe(II)/Fe(III) ratio of 0.5. Open symbols refer to no equilibrium data (pH < 5). (c) Comparison between measured and calculated redox potential in magnetite suspensions. (d) pH-E_H predominance diagram of Fe in the magnetite-maghemite-H_2O system (10 nm particles, $[Fe_3O_4]$ = 0.5 g L^{-1}, in 10 mM NaCl).

We further investigated the behavior of magnetites exhibiting different initial stoichiometries (R_{ini} = 0.1, 0.2, 0.3, 0.4 and 0.5). These were obtained from the same stoichiometric magnetite sample by addition of H_2O_2. Reaction time was increased to 60 days (R_{ini} = 0.3, 0.4) and 320 days (R_{ini} = 0.1, 0.2) in order to ensure that chemical equilibrium is achieved at pH > 5. As for R_{ini} = 0.5, H^+-promoted Fe^{2+} release leads to a decrease of R_{eff} with decreasing pH (Fig. 3b). Interestingly, R_{eff} values of all initial magnetites follow the same trend, once pH falls below a certain value (e.g. at pH < 5.5, R_{eff} values are equal for magnetites with R_{ini} = 0.3, 0.4 and 0.5), evidencing the strong relationship between R_{eff}, pH, and aqueous Fe^{2+}, and suggesting fully reversible release/uptake of Fe(II) by magnetite. The latter was confirmed over a large pH range by adding Fe^{2+} to a suspension of non-stoichiometric magnetite (R_{ini} = 0.1) in order to reach an overall (solid+solution) Fe(II)/Fe(III) ratio of 0.5 (Fig. 3b). Thus, over the whole pH range investigated, final R_{eff} values did not significantly differ from those obtained by release of Fe^{2+} from pristine stoichiometric magnetite.

3.3.4 Chemical thermodynamic modeling of the magnetite-maghemite system

If variations of magnetite stoichiometry cannot be avoided, quantitative prediction of this phenomenon becomes crucial. For this purpose, we consider non-stoichiometric magnetite as a binary solid-solution between maghemite (X = 0) and magnetite (X = 1). In order to describe the thermodynamic equilibrium between a magnetite-maghemite solid-solution and an aqueous solution, it is necessary to ensure that one ion on one structural position is exchanged in the mixing process. Hence, the magnetite oxidation reaction can be formulated as:

$$[Fe_3^{2+}\ Fe_3^{3+}]_{Oh}\ Fe_{3\ Td}^{3+}O_{12}^{2-} + 2\ H^+ \rightleftharpoons\ [Fe_5^{3+}\ \square\ ]_{Oh}Fe_{3\ Td}^{3+}O_{12}^{2-} + Fe^{2+} + H_2 \qquad (4)$$

The Gibbs free energies of formation of the solid-solution ($\Delta G_{ss,nano}$) of magnetite (mt)-maghemite (mm) nanoparticles is expressed by:

$$\Delta G_{ss,nano} = X\Delta G_{mt,nano} + (1-X)\Delta G_{mm,nano} + \Delta G_{mix} \quad (5)$$

The excess free energy of mixing (ΔG_{mix}) can be expressed according to Guggenheim's expansion series:

$$\Delta G_{mix} = X(1-X)RT(a_0 + a_1(2X-1) + \ldots.) \quad (6)$$

Where a_0, a_1, etc. are adjustable so called non-dimensional Guggenheim parameters (Glynn and Reardon, 1990; Glynn, 2000). Tabulated Gibbs free energies of the bulk iron oxides ($\Delta G_{mm,bulk}$ and $\Delta G_{mt,bulk}$) were used (NEA, 2020). Additionally, it was found necessary to consider adjusted surface free energies (referring to hydrated surfaces, γ_{mm} and γ_{mt} in J m^{-2}) of the end-member phases to determine the ΔG of the maghemite and magnetite nanoparticles ($\Delta G_{mm,nano}$ and $\Delta G_{mt,nano}$), in order to precisely match the experimental solubility data (Hiemstra, 2015). Because particle size determined by TEM (Fig. 2c,d,e,f) and crystallite size previously determined by XRD (Chapter 2) (Jungcharoen et al., 2021) did not significantly vary in all our experiments, the surface area was assumed constant (100 m^2 g^{-1}) (Marsac et al., 2017; Demangeat et al., 2018; Cheng et al., 2018). The large Fe^{2+} solubility dataset produced in our study at various pH and R_{ini} was used to calibrate this model, discarding the results obtained at pH < 5 that could not be obtained at chemical equilibrium. The fitting exercise using the geochemical speciation code Phreeplot (PHREEQC-Phreeplot coupling) (Parkhurst and Appelo, 1999; Kinniburgh and Cooper, 2011) gave γ_{mt} = 0.52 ± 0.10 J m^{-2} and γ_{mm} = 0.57 ± 0.29 J m^{-2} consistent with literature data (respectively 0.79 ± 0.28 and 0.57 ± 0.10 J m^{-2}), (Navrotsky et al., 2010) and we found that a single Guggenheim parameter was required in order to obtain an accurate match between model and data (Fig. 3). A negative value of a_0 = -5.49 ± 0.50 confirms the negative ΔG_{mix} previously reported from oxide melt

solution calorimetry for 100-300 nm sized magnetites (Lilova et al., 2012). It demonstrates that non-stoichiometric magnetites are a very special type of solid-solution, in comparison to many other solid-solutions exhibiting positive ΔG_{mix} (Glynn and Reardon, 1990; Glynn, 2000). This may be explained by the fact that mixing of magnetite and maghemite involves generation of vacancies and electron transfer processes rather than mixing of ionic species on a given crystallographic position.

3.3.5 Prediction of oxido-reduction potential in magnetite suspensions

In environmental systems, magnetite plays an important role for the redox speciation of contaminants and, hence, on their fate, transport, bioavailability and toxicity. For instance, magnetite can (i) immobilize uranium by reducing the rather mobile U(VI) to less mobile U(IV), (Latta et al., 2012) (ii) reduce Cr(VI) or nitrobenzene to less toxic Cr(III) or aniline (Peterson et al., 1997; Gorski et al., 2010) or, conversely, (iii) reduce As(V) to a more toxic As(III) (Liu et al., 2015). Therefore, the redox potential (E_H, reported versus the standard hydrogen electrode) in magnetite containing environmental systems is crucial information to predict the behavior and fate of contaminants. Our model was used to predict E_H in magnetite suspensions versus pH. At pH < 7, when pH decreases, all magnetites tend to exhibit the same stoichiometry (Fig. 3b), which leads to similar calculated E_H values (Fig. 3c). Interestingly, the model agreed with experimentally determined E_H values at a Pt electrode, which might be achieved thanks to the large amount of dissolved Fe^{2+} and the small size of the nanoparticles that could react with the electrode (Silvester et al., 2005). At pH > 7, Fe^{2+} is retained in the solid phase, making experimental E_H determination less reliable and a large scatter is observed (open symbols in Fig. 3c) (Nordstrom and Campbell, 2014). Nevertheless, calculated E_H, from +30 mV (R_{ini} = 0.1) to -154 mV (R_{ini} = 0.5) at pH = 7.2,

compared rather well with expected E_H values according to the U(VI)/U(IV) redox chemistry (Latta et al., 2012). This further supports the reliability of the present model. Therefore, our results allow proposing a new pH-E_H predominance diagram of Fe in the magnetite-maghemite-H_2O system ([Fe_3O_4] = 0.5 g L^{-1}, 10 nm particles, in 10 mM NaCl) accounting for the formation of a solid-solution (Fig. 3d). The predominance field of quasi-stoichiometric magnetite (R > 0.495) is rather narrow in the simulated conditions, restricted to circumneutral to alkaline pH (> 6-7 depending on the E_H).

3.4 Discussion

We discussed above how pH controls the redox reactivity of nanomagnetites in aqueous suspension. However, we suspect that interpretations made in a large number of publications have been biased by the side reaction of magnetite with H^+, or inappropriate handling of magnetite suspensions at too low pH values. Indeed, the H^+-promoted dissolution of magnetite nanoparticles is a relatively fast process, as the stoichiometry of nanomagnetites is significantly altered after 24h, although a small magnetite core can persist over a few years surrounded by a maghemite shell. The related Fe^{2+} release should have strong consequences on magnetite surface reactivity. For instance:

(i) The pH of zero-point charge (pH_{zpc}) or the isoelectric point (IEP) of stoichiometric nanomagnetite, key parameters for the prediction of nanoparticle colloidal properties (e.g., aggregation or dispersion), potential coatings or contaminant removal capabilities, are often reported at pH ≈ 6 (e.g. (Sun et al., 1998; Jolsterå et al., 2012)); a pH value that might be hard to investigate experimentally with stoichiometric magnetite.

(ii) Adsorption studies of chemicals onto magnetite nanoparticles at pH < 7 (e.g. (Liu et al., 2015; Schwaminger et al., 2015)) may in fact refer to (quasi-)maghemite surface.

(iii) Investigations of the reduction or Fenton-like (or "peroxidase-like") reactions at pH < 7 do not involve magnetite (Gao et al., 2007; Gumpelmayer et al., 2018) but take advantages of the catalytic activity of maghemite surface, which can be supplied by dissolved Fe^{2+}(Marsac et al., 2017).

(iv) Ligands often used for magnetite surface coatings might also enhance Fe dissolution via the formation of aqueous complexes and, depending on the ligand relative affinity for Fe(II) and Fe(III), affect R_{eff}.

In general, appropriate manipulation of magnetite (e.g. in applied research fields) or prediction of magnetite behavior (e.g. in natural environments, bio/physiological fluids, etc…) must consider various chemical equilibria occurring in aqueous solution because several physico-chemical factors might affect magnetite stoichiometry (E_H, pH, [ligand], etc.).

3.5 Conclusion

"Is it really magnetite?" The systematic and long-term investigations of the effect of pH and oxidation on magnetite stoichiometry in this study clearly show that this is a highly relevant question when interested in magnetite nanoparticles suspended in water: our results show that stoichiometric nanomagnetites are not stable at pH < 7. Because Fe^{2+} content largely controls the physical and chemical properties of magnetite, nanotechnological applications or environmental investigation of magnetite behavior should consider the impact of combined physico-chemical conditions (e.g. pH and E_H, as discussed here) on magnetite stoichiometry. For this purpose, an equilibrium model is proposed to predict these effects. The benefit of such modeling development is beyond the prediction of magnetite stoichiometry in complex aqueous systems because it could also be used to predict physico-chemical properties of magnetite nanoparticles.

Appendix

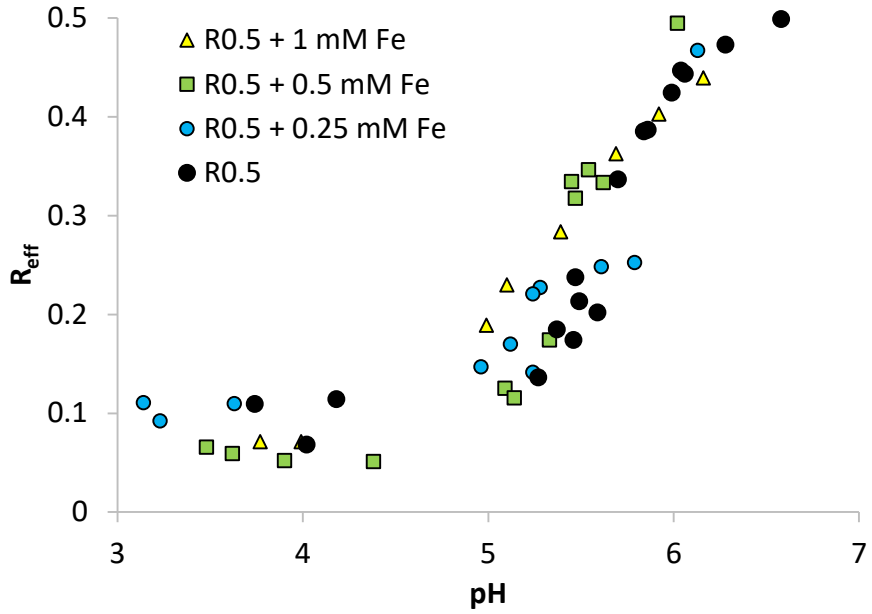

Figure S1. Effect of pH (3-6.5) and addition of dissolved Fe(II) excess (0.25 to 1 mM) on magnetite effective stoichiometry (for R_{ini} = 0.5).

Chapter 4 Influence of organic ligands on the effective stoichiometry of magnetite nanoparticles

Abstract. Magnetite, a ubiquitous mineral in soil and groundwater systems, is of high interest for a variety of applications including environmental remediation, medicine, and catalysis. Its unique properties are mainly due to the presence of Fe^{2+} in its structure. If the transformation of magnetite to maghemite through the oxidation of Fe^{2+} has been well documented, mechanisms involving dissolution processes of Fe^{2+} in aqueous solutions have been overlooked. In the present study, the effects of dissolved organic ligands (EDTA, acetic, lactic and citric acids) on Fe^{2+} solubility and on the stoichiometry (Fe(II)/Fe(III)) of magnetite-maghemite nanoparticles (~10 nm) was investigated. These ligands were chosen for their environmental relevance and because they are widely used as coating agents for nanotechnology applications. Results show insignificant effect of 2 organic ligands (acetate and lactate) on the dissolution of Fe. By contrast, citrate and EDTA enhanced Fe solubility because of the formation of dissolved Fe(II)- and Fe(III)-ligand complexes. Both ligands selectively bound Fe(II) over Fe(III), but EDTA was shown much more selective than citrate. This had drastic impact on magnetite stoichiometry, which dropped from 0.5 to 0.3 in neutral to alkaline pH conditions. The combined effects of oxidation, H^+- and ligand-promoted dissolution of Fe from magnetite could be predicted by using a previously developed magnetite/maghemite solid solution model and by accounting for the formation of dissolved Fe(II)- and Fe(III)-ligand complexes. Therefore, these results show that citrate and EDTA can (i) enhance Fe solubility in presence of magnetite nanoparticles and (ii) modify magnetite stoichiometry, which should drastically effect its properties and might be detrimental for nanotechnology applications.

Résumé. La magnétite, un minéral omniprésent dans les sols et les eaux souterraines, présente un grand intérêt pour une variété d'applications, notamment la remédiation environnementale, la médecine et la catalyse. Ses propriétés uniques sont principalement dues à la présence de Fe^{2+} dans sa structure. Si la transformation de la magnétite en maghémite par oxydation de Fe^{2+} a été bien documentée, les mécanismes impliquant des processus de dissolution de Fe^{2+} dans des solutions aqueuses ont été négligés. Dans cette étude, les effets des ligands organiques dissous (EDTA, acides acétique, lactique et citrique) sur la solubilité du Fe^{2+} et sur la stœchiométrie (Fe(II)/Fe(III)) des nanoparticules de magnétite-maghémite (~10 nm) ont été étudiés. Ces ligands ont été choisis pour leur abondance dans l'environnement et parce qu'ils sont largement utilisés pour l'enrobage de nanoparticules pour des applications en nanotechnologie. Les résultats montrent un effet négligeable de 2 ligands organiques (acétate et lactate) sur la dissolution de Fe. En revanche, le citrate et l'EDTA augmentent la solubilité du Fe en raison de la formation de complexes dissous Fe(II)-ligand et Fe(III)-ligand. Les deux ligands complexent sélectivement le Fe(II) par rapport au Fe(III), mais l'EDTA s'avère beaucoup plus sélectif que le citrate. Cela a un impact drastique sur la stœchiométrie de la magnétite, qui chute de 0,5 à 0,3 dans des conditions de pH neutre à basiques. Les effets combinés de l'oxydation, des H^+ et de la dissolution de Fe induite par les ligand peuvent être prédits en utilisant le modèle de la solution-solide magnétite/maghémite développé précédemment, en tenant compte de la formation de complexes dissous entre le ligands, le Fe(II) et le Fe(III). Par conséquent, ces résultats montrent que le citrate et l'EDTA peuvent (i) améliorer la solubilité du Fe en présence de nanoparticules de magnétite et (ii) modifier la stœchiométrie de la magnétite, ce qui devrait affecter considérablement ses propriétés et pourrait être préjudiciable aux applications nanotechnologiques.

4.1 Introduction

Magnetite nanoparticles have been studied extensively for various scopes (medicine, high-technology, environmental treatment, catalysis, etc.) owing to intrinsic magnetite properties (magnetic, semi-conductor, redox, etc.) (Sherman, 1987; Goss, 1988; Walz, 2002; Usman et al., 2018) and their small size leading to a large reactive surface area. Indeed, magnetite nanoparticles are potentially important roles in various environmental remediations such as degradation or sorption of organic and inorganic contaminants (Klausen et al., 1995; Huber, 2005; Gorski and Scherer, 2009; Singer et al., 2012).

The environmental conditions, such as pH and redox potential (E_h) can lead to magnetite (Fe_3O_4) transformation to maghemite (Fe_2O_3) according to equations 1 and 2, respectively:

$$Fe_3O_4 + 2H^+ \rightleftharpoons Fe_2O_3 + H_2O + Fe^{2+} \quad (1)$$

$$2\ Fe_3O_4 + ½\ O_2 \rightleftharpoons 3\ Fe_2O_3 \quad (2)$$

In fact, magnetite-maghemite solid-solutions can form, so called non-stoichiometric magnetites. The Fe(II) to Fe(III) concentration ratio defines magnetite stoichiometry (R) and varies between 0 (maghemite) to 0.5 (magnetite).

$$R = Fe(II)/Fe(III) \quad (3)$$

Magnetite stoichiometry largely controls the physico-chemical properties of the nanoparticles. The Fe(II)/Fe(III) ratio affects, for example, (i) reduction kinetics (Gorski and Scherer, 2010) and (ii) adsorption capacity of organic contaminants (Tombácz et al., 2013; Cheng et al., 2018), heavy metals (Catalette et al., 1998; Giraldo et al., 2013).

When the nanoparticles are released into soil and groundwater, they might not only be sensitive to pH and E_h but also to the presence of organic acids occurring in the soil and groundwater. In the rhizosphere, Low-Molecular-Weight Organic Acids (LMWOAs) play an important role in metal tolerance and plant-microbe interactions operating at root and soil interface (López-Bucio et al., 2000). Some of LMWOAs are microbial metabolites and crucial plant exudates. It is often considered that acetic and lactic acids are more emanating from rhizosphere bacteria (Jones, 1998). The LMWOAs are present in all natural soils but their concentrations may differ considerably. Furthermore, citric acid is efficiently used ligand to modify the surface of iron oxide nanoparticles in a variety of syntheses (Hui et al., 2008; Liu et al., 2009; Jensen et al., 2014) and applications (Laurent et al., 2008) including wastewater purification (Baseri and Tizro, 2017), NMR imaging (Fan et al., 2010; Mazarío et al., 2015; Lee et al., 2015), and biomolecule extraction (Nigam et al., 2011). Because it can make the complex water-soluble, stable, and dispersed for further applications. In addition to this, EDTA is one of the most chelating agents for environmental treatment (Keny et al., 2005; Xu et al., 2011; Wang et al., 2012) and medicine therapy (Yi et al., 2014; Daoush, 2017) and usually used to determine the bioavailability of elements for plant due to its chelating behavior analogous to (phyto-)siderophores.

The functional groups of organic molecules might affect and modify the reactivity of magnetite entirely or partially (Borghi et al., 1989; Xu et al., 2011; Magdalena et al., 2018). Indeed, the magnetite nanoparticles and their magnetic characteristics are significantly affected by carboxylates. LMWOAs and EDTA contain 1 or more carboxylic groups. For example, the citric acid molecule is used to functionalized magnetite surface by utilizing the coordination of carboxylate functionalities of the citrate depending on the steric necessity and curvature of the surface (Sahoo et al., 2005; Dheyab et al., 2020). Hence, the changes induced by citric acid

molecules adsorbed on the nanoparticle surface are considerable to understand its mechanism. The addition of EDTA to form EDTA-functionalized magnetite nanoparticles were also investigated to change the mechanism of nucleation and nanostructure growth (Magdalena et al., 2018).

Until now, very a little is known about the effects of biomolecules of plants or microbial origin on Fe release by magnetite and on the magnetite stoichiometry. In order to deeply understand the determinant factors for the magnetite solubility, the effect of each organic needs to be investigated individually. Moreover, no predictive model of the effect of the environmental factors with the presence of organic molecules has been developed yet with magnetite. The objective of this study was to determine the effect of organics on Fe solubility of stoichiometric magnetite and on magnetite nanoparticles with different stoichiometries and compare geochemical modeling under various environmental conditions in presence of 4 organic acids:acetate, citrate, lactate which are all naturally presented in soils (Feng et al., 2005), and EDTA, an organic molecule model for chelating agents like (phyto-)siderophores.

4.2 Materials and Methods

4.2.1 Chemical reagents and materials

All chemicals were of analytical grade or better. Iron(III) chloride hexahydrate ($FeCl_3 \cdot 6H_2O$) and Iron(II) chloride tetrahydrate ($FeCl_2 \cdot 4H_2O$) were purchased from AnalaR NORMAPUR. Hydrogen peroxide (H_2O_2), acetate, citrate, lactate, and EDTA were obtained from Sigma-Aldrich. The sample solutions were prepared with ultrapure "Milli-Q" water (specific resistivity which is 18.2 $M\Omega cm^{-1}$). All experiments were carried out in an anaerobic chamber (N_2-glovebox, JACOMEX, $O_{2(g)} < 1$ ppm), and all solutions were purged with $N_{2(g)}$ for at least 12 h inside the glovebox before use.

4.2.2 Synthesis and characterization of magnetites with various stoichiometries

A stoichiometric magnetite (R0.5) has been firstly synthesized in N_2-glove box following a well-known protocol, which produces ~10 nm particles (Demangeat et al., 2018; Jungcharoen et al., 2021). Stoichiometric magnetite (R0.5) was prepared by involving a room temperature aqueous precipitation method in an anaerobic chamber (JACOMEX). After the synthesis, washing was made at pH 8.5 (using NaOH) to avoid the release of Fe^{2+}, as observed in previous work (Marsac et al., 2017; Cheng et al., 2018), and thus, to guarantee the stoichiometry R0.5.

Specific stoichiometric amounts of H_2O_2 were added to R0.5 to produce two sets of partly oxidized non-stoichiometric magnetites (R0.1 and R0.3) (Gorski and Scherer, 2010; Cheng et al., 2018). The non-stoichiometric magnetites were washed with ultrapure water (at pH = 8.5) to remove residual H_2O_2. Effective Fe(II)/Fe(III) ratios (R_{eff}) were determined by acid digestion of magnetites in 0.6 M HCl during 3 days, followed by spectrophotometric determination of dissolved

[Fe(II)] and total [Fe] (= [Fe(III)] + [Fe(II)]) using the 1-10 phenanthroline colorimetric method (Fortune and Mellon, 1938). Repetition of acid digestion followed by spectrophotometry led to an error of ±0.01 on the determination of R_{eff}. Results were in excellent agreement with values expected from the amount of added H_2O_2, as in previous studies (Gorski and Scherer, 2010; Cheng et al., 2018; Jungcharoen et al., 2021).

4.2.3 Batch studies

Equilibrium studies were conducted for a total of 6.5 mM of Fe (~0.5 g/L of magnetite) and in 15mL tubes containing 10 mL of solution following the same procedure as our previous study (Jungcharoen et al., 2021). All magnetite suspensions (R0.1, R0.3 and R0.5) were prepared in 10 mM NaCl. Magnetite solubility was investigated in the presence of 1 mM organic ligand (acetic, lactic, citric acids, and EDTA). The Fe solubility was studied in different pH conditions (pH 5-11) by using HCl and NaOH for pH adjustment (no buffer was used). Results in the absence of dissolved ligands, denoted as "bare magnetite", were taken from our previous study (Jungcharoen et al., 2021). The samples of all studies were stirred during 20 days in order to confirm the equilibrium for pH above around 5 (Sun et al., 1998; Jungcharoen et al., 2021). In the absence of organic ligands (bare magnetite nanoparticles), an almost complete release of Fe(II) from the magnetite nanoparticles is expected at pH < 5. In addition, strong kinetic limitations make equilibrium study difficult to perform (Chapter 3). Consequently, the investigated ligands might hardly show an effect on Fe solubility at pH < 5 in the present study. For these reasons, experiments were limited to pH ≥ 5.

After 20 days, pH and ORP were measured using Pt electrod prior to the sampling of an aliquot for further analysis. ORP reading was converted to E_h by correcting for the electrode

potential of the reference Ag/AgCl electrode (E_{ref}). A commercial redox-buffer (220 mV, Hach) was used for calibration. An equilibrium time of 15 minutes was applied for all E_h measurements (Marsac et al., 2015). The suspension was stirred prior to the E_h measurements. The electrode surface was periodically cleaned by exposing it to 0.1 M HCl for 1 h (Teasdale et al., 1998). After recording pH end E_H, an aliquot was filtered using 0.2 µm cellulose acetate filters (Sartorius Minisart). The absence of magnetite nanoparticles in the filtrates were checked by dynamic light scattering (DLS; VASCO Flex) in order to confirm no interferences during the measurement of Fe by spectrophotometer. However, DLS analysis showed that citric acid increased the colloidal stability of Fe nanoparticles. Hence, ultrafiltration experiments at 5kDa (Vivaspin 15RH12, Sartorius) were additionally performed to eliminate Fe nanoparticles. After (ultra)filtration, [Fe(II)] and total [Fe] were measured by spectrophotometry using the 1-10 phenantroline colorimetric method. The error on [Fe] determination was assumed equal to 5 %. It was possible to calculate the effective Fe(II)/Fe(III) ratio (R_{eff}) knowing the total [Fe(II)] and [Fe(III)] in the suspension (i.e. solution) and dissolved $[Fe(II)]_{aq}$ and $[Fe(III)]_{aq}$ after filtration, according to the following Equation 4.

$$R_{eff} = ([Fe(II)]_{Total} - [Fe(II)]_{aq}) / ([Fe(III)]_{Total} - [Fe(III)]_{aq}) \quad (4)$$

Concentration of organic ligands were determined by dissolved organic carbon analysis (Schimadzu TOC-L) after (ultra)filtration in order to quantify ligands adsorption to magnetite.

4.2.4 XMCD characterization

X-ray absorption spectra (XAS) and X-ray magnetic circular dichroism (XMCD) provide key insights into magnetite stoichiometry (R=Fe(II)/Fe(III)) (Pellegrin et al., 1999; Carvallo et al., 2008; Coker et al., 2008; Jiménez-Villacorta et al., 2011; Peng et al., 2018). The XAS and XMCD

signals were recorded at the Fe $L_{2,3}$ edges (700 – 730 eV) on the DEIMOS beamline at the synchrotron light source SOLEIL. The measurement protocol was detailed in our previous studies (Sartori et al., 2019; Jungcharoen et al., 2021).

4.2.5 Geochemical modeling

Calculations were made using the geochemical speciation code PHREEQC (version 2) (Parkhurst and Appelo, 1999) and the database "Minteq.v4.dat". According to a previous study, the magnetite oxidation reaction can be formulated as:

$$[Fe_3^{2+}\ Fe_3^{3+}]_{Oh}\ Fe_{3\,Td}^{3+}O_{12}^{2-} + 2\ H^+ \rightleftharpoons\ [Fe_5^{3+}\ \square\ ]_{Oh}Fe_{3\,Td}^{3+}O_{12}^{2-} + Fe^{2+} + H_2 \qquad (5)$$

The Gibbs free energies of formation of the solid-solution ($\Delta G_{ss,nano}$) of magnetite (mt)-maghemite (mm) nanoparticles is expressed by:

$$\Delta G_{ss,nano} = X\Delta G_{mt,nano} + (1\text{-}X)\Delta G_{mm,nano} + \Delta G_{mix} \qquad (6)$$

Where X, with $0 \leq X \leq 1$, defines the fraction of magnetite in the mixture. The excess free energy of mixing (ΔG_{mix}) can be expressed according to Guggenheim's expansion series (Guggenheim, 1937; Glynn, 2000) :

$$\Delta G_{mix} = a_0\, X(1\text{-}X)RT \qquad (7)$$

Where a_0 is the specific Guggenheim's parameter for the magnetite-maghemite solid-solution system. The Gibbs free energies of formation of the magnetite and maghemite nanoparticles was calculated from the corresponding values of the bulk iron oxides ($\Delta G_{mm,bulk}$ and $\Delta G_{mt,bulk}$), surface free energies (referring to hydrated surfaces, γ_{mm} and γ_{mt} in J m^{-2}) and assuming that surface area was assumed constant (100 $m^2\ g^{-1}$) (Marsac et al., 2017; Demangeat et al., 2018).

Fe(II) and Fe(II) complexation reactions and constants with all ligands are included in the database "Minteq.v4.dat". However, preliminary test with available citrate reactions gave unsatisfactory results. Therefore, reactions and constants with citrate were taken from a more recent study (Table S1) (Vukosav et al., 2012).

4.3 Results and discussion

4.3.1 Effect of organics on the dissolution of stoichiometric magnetite

The solubility of iron strongly depends on pH both in the absence and the presence of organic ligands (Borghi et al., 1989; Keny et al., 2005; Yi et al., 2014; Jungcharoen et al., 2021). Figure 1a compares total dissolved Fe concentration ($[Fe]_{tot} = [Fe(II)]_{aq} + [Fe(III)]_{aq}$) versus pH measured in solution in presence of stoichiometric magnetite (R0.5) and each of the 4 organic ligands. In the absence of organic ligands (bare magnetite nanoparticles), $[Fe]_{tot}$ increases with decreasing pH due to the proton-promoted Fe(II) release. The presence of acetic or lactic acid did not increse $[Fe]_{tot}$ at any pH value (Figure 1a). This is due to the weak binding of Fe to these ligands (Gotić and Musić, 2008; Zhao et al., 2009). By contrast, $[Fe]_{tot}$ increased in the presence of citric acid at circum-neutral pH (6-8), and in the presence of EDTA, at any pH investigated (5-11). For instance, at pH ≈ 7, $[Fe]_{tot}$ is below detection limit for magnetite in the absence of organic ligand or in presence of acetic acid and lactic acid, but it is equal to ca. 200 μM for citric acid and 900 μM for EDTA. Fe release was larger with EDTA than with citrate because the former is a stronger Fe chelating agent (Alderman et al., 2009; Mies et al., 2006;Holmén & Casey, 1996; Kalinowski et al., 2000). This can be related to the number of binding groups in the molecule: EDTA may form hexadentate complexes with metal ions as it contains four carboxylic groups and two amines (Blesa et al., 1984; Shailaja and Narasimhan, 1991; Yi et al., 2014), while citrate

includes three carboxylic groups and one OH group that might also be involved in the complex formation (Hamm et al., 1954; Răcuciu et al., 2006; Vukosav et al., 2012).

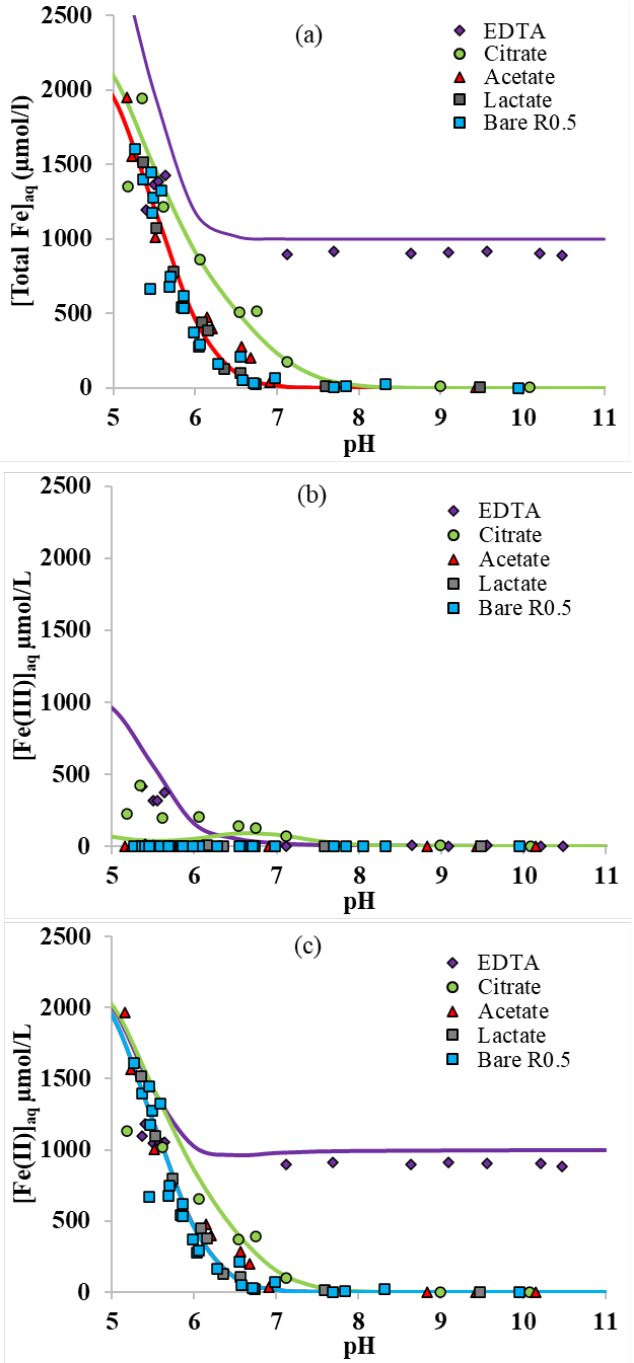

Figure 1. (a) Total dissolved [Fe], (b) dissolved [Fe(III)] and (c) dissolved [Fe(II)], as a function of pH for R0.5 in presence of 1 mM of each ligand in 10 mM NaCl. Lines correspond to magnetite-maghemite solid solution modelling results.

The adsorption of ligands on nanomagnetite was determined and plotted in Figure S1. No significant adsorption of acetate and lactate was determined, in line with their weak binding to iron oxides in general (see e.g. (Norén and Persson, 2007)) and the very large surface loadings investigated in the present work (i.e. 50 m^2 g^{-1} of reactive surface with 10^{-3} mol L^{-1} of ligand). EDTA adsorption was also negligible, although it is know to form strong complexes at mineral surfaces (Borghi et al., 1989; Keny et al., 2005; Yi et al., 2014), because of the large [EDTA] investigated and the formation of aqueous Fe-EDTA complexes that limit EDTA adsorption. Indeed, according to the sorption isotherm data of Blesa et al. (1984), we estimated that less than 5% adsorption can be expected in the presently investigated conditions. By contrast with other ligands, citrate adsorption was significant and equal to about 10% over the whole pH range investigated. This phenomenon must be taken into account because it is expected to affects Fe solubility in our study.

Thanks to spectrophotometric method, it is possible to differentiate dissolved Fe^{3+} and Fe^{2+}, and hence, to study their intrinsic solubility versus pH (Figures 1b,c). In the absence of ligand, $[Fe(III)]_{aq}$ is below the detection limit as shown in Figure 1b, that is, total Fe solubility is due to the preferential dissolution of Fe(II) over Fe(III) (Figure 1c) (Jolivet and Tronc, 1988; Sun et al., 1998) (Chapter 3). No significant effect of both acetic and lactic acids on dissolved Fe(II) and Fe(III) concentrations is observed (Figures 1b,c). By contrast, the solubility of both Fe(II) and Fe(III) was enhanced by their complexation to citrate and EDTA. While [Fe(III)] was comparable in the presence of both ligands (Figures 1b), Fe(II) binding to EDTA was much stronger than to

citrate (Figures 1c). Because Fe(II) solubility is large at pH < 7 in the absence of ligand (Chapter 3), Fe(II)-ligand complexation was plotted by subtracting [Fe(II)] released from the bare magnetite modality. The concentration of Fe(II) bound to EDTA ([Fe(II)-EDTA]) is compared to [Fe(III)-EDTA] in Figure 2a. Large values of [Fe(III)-EDTA] are measured at pH~5.5, by constrast with [Fe(II)-EDTA] values that are close to 0. When pH increase, [Fe(III)-EDTA] it drops to 0 for pH values above 7 wherease [Fe(II)-EDTA] increases up to ~900 µM and remains nealy constant up to pH = 11. Hence, EDTA more selectively binds (i) Fe(III) than Fe(II) at pH~5.5 and (ii) Fe(II) than Fe(III) at pH>7. The concentration of Fe(II) bound to citrate ([Fe(II)-Citrate]) is compared to [Fe(III)-Citrate] in Figure 2b. Like EDTA, citrate more selectively binds Fe(III) than Fe(II) at pH values around 5.5 because [Fe(II)-Citrate] ≈ 0 while [Fe(III)-Citrate] value is maximal. [Fe(II)-Citrate] increases with pH and reaches a maximum at pH values between 6 and 7, and decreases above. At pH 6-7, citrate binds slightly more selectively Fe(II) than Fe(III) and become non-selective between pH 7 and 8.

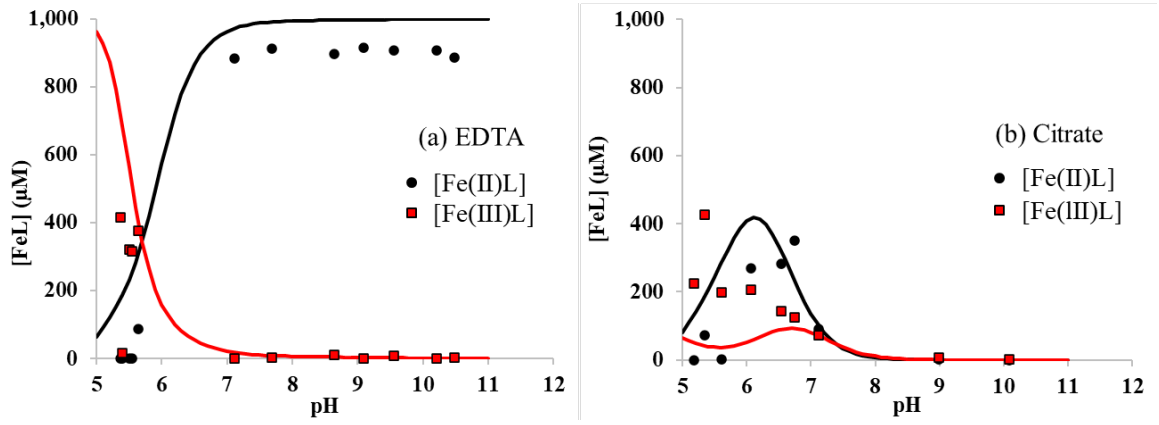

Figure 2. Concentrations of Fe(II) and Fe(III) complexed to (a) citrate and (b) EDTA as a function of pH for R0.5 in presence of 1 mM of each ligand in 10 mM NaCl. Lines correspond to magnetite-maghemite solid solution modelling results.

4.3.2 Solid phase analysis of stoichiometric magnetite

The selective binding of Fe(II) and Fe(III) may influence magnetite stoichiometry. The effective stoichiometry (R_{eff}, Equation 4) of R0.5 is shown on Figure 3a versus pH in the absence and presence of organic ligand. Equation 4 depends on the solubilization of Fe(II) and Fe(III), which may be ligand-induced and implicitly depend on pH and ligand concentration. For instance, values of R_{eff} of bare magnetite decrease with decreasing pH because of the solubilization of Fe(II) while that of Fe(III) is negligible (Figure 2a, Chapter 3). Acetic acid and lactic acid had little effect on the solubility of Fe and, hence, on R_{eff} in agreement with results shown in Figure 2a. For pH < 5.5, where selective binding of Fe(III) occurs, no clear impact of either EDTA or citrate on R_{eff} can be noticed because the very high $[Fe(II)]_{aq}$ found due to the H^+-promoted dissolution process. For $5.5 \leq pH \leq 7$, citrate only slightly affects R_{eff} due to selective binding Fe(II) over Fe(III) as discussed above. By contrast, the presence of EDTA dramatically decreases R_{eff} from 0.5 to 0.3 which remains then stable at this value at pH above 5.5.

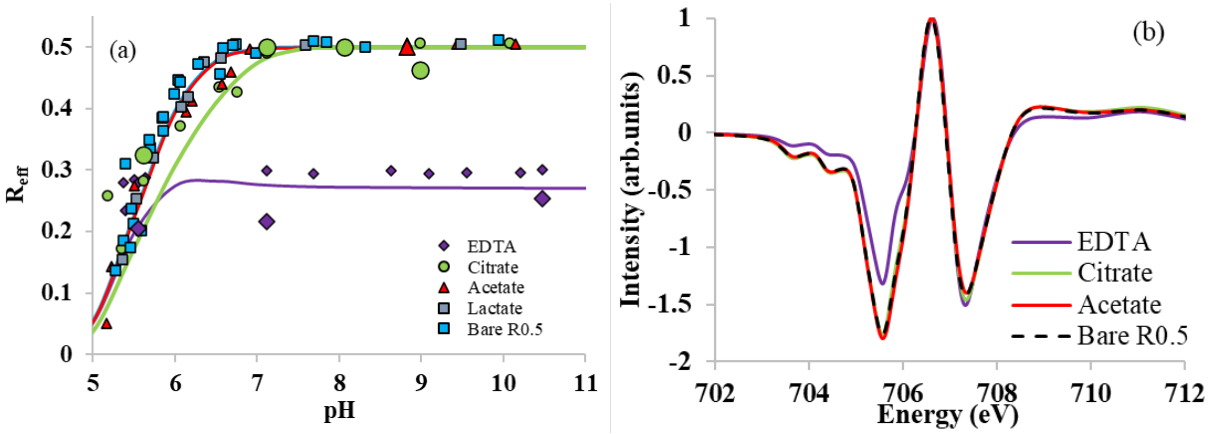

Figure 3. (a) R_{eff} as a function of pH for R0.5 in presence of 1 mM of each ligand in 10 mM NaCl. Lines correspond to magnetite- maghemite solid solution modelling results. Large symbols correspond to R_{eff} determined by X-ray magnetism circular dichroism (XMCD). (b) normalized

XMCD spectra at the Fe L_3-edge of R0.5 in absence (pH 7) and presence of ligands (citrate and EDTA at pH 7; acetate at pH = 9).

To confirm these observations, solid phases of some samples were analyzed by XMCD at the Fe L_3-edge. XMCD spectra (Figure 3b) exhibit three main peaks at the L_3-edge. The peak S_1 (at 705.5 eV) corresponds to both Fe(II) and Fe(III) on O_h sites, but is dominated by Fe(II). The peak S_2 (at 706.6 eV) corresponds to the contribution of Fe(III) in T_d sites while the peak S_3 (at 707.3 eV) is attributed to Fe(III) in O_h sites. S_1 and S_3 are coupled antiparallel to S_2 due to the ferromagnetic behavior of the inverse spinel structure of $Fe_{3-\delta}O_4$ nanoparticles. Because XMCD spectrum of stoichiometric magnetite with acetate (pH 9) and citrate (ca. pH 7) are similar to the bare one at pH = 7, acetate and citrate do not significantly affect magnetite stoichiometry, in agreement with wet chemistry results (Figure 3a). By contrast, the presence of EDTA and magnetite nanoparticles (pH 7) strongly decreased S_1 intenstity because of the large binding of Fe(II) in solution. XMCD spectra were recorded at different pH values for citrate (5.5, 7, 8 and 9) and EDTA (5.5, 7 and 10.5). By using a linear combination fit (LCF) procedure, R_{eff} could be determined and plotted in Figure 3a (Jungcharoen et al., 2021). LCF results are in relatively good agreement with wet chemistry data, although slightly smaller for EDTA. The discrepancy between spectrophotometric determination of dissolved Fe(II) and XMCD might suggest the presence of a small amount of adsorbed Fe(II) ions that are not detected by XMCD because magnetically silent. This might be due to the presence of ternary magnetite-Fe(II)-EDTA (or magnetite-EDTA-Fe(II)) complexes (Blesa et al., 1984).

4.3.3 Effect of organics on magnetite with different stoichiometries

Magnetites with different initial stoichiometries (R0.1 and R0.3) were synthesized by oxidizing R0.5 with H_2O_2. Then, the impact of initial stochiometry on the dissolved [Fe(III)], dissolved [Fe(II)], and effective stoichiometry of magnetite in the presence of acetate, citrate and EDTA was studied. The adsorption of the ligands to the magnetite surface was also monitored but the results were found almost independent to the initial stoichiometry (Figure S1). Acetate had no significant impact of Fe solubility in any case in presence of R0.1 and R0.3, as previously observed for R0.5 (Figure S1). Figures 4a and 4b show respectively dissolved [Fe(III)] and [Fe(II)] in the presence of citrate. Both concentrations decrease with increasing pH for all stoichiometries. Interstingly, [Fe(III)] and [Fe(II)] are found weakly dependent to initial magnetite stoichiometry in presence of citrate, which affected R_{eff} values similarly to the experiments with R0.5 (Figure 4c). By contrast, in presence of EDTA, [Fe(III)] is found to increase when magnetite initial stoichiometry decreases (Figure 4d), while [Fe(II)] decreases (Figure 4e). This can be explained by the competitive effects between Fe(II) and Fe(III) for EDTA binding. Fe(II)-EDTA complexes are favored in presence of Fe(II)-rich nanoparticles (i.e. R0.5) whereas, in presence of a limited amount of Fe(II) (i.e. R0.1), Fe(III)-EDTA complexation becomes important. Because variations of both [Fe(III)] and [Fe(II)] with pH remain relatively small at pH > 6, corresponding R_{eff} values remain constant with pH for each magnetite (Figure 4f) according to Equation 4. Indeed, EDTA is a 1: 1 chelating molecule, involving the solubilization of 1 mM Fe per 1 mM EDTA. Thus, the amount of solubilized Fe^{2+} is stable as soon as all EDTA molecules are already under complexes

EDTA-Fe form. Therefore, R_{eff} values remain constant for R_{ini} = 0.5 and 0.3 at the pH upper to 7. Concerning R_{ini} 0.1, R_{eff} is also stable but at almost the same value that at the beginning of the experiment, due to the limited amount of Fe(II) leading to the formation of Fe(III)-EDTA complexes. Therefore, the presence of EDTA strongly decreases the effective stoichiometry of magnetites. This decrease is according to the amount of Fe(II) present within the magnetite.

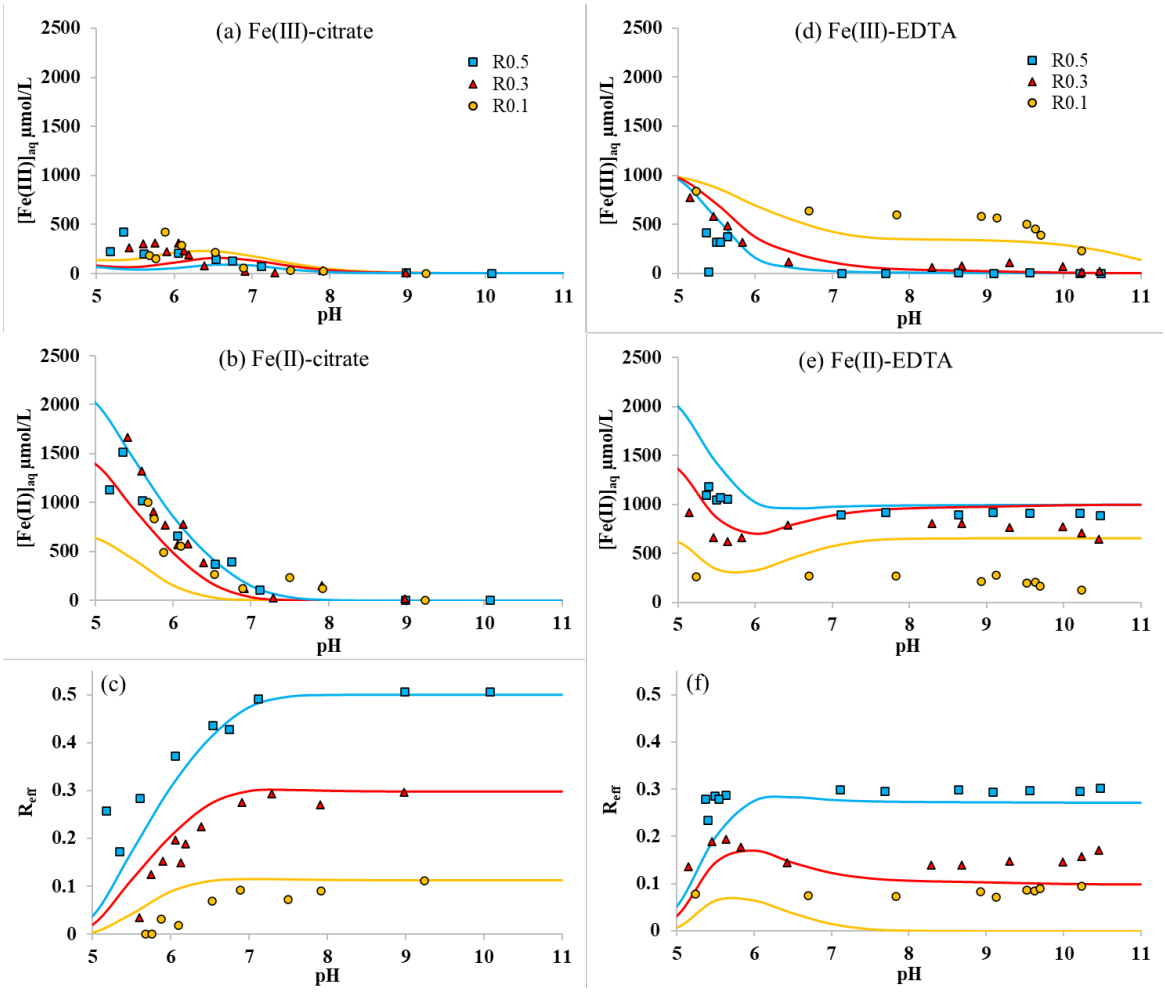

Figure 4. Fe(III) and Fe(II) solubility, and corresponding R_{eff} versus pH in the presence of 1mM citrate (a,b,c) or EDTA (d,e,f) and magnetites with different initial stoichiometries (R0.1, R0.3 and R0.5) in 10 mM NaCl. Lines correspond to magnetite-maghemite solid solution modelling results.

4.3.4 Modeling

As an attempt to account for citrate adsorption to magnetite, we used a surface complexation model, previously developed for the adsorption of another organic molecule (nalidixic acid, NA) (Cheng et al., 2018; Deng et al., 2020). We applied the same formalism and equations by assuming that citrate binds to two surface hydroxyl groups by involving two of its carboxylates, while the third carboxylic groups and the alcohol groups are, respectively, deprotonated and protonated:

$$2 \equiv FeOH + 2\ H^{+} + CitrateH^{3-} \rightleftharpoons (\equiv Fe)_2 CitrateH^{-} + 2\ H_2O \quad (8)$$

Because of the very high surface loading, the available site density was raised from 1.5 to 3 nm^{-2}, which might traduce the involvement of sites that are not necessary at lower loadings investigated for NA. The present work did not provide enough data to model an effect of magnetite stoichiometry on citrate adsorption (Figure S1b). Therefore, a single log K value for Equation 8 was used. The value (27.6) was similar to that of NA on stoichiometric magnetite (25.5).

Thanks to the chemical thermodynamic modeling of magnetite-maghemite at solid solution (Chapter 3), it was possible to predict the solubility of total Fe, dissolved [Fe(III)], [Fe(II)], and R_{eff} in the presence of the ligands. Modeling results are depicted in each figure of this manuscript, when relevant (Figures 1-4). As expected, the model predicts no significant effect of acetate and lactate on Fe behavior (Figures 1, 2a and S2). Although (i) $[Fe(III)]_{aq}$ is underestimated at pH < 6.5 for all R_{ini} (Figures 1b, 2b and 4a) and (ii) $[Fe(II)]_{aq}$ is underestimated for R_{ini} = 0.1 (Figure 4b), the effect of citrate on Fe(II/III) solubility and magnetite stoichiometry (Figures 3a and 4c) is relatively well captured. The effect of EDTA is also relatively well predicted. Fe(II)-EDTA complexation is slightly overestimated (Figures 1a, 1c, 2a, 4e). However, if the resulting R_{eff} is underestimated, the model falls between the wet chemistry and XMCD data (Figure 3a). The

largest discrepancies are observed for R_{ini} = 0.1, where the model predicts a complete release of Fe(II). This has two consequences: (i) Fe(II) competitive effect on Fe(III)-EDTA is too strong so Fe(III) solubility is underestimated and (ii) R_{eff} drops to 0 for pH > 7.5. As previously shown, (chapter 3) the complete release of Fe(II) might be kinetically limited and could take several years to reach a steady-state, especially for R_{eff} < 0.1, which would explain the discrepancies with the model.

Prediction of the redox potential of the magnetite suspensions were also made in the presence of ligands and compared to the measured data. As previously suggested for bare magnetite, (chapter 3) at pH < 7, experimental determination of the E_H values with a Pt electrode might be achieved thanks to the large amount of dissolved Fe^{2+} and the small size of the nanoparticles that could react with the electrode (Silvester et al., 2005). At pH > 7, Fe^{2+} is retained in the solid phase, making experimental E_H determination less reliable and a large scatter is observed (Fig. S3c) (Nordstrom and Campbell, 2014). Accordingly, in the presence of all ligands, experimental and model E_H values agree because magnetite stoichiometry and Fe(II) dissolution are primarily controlled by the pH. For pH > 7, experimental data for citrate and acetate might not be reliable. In these conditions, the model predicts not big difference between E_h values in the presence or absence of these ligands. By contrast, in the presence of EDTA, $[Fe(II)]_{aq}$ is large. Both experimental and calculated E_h values were found larger to the bare magnetite modality, because EDTA binding stabilizes Fe(II) over Fe(III) at pH 7 and make it a weaker reductant.

4.4 Environmental Implications

Nanomagnetite with different stoichiometries may be present in environmental systems and their compositions are dependent on pH and redox conditions, and the presence of organic ligands

in soils. This study investigated the effects of several small organic ligands, which can be found in soils and soil solutions such as acetate, lactate, citrate, and the effect of EDTA which can model natural chelating agent effects like (phyto-)siderophores. Results showed insignificant effect of 2 organics ligands (acetic and lactic acid) on the solubility of magnetite. By contrast, citrate and EDTA can modify significantly magnetite solubility, by comparison with experiments without organic molecules. Furthermore, citrate and EDTA were shown to also affect magnetite effective stoichiometry because of the stronger complexation with Fe(II) than FeIII) by citrate and EDTA in our experimental conditions. By accounting for the complexation of Fe(II) and Fe(III) by citric acid and EDTA, Fe solubility is relatively well predicted. The findings suggest that (i) the solubility of Fe is not only dependent on the pH conditions, (ii) ligand-controlled dissolution processes should be taken into account for the chemical stability of magnetite. The occurrence of these organic effects over a range of environmentally relevant conditions recommends that the ligand- controlled dissolution might be influential in the use of magnetite nanoparticles for biological Fe acquisition in agriculture, natural systems, and in redox transition zones. Finally, these results show that the use of organic ligand for some nanotechnological applications of magnetite (e.g. citrate in order to ameliorate the colloidal stability of stoichiometric magnetite) should be performed with attention because processes like Fe release could significantly modify initial surface properties expected.

Appendix

Table S1. Ferric and ferrous citrate species in aqueous solution by following (Silva et al., 2009) for the database in PHREEQC.

	log K
Fe(III)LH	25.69
$Fe(III)L_2^{5-}$	36.27
$Fe(III)HL_2^{4-}$	41.4
$Fe(III)H_2L_2^{3-}$	47.46
$Fe(II)LH^{-}$	19.43
$Fe(II)L_2^{6-}$	Not used

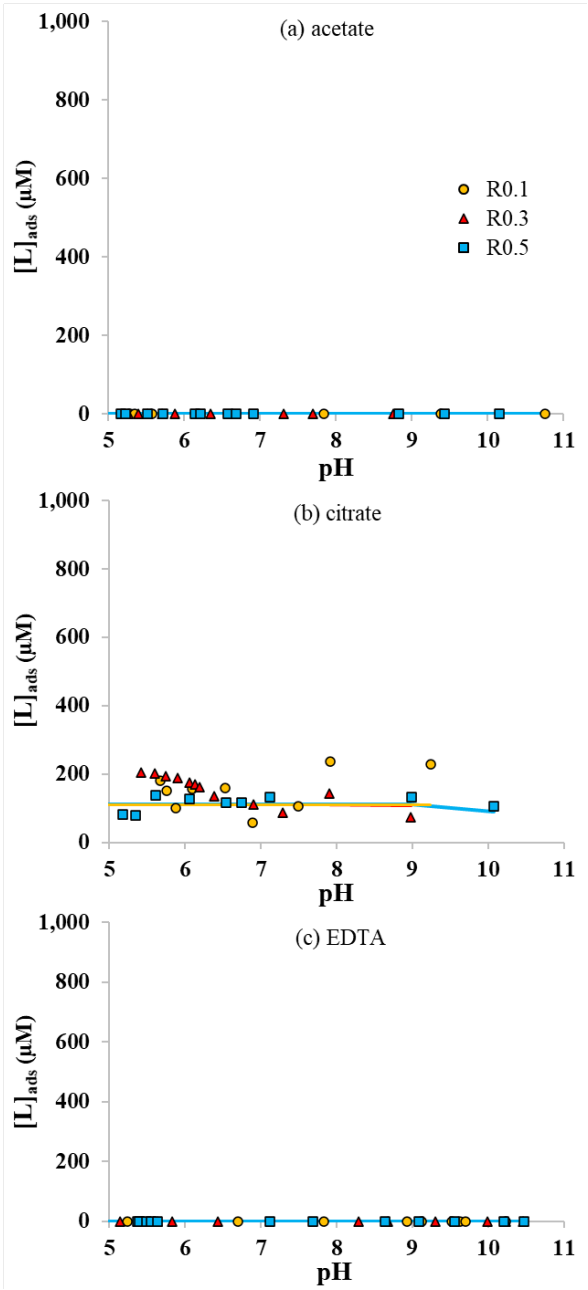

Figure S1. the ligands' adsorption ($[L]_{ads}$) on magnetite nanopartiocles as a function of pH for R0. 1, R0.3, and R0.5 in presence of 1 mM of (a) acetate, (b) citrate, and (c) EDTA in 10 mM NaCl. Lines correspond to magnetite-maghemite solid solution modelling results.

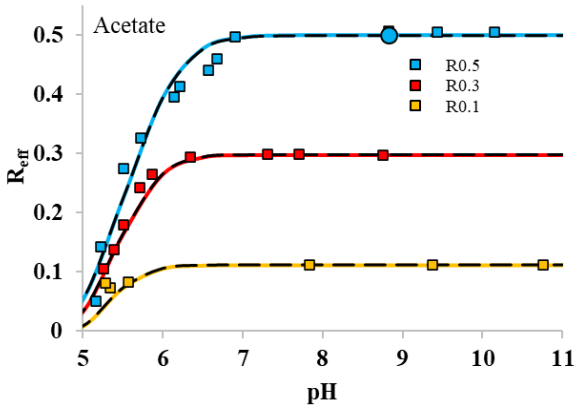

Figure S2. R_{eff} versus pH in the absence (black dashed line) and presence of acetate and magnetites with different initial stoichiometries (R0.1, R0.3 and R0.5) in 10 mM NaCl. A large cycle symbol was determined by XMCD. Colored lines correspond to magnetite- maghemite solid solution modelling results.

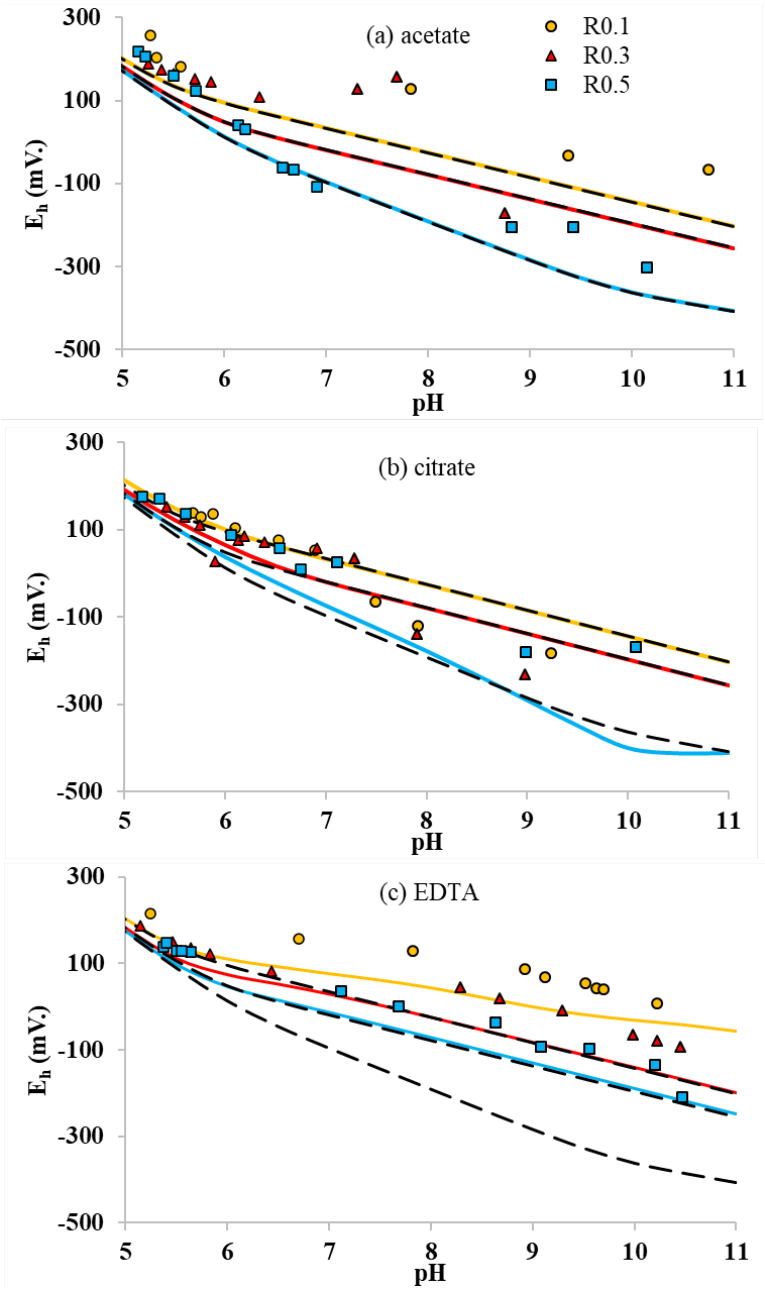

Figure S3. E_h as a function of pH for R0.1, R0.3, and R0.5 in absence (black dashed line) and presence of 1 mM of acetate, citrate, and EDTA in 10 mM NaCl. Coloured lines correspond to magnetite-maghemite solid solution modelling results.

Chapter 5 Conclusions and perspectives

Conclusions and perspectives

Magnetite stoichiometry (R = Fe(II)/Fe(III)) strongly controls its magnetic, catalytic, and redox properties (Usman et al., 2018). Determination of the factors and mechanisms responsible for its variation is highly relevant owing to its extensive applications in many fields (Wang et al., 2010; Zhu et al., 2011; Xu et al., 2012; Li, 2014; Nidheesh, 2015; Zanganeh et al., 2016) and the key role played by magnetite in many environmental systems (Byrne et al., 2015). However, beside the effect of oxidants (e.g. O_2 or H_2O_2) on the transformation of magnetite into maghemite, the effect of several other environmental factors has been overlooked (Gorski and Scherer, 2009; Gorski et al., 2010). Consequently, the thesis aims at developing a numerical model for the magnetite-maghemite solid solution capable of the prediction of the stability and redox reactivity of nanomagnetite in aqueous solution. To do so, the combined effects of oxidation, H^+- and ligand-promoted dissolution of Fe from magnetite were investigated and an accurate characterization of magnetite nanoparticles.

5.1 Conclusions

Chapter 2 examined the effect of redox conditions and dissolved Fe^{2+} on nanomagnetite stoichiometry by wet chemistry, XRD, XAS, and XMCD (Jungcharoen et al., 2021). In particular, XMCD signals have been used to further characterize the complex reactions involved in the magnetite/maghemite system upon oxidation and recharge processes (Pellegrin et al., 1999; Signorini et al., 2006; Carvallo et al., 2008; Coker et al., 2008; Jiménez-Villacorta et al., 2011; Kuzmin and Chaboy, 2014; Peng et al., 2018; Stoerzinger et al., 2019), *e.g.* decreasing R from 0.5 to 0.1 using H_2O_2 or increasing from 0.1 to 0.5 through dissolved Fe^{2+} amendment, or interaction

of stoichiometric magnetite (R0.5) with an excess of aqueous Fe^{2+}. The results show a significant increase in XMCD signals upon these three processes. This was attributed to surface recrystallization processes, induced by oxidation as well as Fe^{2+} diffusion into the solid phase and/or redistribution of electron equivalents between the aqueous solution and the magnetite bulk, leading to decreased spin canting effects that altered XMCD signals (Signorini et al., 2006; Graf et al., 2015). The major outcome of this chapter is that XMCD analysis cannot easily determine molar fraction of magnetite because it depends on both R and surface spin canting (Brice-Profeta et al., 2005; Signorini et al., 2006; Graf et al., 2015). A more accurate method for the determination of magnetite stoichiometry by XMCD is proposed for the presently investigated 10 nm magnetite (Jungcharoen et al., 2021).

Chapter 3 investigated the combined effects of oxidation and pH on the solubility of Fe from nanomagnetite (≈ 10nm) in aqueous suspensions. While Fe(III) was not significantly dissolved, aqueous Fe(II) concentration increased with decreasing pH and increasing initial stoichiometry (R_{ini}) of the magnetite (Gorski et al., 2012; Peng et al., 2018). It could be concluded that corresponding effective stoichiometry (R_{eff}) of magnetite could be effectively controlled by pH, redox condition, and recharge (Gorski and Scherer, 2009; Gorski et al., 2010; Cheng et al., 2018). In particular, results show that stoichiometric magnetite cannot actually exist at pH < 7 because of the incongruent dissolution on Fe(II) with respect to Fe(III) (Gao et al., 2007; Liu et al., 2015; Schwaminger et al., 2015; Gumpelmayer et al., 2018). The long-term (~1.5 year) kinetic results indicated two stages concerning Fe(II) release from magnetite. The H^+-promoted dissolution of Fe(II) is relatively fast (i.e. it proceeds within few days) until the maghemite shell at the nanoparticle surface becomes large enough, which occurs for $R_{eff} \approx 0.1$ (Jolivet and Tronc, 1988). The Fe(II) release process becomes much slower for $R_{eff} < 0.1$, and even slows down further

as the Fe(II)-depleted outer rim grows thicker while the core shrinks (Jolivet and Tronc, 1988; Sun et al., 1998). Nevertheless, because reaction products of magnetite with H^+, H_2O_2 or Fe^{2+} were similar, an equilibrium was assumed for all samples reaching $R_{eff} > 0.1$ after 20 days(Sun et al., 1998). Hence, a thermodynamic model for the magnetite-maghemite solid-solution was developed to predict the combined effects of oxidation and pH on magnetite stoichiometry.

Chapter 4 aimed to determine the effect of organic ligands (acetate, lactate, citrate and EDTA) on the stoichiometry of magnetite. These ligands were chosen because of their environmental relevance because (i) they can naturally be found in soils as common LMWOA (e.g. produced in the rhizosphere) (Jones, 1998), (ii) they can be used for environmental remediation (e.g. citrate, EDTA) and (iii) they are often used as coating agents to modify the surface properties of nanoparticles (Keny et al., 2005; Xu et al., 2011; Wang et al., 2012; Baseri and Tizro, 2017). Results showed insignificant effect of 2 organics ligands (acetic and lactic acid) on the solubility of magnetite (Gotić and Musić, 2008; Zhao et al., 2009). By contrast, citrate and EDTA can modify significantly magnetite solubility (Alderman et al., 2009; Mies et al., 2006;Holmén & Casey, 1996; Kalinowski et al., 2000), by comparison with experiments without organic molecules. Furthermore, citrate and EDTA were shown to also affect magnetite effective stoichiometry because of the stronger complexation with Fe(II) than Fe(III) in our experimental conditions. By accounting for the complexation of Fe(II) and Fe(III) by citric acid (Hamm et al., 1954; Răcuciu et al., 2006; Vukosav et al., 2012) and EDTA (Blesa et al., 1984; Shailaja and Narasimhan, 1991; Yi et al., 2014), Fe solubility is relatively well predicted using the magnetite-maghemite solid-solution model. The findings suggest that the solubility of Fe is not only dependent on the pH conditions, but ligand-controlled dissolution processes should be considered for the chemical stability of magnetite.

5.2 Implications

This fundamental research revealed the prediction of magnetite solubility and the stoichiometry of magnetite under a wide range of environmental conditions (the presence of oxygen, redox condition, Fe^{2+} ions content and the presence of some organic ligands). The findings from this thesis insight our understanding of the impact of the environmental conditions on the stoichiometry of magnetite nanoparticles, demonstrate that it is possible to tune the stoichiometry of magnetite by modifying pH, redox conditions and Fe(II) concentrations, and reveal that the stoichiometric nano-magnetite suspension is no more than a quasi-maghemite phase with dissolved [Fe(II)] at pH < 7. Hence, like the stoichiometry plays a key role on the physico-chemical properties of magnetite, nanotechnological applications (environmental remediation, drug delivery, and catalyst) or environmental investigations of magnetite behavior should consider the impact of combined physico-chemical conditions (e.g. pH and E_H, as discussed here) on magnetite stoichiometry. Moreover, the magnetite-maghemite solid solution model could be an essential tool for the use of organic ligand (e.g. citrate and EDTA) in order to ameliorate the colloidal stability of stoichiometric magnetite and for biological Fe acquisition in agriculture, natural systems, and in redox transition zones. Hence, these results call for the reconsideration of how to assess the properties of magnetite nanoparticles before nanotechnological applications in solution under the influence of a variety of conditions. In addition, the benefits of this thesis will help to enhance any decision support tools for environmental remediation in field scale, drug design, and other nanotechnology applications.

5.3 Perspectives

5.3.1 Perspective in the short term

Although the research scope of this thesis focused on the impacts of environmentally relevant conditions on the stoichiometry of magnetite nanoparticles in aqueous solution (batch scale), it should be more studied with complex molecules. For example, refractory natural organic matters (NOMs) present in soils and natural systems like humic substances. Humic substances represent a pool of NOMs which is more complex and richer in acidic functional groups and certainly able to impact the solubility of magnetite as citric acid studied in this work. In addition, NOM can play a role of electron donor or acceptor depending on its oxidation state (Klüpfel et al., 2014). Therefore, magnetite in the presence of humic substances should be studied under various pH and Eh conditions. In particular, special attention of how NOM can affect magnetite stoichiometry should be taken.

In addition, the transport of nanomagnetite should be considered in order to determine its fate and that of associated elements when applied in soil remediation. The present work suggests that the effect of stoichiometry of magnetite nanoparticles on its transport in soils should be investigated. The transformation of magnetite nanoparticles may affect aggregation and dispersion processes during the transport due to the modification of its surface during the release of Fe(II) in soils. In addition, further characterization of nano-particles surface state and structure, especially the determination of their surface charge because it is one of the key parameters for the prediction of nanoparticle colloidal behavior, might be required to interpret the results and to develop reactive transport models. Investigations of the transport of magnetite in soils via column experiments

might be an interesting step before applying in the field scale, in order to develop upscaling approaches.

5.3.2 Perspective in the long term

Ideal laboratory conditions for various applications of magnetite nanoparticles have been investigated already. Although many fundamental aspects have to be discovered, as it is the case in this manuscript, investigations at the field scale are also required to solve any problems in the real world. For example, magnetite nanoparticle can be injected by geoprobe (Zhang et al., 2019) in order to treat groundwater contaminations. The most significant factors of groundwater properties are pH, organic ligands, carbon content, Eh and microbes which might affect the transformation of contaminants. However, if many studies showed that magnetite if a powerful nanotechnological tool in environmental remediation strategies, the present work showed that much caution should be taken when handling it because it might rapidly be transformed to maghemite, even in reducing conditions, if pH is too low or organic ligand concentration is too high. The findings of the present work might be used to optimize the used of magnetite nanoparticles. For instance, the removal efficiency of magnetite nanoparticles and nano zero valent iron on heavy metals and chlorinated compounds could be compared.

In another context, the interesting applications of magnetite nanoparticles are drug design for cancer therapy (Liu et al., 2013; Bauer et al., 2016) and magnetic resonance imaging (Wei et al., 2017). Due to magnetite modification by various complex organic ligands and/ or polymers, it might reduce or increase the stoichiometry of magnetite and its properties. Therefore, the efficient way is to predict the optimal parameters (concentration of ligands, magnetite suspension, and pH

condition, etc.) from the solid solution model in order to save time, reduce the cost of chemicals and materials, eliminate the contaminants (zero waste as we can), allowing a good medical design.

References

Abushrida A., Elhuni I., Taresco V., Marciani L., Stolnik S. and Garnett M. C. (2020) A simple and efficient method for polymer coating of iron oxide nanoparticles. *Journal of Drug Delivery Science and Technology* **55**, 101460.

Ahmed I. A. M. and Maher B. A. (2018) Identification and paleoclimatic significance of magnetite nanoparticles in soils. *Proc Natl Acad Sci USA* **115**, 1736–1741.

Alderman B. W., Ratliff A. E. and Wirgau J. I. (2009) A mechanistic study of ferrioxamine B reduction by the biological reducing agent ascorbate in the presence of an iron(II) chelator. *Inorganica Chimica Acta* **362**, 1787–1792.

Auffan M., Rose J., Bottero J.-Y., Lowry G. V., Jolivet J.-P. and Wiesner M. R. (2009) Towards a definition of inorganic nanoparticles from an environmental, health and safety perspective. *Nature Nanotech* **4**, 634–641.

Balzar D., Audebrand N., Daymond M. R., Fitch A., Hewat A., Langford J. I., Le Bail A., Louër D., Masson O., McCowan C. N., Popa N. C., Stephens P. W. and Toby B. H. (2004) Size–strain line-broadening analysis of the ceria round-robin sample. *J Appl Cryst* **37**, 911–924.

Baseri H. and Tizro S. (2017) Treatment of nickel ions from contaminated water by magnetite based nanocomposite adsorbents: Effects of thermodynamic and kinetic parameters and modeling with Langmuir and Freundlich isotherms. *Process Safety and Environmental Protection* **109**, 465–477.

Bauer L. M., Situ S. F., Griswold M. A. and Samia A. C. S. (2016) High-performance iron oxide nanoparticles for magnetic particle imaging – guided hyperthermia (hMPI). *Nanoscale* **8**, 12162–12169.

Blesa M. A., Borghi E. B., Maroto A. J. G. and Regazzoni A. E. (1984) Adsorption of EDTA and Iron-EDTA Complexes on Magnetite and the Mechanism of Dissolution of Magnetite by EDTA. *Journal of Colloid and Interface Science* **98**, 11.

Bliem R., McDermott E., Ferstl P., Setvin M., Gamba O., Pavelec J., Schneider M. A., Schmid M., Diebold U., Blaha P., Hammer L. and Parkinson G. S. (2014) Subsurface cation vacancy stabilization of the magnetite (001) surface. *Science* **346**, 1215–1218.

Boily J.-F. and Kozin P. A. (2014) Particle morphological and roughness controls on mineral surface charge development. *Geochimica et Cosmochimica Acta* **141**, 567–578.

Borghi E. B., Regazzoni A. E., Maroto A. J. G. and Blesa M. A. (1989) Reductive dissolution of magnetite by solutions containing EDTA and FeII. *Journal of Colloid and Interface Science* **130**, 299–310.

Bourgeois F., Gergaud P., Renevier H., Leclere C. and Feuillet G. (2013) Low temperature oxidation mechanisms of nanocrystalline magnetite thin film. *Journal of Applied Physics* **113**, 013510.

Brice-Profeta S., Arrio M.-A., Tronc E., Menguy N., Letard I., Cartier dit Moulin C., Noguès M., Chanéac C., Jolivet J.-P. and Sainctavit Ph. (2005) Magnetic order in - nanoparticles: a XMCD study. *Journal of Magnetism and Magnetic Materials* **288**, 354–365.

Brown D. A., Sherriff B. L. and Sawicki J. A. (1997) Microbial transformation of magnetite to hematite. *Geochimica et Cosmochimica Acta* **61**, 3341–3348.

Byrne J. M., Klueglein N., Pearce C., Rosso K. M., Appel E. and Kappler A. (2015) Redox cycling of Fe(II) and Fe(III) in magnetite by Fe-metabolizing bacteria. *Science* **347**, 1473–1476.

Carvallo C., Sainctavit P., Arrio M.-A., Menguy N., Wang Y., Ona-Nguema G. and Brice-Profeta S. (2008) Biogenic vs. abiogenic magnetite nanoparticles: A XMCD study. *American Mineralogist* **93**, 880–885.

Catalette H., Dumonceau J. and Ollar P. (1998) Sorption of cesium, barium and europium on magnetite. *Journal of Contaminant Hydrology* **35**, 151–159.

Cheng W., Marsac R. and Hanna K. (2018) Influence of Magnetite Stoichiometry on the Binding of Emerging Organic Contaminants. *Environ. Sci. Technol.* **52**, 467–473.

Coker V. S., Pearce C. I., Pattrick R. A. D., van der Laan G., Telling N. D., Charnock J. M., Arenholz E. and Lloyd J. R. (2008) Probing the site occupancies of Co-, Ni-, and Mn-substituted biogenic magnetite using XAS and XMCD. *American Mineralogist* **93**, 1119–1132.

Cornell R. M. and Schwertmann U. (2003) *The Iron Oxides: Structure, Properties, Reactions, Occurences and Uses, Second Edition*., Wiley-VCH: Weinheim.

Dadashi S., Poursalehi R. and Delavari H. (2015) Structural and Optical Properties of Pure Iron and Iron Oxide Nanoparticles Prepared via Pulsed Nd:YAG Laser Ablation in Liquid. *Procedia Materials Science* **11**, 722–726.

Daffé N., Choueikani F., Neveu S., Arrio M.-A., Juhin A., Ohresser P., Dupuis V. and Sainctavit P. (2018) Magnetic anisotropies and cationic distribution in CoFe2O4 nanoparticles prepared by co-precipitation route: Influence of particle size and stoichiometry. *Journal of Magnetism and Magnetic Materials* **460**, 243–252.

Daoush W. M. (2017) Co-Precipitation and Magnetic Properties of Magnetite Nanoparticles for Potential Biomedical Applications. *JNMR*.

Darbandi M., Stromberg F., Landers J., Reckers N., Sanyal B., Keune W. and Wende H. (2012) Nanoscale size effect on surface spin canting in iron oxide nanoparticles synthesized by the microemulsion method. *J. Phys. D: Appl. Phys.* **45**, 195001.

Demangeat E., Pédrot M., Dia A., Bouhnik-le-Coz M., Grasset F., Hanna K., Kamagate M. and Cabello-Hurtado F. (2018) Colloidal and chemical stabilities of iron oxide nanoparticles in aqueous solutions: the interplay of structural, chemical and environmental drivers. *Environ. Sci.: Nano* **5**, 992–1001.

Deng J., Bae S., Yoon S., Pasturel M., Marsac R. and Hanna K. (2020) Adsorption capacity of the corrosion products of nanoscale zerovalent iron for emerging contaminants. *Environ. Sci.: Nano* **7**, 3773–3782.

Dheyab M. A., Aziz A. A., Jameel M. S., Noqta O. A., Khaniabadi P. M. and Mehrdel B. (2020) Simple rapid stabilization method through citric acid modification for magnetite nanoparticles. *Sci Rep* **10**, 10793.

F. Hasany S., Ahmed I., J R. and Rehman A. (2013) Systematic Review of the Preparation Techniques of Iron Oxide Magnetic Nanoparticles. *NN* **2**, 148–158.

Faivre D. and Godec T. U. (2015) From Bacteria to Mollusks: The Principles Underlying the Biomineralization of Iron Oxide Materials. *Angewandte Chemie International Edition* **54**, 4728–4747.

Faivre D., Menguy N., Guyot F., Lopez O. and Zuddas P. (2005) Morphology of nanomagnetite crystals: Implications for formation conditions. *American Mineralogist* **90**, 1793–1800.

Fan H.-M., Olivo M., Shuter B., Yi J.-B., Bhuvaneswari R., Tan H.-R., Xing G.-C., Ng C.-T., Liu L., Lucky S. S., Bay B.-H. and Ding J. (2010) Quantum Dot Capped Magnetite Nanorings as High Performance Nanoprobe for Multiphoton Fluorescence and Magnetic Resonance Imaging. *J. Am. Chem. Soc.* **132**, 14803–14811.

Fassbinder J. W., Stanjek H. and Vali H. (1990) Occurrence of magnetic bacteria in soil. *Nature* **343**, 161–163.

Feng M.-H., Shan X.-Q., Zhang S.-Z. and Wen B. (2005) Comparison of a rhizosphere-based method with other one-step extraction methods for assessing the bioavailability of soil metals to wheat. *Chemosphere* **59**, 939–949.

Fortin J.-P., Wilhelm C., Servais J., Ménager C., Bacri J.-C. and Gazeau F. (2007) Size-Sorted Anionic Iron Oxide Nanomagnets as Colloidal Mediators for Magnetic Hyperthermia. *J. Am. Chem. Soc.* **129**, 2628–2635.

Fortune W. B. and Mellon M. G. (1938) Determination of Iron with o-Phenanthroline: A Spectrophotometric Study. *Ind. Eng. Chem. Anal. Ed.* **10**, 60–64.

Gaboriaud F. and Ehrhardt J.-J. (2003) Effects of different crystal faces on the surface charge of colloidal goethite (α-FeOOH) particles: An experimental and modeling study. *Geochimica et Cosmochimica Acta* **67**, 967–983.

Gao L., Zhuang J., Nie L., Zhang J., Zhang Y., Gu N., Wang T., Feng J., Yang D., Perrett S. and Yan X. (2007) Intrinsic peroxidase-like activity of ferromagnetic nanoparticles. *Nature Nanotech* **2**, 577–583.

Giraldo L., Erto A. and Moreno-Piraján J. C. (2013) Magnetite nanoparticles for removal of heavy metals from aqueous solutions: synthesis and characterization. *Adsorption* **19**, 465–474.

Glynn P. (2000) Solid-Solution Solubilities and Thermodynamics: Sulfates, Carbonates and Halides. *Reviews in Mineralogy and Geochemistry* **40**, 481–511.

Glynn P. D. and Reardon E. J. (1990) Solid-solution aqueous-solution equilibria; thermodynamic theory and representation. *American Journal of Science* **290**, 164–201.

Gorski C. A., Handler R. M., Beard B. L., Pasakarnis T., Johnson C. M. and Scherer M. M. (2012) Fe Atom Exchange between Aqueous Fe $^{2+}$ and Magnetite. *Environ. Sci. Technol.* **46**, 12399–12407.

Gorski C. A., Nurmi J. T., Tratnyek P. G., Hofstetter T. B. and Scherer M. M. (2010) Redox Behavior of Magnetite: Implications for Contaminant Reduction. *Environ. Sci. Technol.* **44**, 55–60.

Gorski C. A. and Scherer M. M. (2010) Determination of nanoparticulate magnetite stoichiometry by Mossbauer spectroscopy, acidic dissolution, and powder X-ray diffraction: A critical review. *American Mineralogist* **95**, 1017–1026.

Gorski C. A. and Scherer M. M. (2009) Influence of Magnetite Stoichiometry on Fe ^{II} Uptake and Nitrobenzene Reduction. *Environ. Sci. Technol.* **43**, 3675–3680.

Goss C. J. (1988) Saturation magnetisation, coercivity and lattice parameter changes in the system Fe3O4-γFe2O3, and their relationship to structure. *Physics and Chemistry of Minerals* **16**, 164–171.

Gotić M., Koščec G. and Musić S. (2009) Study of the reduction and reoxidation of substoichiometric magnetite. *Journal of Molecular Structure* **924–926**, 347–354.

Gotić M. and Musić S. (2008) Synthesis of Nanocrystalline Iron Oxide Particles in the Iron(III) Acetate/Alcohol/Acetic Acid System. *Eur. J. Inorg. Chem.* **2008**, 966–973.

Graf C., Goroncy C., Stumpf P., Weschke E., Boeglin C., Ronneburg H. and Rühl E. (2015) Local Magnetic and Electronic Structure of the Surface Region of Postsynthesis Oxidized Iron Oxide Nanoparticles for Magnetic Resonance Imaging. *J. Phys. Chem. C* **119**, 19404–19414.

Guggenheim E. A. (1937) The theoretical basis of Raoult's law. *Trans. Faraday Soc.* **33**, 151.

Gumpelmayer M., Nguyen M., Molnár G., Bousseksou A., Meunier B. and Robert A. (2018) Magnetite Fe3O4 Has no Intrinsic Peroxidase Activity, and Is Probably not Involved in Alzheimer's Oxidative Stress. *Angewandte Chemie International Edition* **57**, 14758–14763.

Hamm R. E., Shull C. M. and Grant D. M. (1954) Citrate Complexes with Iron(II) and Iron(III) [1]. *J. Am. Chem. Soc.* **76**, 2111–2114.

Handler R. M., Beard B. L., Johnson C. M. and Scherer M. M. (2009) Atom Exchange between Aqueous Fe(II) and Goethite: An Fe Isotope Tracer Study. *Environ. Sci. Technol.* **43**, 1102–1107.

Hansel C. M., Benner S. G. and Fendorf S. (2005) Competing Fe(II)-Induced Mineralization Pathways of Ferrihydrite. *Environ. Sci. Technol.* **39**, 7147–7153.

He H., Zhong Y., Liang X., Tan W., Zhu J. and Yan WANG C. (2015) Natural Magnetite: an efficient catalyst for the degradation of organic contaminant. *Sci Rep* **5**, 10139.

Hiemstra T. (2015) Formation, stability, and solubility of metal oxide nanoparticles: Surface entropy, enthalpy, and free energy of ferrihydrite. *Geochimica et Cosmochimica Acta* **158**, 179–198.

Hiemstra T. and van Riemsdijk W. H. (2007) Adsorption and surface oxidation of Fe(II) on metal (hydr)oxides. *Geochimica et Cosmochimica Acta* **71**, 5913–5933.

Holmén B. A. and Casey W. H. (1996) Hydroxamate ligands, surface chemistry, and the mechanism of ligand-promoted dissolution of goethite [alpha -FeOOH(s)]. *Geochimica et Cosmochimica Acta* **60**, 4403–4416.

Huber D. L. (2005) Synthesis, Properties, and Applications of Iron Nanoparticles. *Small* **1**, 482–501.

Hui C., Shen C., Yang T., Bao L., Tian J., Ding H., Li C. and Gao H.-J. (2008) Large-Scale Fe_3O_4 Nanoparticles Soluble in Water Synthesized by a Facile Method. *J. Phys. Chem. C* **112**, 11336–11339.

Ikoba U., Peng H., Li H., Miller C., Yu C. and Wang Q. (2015) Nanocarriers in therapy of infectious and inflammatory diseases. *Nanoscale* **7**, 4291–4305.

Ito A., Shinkai M., Honda H. and Kobayashi T. (2005) Medical application of functionalized magnetic nanoparticles. *Journal of Bioscience and Bioengineering* **100**, 1–11.

Jensen K. M. Ø., Andersen H. L., Tyrsted C., Bøjesen E. D., Dippel A.-C., Lock N., Billinge S. J. L., Iversen B. B. and Christensen M. (2014) Mechanisms for Iron Oxide Formation under Hydrothermal Conditions: An *in Situ* Total Scattering Study. *ACS Nano* **8**, 10704–10714.

Jiménez-Villacorta F., Prieto C., Huttel Y., Telling N. D. and van der Laan G. (2011) X-ray magnetic circular dichroism study of the blocking process in nanostructured iron-iron oxide core-shell systems. *Phys. Rev. B* **84**, 172404.

Jolivet J.-P., Chanéac C. and Tronc E. (2004) Iron oxide chemistry. From molecular clusters to extended solid networks. *Chem. Commun.*, 481–483.

Jolivet J.-P. and Tronc E. (1988) Interfacial electron transfer in colloidal spinel iron oxide. Conversion of Fe3O4-γFe2O3 in aqueous medium. *Journal of Colloid and Interface Science* **125**, 688–701.

Jolsterå R., Gunneriusson L. and Holmgren A. (2012) Surface complexation modeling of Fe3O4–H+ and Mg(II) sorption onto maghemite and magnetite. *Journal of Colloid and Interface Science* **386**, 260–267.

Jones A. M., Collins R. N., Rose J. and Waite T. D. (2009) The effect of silica and natural organic matter on the Fe(II)-catalysed transformation and reactivity of Fe(III) minerals. *Geochimica et Cosmochimica Acta* **73**, 4409–4422.

Jones D. L. (1998) Organic acids in the rhizosphere – a critical review. *Plant and Soil* **205**, 25–44.

Jungcharoen P., Pédrot M., Choueikani F., Pasturel M., Hanna K., Heberling F., Tesfa M. and Marsac R. (2021) Probing the effects of redox conditions and dissolved Fe2+ on nanomagnetite stoichiometry by wet chemistry, XRD, XAS and XMCD. *Environ. Sci.: Nano*.

Kalinowski B. E., Liermann L. J., Givens S. and Brantley S. L. (2000) Rates of bacteria-promoted solubilization of Fe from minerals: A review of problems and approaches. *CHEM. GEOL.* **169**, 357–370.

Keny S. J., Kumbhar A. G., Venkateswaran G. and Kishore K. (2005) Radiation effects on the dissolution kinetics of magnetite and hematite in EDTA- and NTA-based dilute chemical decontamination formulations. *Radiation Physics and Chemistry* **72**, 475–482.

Kim W., Suh C.-Y., Cho S.-W., Roh K.-M., Kwon H., Song K. and Shon I.-J. (2012) A new method for the identification and quantification of magnetite-maghemite mixture using conventional X-ray diffraction technique. *Talanta* **94**, 348–352.

Kinniburgh D. G. and Cooper D. M. (2011) PhreePlot: Creating graphical output with PHREEQC.

Kirschvink J. L., Walker M. M. and Diebel C. E. (2001) Magnetite-based magnetoreception. *Curr Opin Neurobiol* **11**, 462–467.

Kirschvink J. L., Winklhofer M. and Walker M. M. (2010) Biophysics of magnetic orientation: strengthening the interface between theory and experimental design. *J. R. Soc. Interface.* **7**.

Klausen Joerg., Troeber S. P., Haderlein S. B. and Schwarzenbach R. P. (1995) Reduction of Substituted Nitrobenzenes by Fe(II) in Aqueous Mineral Suspensions. *Environ. Sci. Technol.* **29**, 2396–2404.

Klüpfel L., Piepenbrock A., Kappler A. and Sander M. (2014) Humic substances as fully regenerable electron acceptors in recurrently anoxic environments. *Nature Geosci* **7**, 195–200.

Kobayashi A., Horikawa M., Kirschvink J. L. and Golash H. N. (2018) Magnetic control of heterogeneous ice nucleation with nanophase magnetite: Biophysical and agricultural implications. *PNAS* **115**, 5383–5388.

Kolhatkar A., Jamison A., Litvinov D., Willson R. and Lee T. (2013) Tuning the Magnetic Properties of Nanoparticles. *IJMS* **14**, 15977–16009.

Konhauser K. O., Kappler A. and Roden E. E. (2011) Iron in Microbial Metabolisms. *Elements* **7**, 89–93.

Kostka J. E., Dalton D. D., Skelton H., Dollhopf S. and Stucki J. W. (2002) Growth of Iron(III)-Reducing Bacteria on Clay Minerals as the Sole Electron Acceptor and Comparison of Growth Yields on a Variety of Oxidized Iron Forms. *Appl Environ Microbiol* **68**, 6256–6262.

Kostka J. E. and Nealson K. H. (1995) Dissolution and reduction of magnetite by bacteria. *Environ Sci Technol* **29**, 2535–2540.

Kuzmin A. and Chaboy J. (2014) EXAFS and XANES analysis of oxides at the nanoscale. *IUCrJ* **1**, 571–589.

van der Laan G. and Figueroa A. I. (2014) X-ray magnetic circular dichroism—A versatile tool to study magnetism. *Coordination Chemistry Reviews* **277–278**, 95–129.

Latta D. E., Gorski C. A., Boyanov M. I., O'Loughlin E. J., Kemner K. M. and Scherer M. M. (2012) Influence of Magnetite Stoichiometry on UVI Reduction. *Environ. Sci. Technol.* **46**, 778–786.

Laurent S., Forge D., Port M., Roch A., Robic C., Vander Elst L. and Muller R. N. (2008) Magnetic Iron Oxide Nanoparticles: Synthesis, Stabilization, Vectorization, Physicochemical Characterizations, and Biological Applications. *Chem. Rev.* **108**, 2064–2110.

Lee N., Yoo D., Ling D., Cho M. H., Hyeon T. and Cheon J. (2015) Iron Oxide Based Nanoparticles for Multimodal Imaging and Magnetoresponsive Therapy. *Chem. Rev.* **115**, 10637–10689.

Li C. (2014) A targeted approach to cancer imaging and therapy. *Nature Mater* **13**, 110–115.

Li Z., Chanéac C., Berger G., Delaunay S., Graff A. and Lefèvre G. (2019) Mechanism and kinetics of magnetite oxidation under hydrothermal conditions. *RSC Adv.* **9**, 33633–33642.

Lilova K. I., Xu F., Rosso K. M., Pearce C. I., Kamali S. and Navrotsky A. (2012) Oxide melt solution calorimetry of Fe2+-bearing oxides and application to the magnetite–maghemite (Fe3O4–Fe8/3O4) system. *American Mineralogist* **97**, 164–175.

Lin S.-S. and Gurol M. D. (1998) Catalytic Decomposition of Hydrogen Peroxide on Iron Oxide: Kinetics, Mechanism, and Implications. *Environ. Sci. Technol.* **32**, 1417–1423.

Lin X.-M. and Samia A. C. S. (2006) Synthesis, assembly and physical properties of magnetic nanoparticles. *J. Magn. Magn. Mater.* **305**, 100–109.

Lininger C. N., Brady N. W. and West A. C. (2018) Equilibria and Rate Phenomena from Atomistic to Mesoscale: Simulation Studies of Magnetite. *Acc. Chem. Res.* **51**, 583–590.

Lippert P. C. (2008) Big discovery for biogenic magnetite. *PNAS* **105**, 17595–17596.

Liu C.-H., Chuang Y.-H., Chen T.-Y., Tian Y., Li H., Wang M.-K. and Zhang W. (2015) Mechanism of Arsenic Adsorption on Magnetite Nanoparticles from Water: Thermodynamic and Spectroscopic Studies. *Environ. Sci. Technol.* **49**, 7726–7734.

Liu G., Gao J., Ai H. and Chen X. (2013) Applications and Potential Toxicity of Magnetic Iron Oxide Nanoparticles. *Small* **9**, 1533–1545.

Liu J., Sun Z., Deng Y., Zou Y., Li C., Guo X., Xiong L., Gao Y., Li F. and Zhao D. (2009) Highly Water-Dispersible Biocompatible Magnetite Particles with Low Cytotoxicity Stabilized by Citrate Groups. *Angew. Chem. Int. Ed.* **48**, 5875–5879.

López-Bucio J., Nieto-Jacobo M. F., Ramírez-Rodríguez V. and Herrera-Estrella L. (2000) Organic acid metabolism in plants: from adaptive physiology to transgenic varieties for cultivation in extreme soils. *Plant Science* **160**, 1–13.

Lu A.-H., Salabas E. L. and Schüth F. (2007) Magnetic Nanoparticles: Synthesis, Protection, Functionalization, and Application. *Angew. Chem. Int. Ed.* **46**, 1222–1244.

Magdalena A. G., Silva I. M. B., Marques R. F. C., Pipi A. R. F., Lisboa-Filho P. N. and Jafelicci M. (2018) EDTA-functionalized Fe3O4 nanoparticles. *Journal of Physics and Chemistry of Solids* **113**, 5–10.

Maher B. A. and Taylor R. M. (1988) Formation of ultrafine-grained magnetite in soils. *Nature* **336**, 368–370.

Mahmoudi M., Sant S., Wang B., Laurent S. and Sen T. (2011) Superparamagnetic iron oxide nanoparticles (SPIONs): Development, surface modification and applications in chemotherapy. *Advanced Drug Delivery Reviews* **63**, 24–46.

Marín T., Montoya P., Arnache O. and Calderón J. (2016) Influence of Surface Treatment on Magnetic Properties of Fe_3O_4 Nanoparticles Synthesized by Electrochemical Method. *J. Phys. Chem. B* **120**, 6634–6645.

Marsac R., Banik N. lal, Lützenkirchen J., Marquardt C. M., Dardenne K., Schild D., Rothe J., Diascorn A., Kupcik T., Schäfer T. and Geckeis H. (2015) Neptunium redox speciation at the illite surface. *Geochimica et Cosmochimica Acta* **152**, 39–51.

Marsac R., Pasturel M. and Hanna K. (2017) Reduction Kinetics of Nitroaromatic Compounds by Titanium-Substituted Magnetite. *J. Phys. Chem. C* **121**, 11399–11406.

Marshall T. A., Morris K., Law G. T. W., Mosselmans J. F. W., Bots P., Parry S. A. and Shaw S. (2014) Incorporation and Retention of 99-Tc(IV) in Magnetite under High pH Conditions. *Environ. Sci. Technol.* **48**, 11853–11862.

Massart R. (1981) Preparation of aqueous magnetic liquids in alkaline and acidic media. *IEEE Transactions on Magnetics* **17**, 1247–1248.

Mazarío E., Sánchez-Marcos J., Menéndez N., Cañete M., Mayoral A., Rivera-Fernández S., de la Fuente J. M. and Herrasti P. (2015) High Specific Absorption Rate and Transverse Relaxivity Effects in Manganese Ferrite Nanoparticles Obtained by an Electrochemical Route. *J. Phys. Chem. C* **119**, 6828–6834.

Melton E. D., Swanner E. D., Behrens S., Schmidt C. and Kappler A. (2014) The interplay of microbially mediated and abiotic reactions in the biogeochemical Fe cycle. *Nat Rev Microbiol* **12**, 797–808.

Mies K. A., Wirgau J. I. and Crumbliss A. L. (2006) Ternary Complex Formation Facilitates a Redox Mechanism for Iron Release from a Siderophore. *Biometals* **19**, 115–126.

Morelová N., Finck N., Lützenkirchen J., Schild D., Dardenne K. and Geckeis H. (2020) Sorption of americium / europium onto magnetite under saline conditions: Batch experiments, surface complexation modelling and X-ray absorption spectroscopy study. *Journal of Colloid and Interface Science* **561**, 708–718.

Mouritsen H. and Ritz T. (2005) Magnetoreception and its use in bird navigation. *Curr Opin Neurobiol* **15**, 406–414.

Narayanan K. B. and Sakthivel N. (2010) Biological synthesis of metal nanoparticles by microbes. *Advances in Colloid and Interface Science* **156**, 1–13.

Naseem T. and Farrukh M. A. (2015) Antibacterial Activity of Green Synthesis of Iron Nanoparticles Using *Lawsonia inermis* and *Gardenia jasminoides* Leaves Extract. *Journal of Chemistry* **2015**, 1–7.

Navrotsky A., Ma C., Lilova K. and Birkner N. (2010) Nanophase Transition Metal Oxides Show Large Thermodynamically Driven Shifts in Oxidation-Reduction Equilibria. *Science* **330**, 199–201.

NEA (2020) Chemical Thermodynamics of Iron, Part 2. *Nuclear Energy Agency (NEA)*.

Nidheesh P. V. (2015) Heterogeneous Fenton catalysts for the abatement of organic pollutants from aqueous solution: a review. *RSC Adv.* **5**, 40552–40577.

Nigam S., Barick K. C. and Bahadur D. (2011) Development of citrate-stabilized Fe3O4 nanoparticles: Conjugation and release of doxorubicin for therapeutic applications. *Journal of Magnetism and Magnetic Materials* **323**, 237–243.

Nordstrom D. K. and Campbell K. M. (2014) 7.2 - Modeling Low-Temperature Geochemical Processes. In *Treatise on Geochemistry (Second Edition)* (eds. H. D. Holland and K. K. Turekian). Elsevier, Oxford. pp. 27–68.

Norén K. and Persson P. (2007) Adsorption of monocarboxylates at the water/goethite interface: The importance of hydrogen bonding. *Geochimica et Cosmochimica Acta* **71**, 5717–5730.

Norouzi M., Yathindranath V., Thliveris J. A., Kopec B. M., Siahaan T. J. and Miller D. W. (2020) Doxorubicin-loaded iron oxide nanoparticles for glioblastoma therapy: a combinational approach for enhanced delivery of nanoparticles. *Sci Rep* **10**, 11292.

Ohresser P., Otero E., Choueikani F., Chen K., Stanescu S., Deschamps F., Moreno T., Polack F., Lagarde B., Daguerre J.-P., Marteau F., Scheurer F., Joly L., Kappler J.-P., Muller B., Bunau O. and Sainctavit Ph. (2014) DEIMOS: A beamline dedicated to dichroism measurements in the 350–2500 eV energy range. *Review of Scientific Instruments* **85**, 013106.

Pan Z., Bártová B., LaGrange T., Butorin S. M., Hyatt N. C., Stennett M. C., Kvashnina K. O. and Bernier-Latmani R. (2020) Nanoscale mechanism of UO 2 formation through uranium reduction by magnetite. *Nature Communications* **11**, 4001.

Park J., An K., Hwang Y., Park J.-G., Noh H.-J., Kim J.-Y., Park J.-H., Hwang N.-M. and Hyeon T. (2004) Ultra-large-scale syntheses of monodisperse nanocrystals. *Nature Mater* **3**, 891–895.

Park J., Lee E., Hwang N.-M., Kang M., Kim S. C., Hwang Y., Park J.-G., Noh H.-J., Kim J.-Y., Park J.-H. and Hyeon T. (2005) One-Nanometer-Scale Size-Controlled Synthesis of Monodisperse Magnetic Iron Oxide Nanoparticles. *Angewandte Chemie International Edition* **44**, 2872–2877.

Parkhurst D. L. and Appelo C. A. J. (1999) *User's guide to PHREEQC (Version 2) : a computer program for speciation, batch-reaction, one-dimensional transport, and inverse geochemical calculations*., Water-resources Investigation Report 99–4259. USGS, Denver, Colorado.

Pearce C. I., Qafoku O., Liu J., Arenholz E., Heald S. M., Kukkadapu R. K., Gorski C. A., Henderson C. M. B. and Rosso K. M. (2012) Synthesis and properties of titanomagnetite (Fe3−xTixO4) nanoparticles: A tunable solid-state Fe(II/III) redox system. *Journal of Colloid and Interface Science* **387**, 24–38.

Pellegrin E., Hagelstein M., Doyle S., Moser H. O., Fuchs J., Vollath D., Schuppler S., James M. A., Saxena S. S., Niesen L., Rogojanu O., Sawatzky G. A., Ferrero C., Borowski M. \, Tjernberg O. and Brookes

N. B. (1999) Characterization of Nanocrystalline g-Fe2O3 with Synchrotron Radiation Techniques. **215**, 797–801.

Peng H., Pearce C. I., Huang W., Zhu Z., N'Diaye A. T., Rosso K. M. and Liu J. (2018) Reversible Fe(II) uptake/release by magnetite nanoparticles. *Environ. Sci.: Nano* **5**, 1545–1555.

Peterson M. L., White A. F., Brown Gordon E. and Parks G. A. (1997) Surface Passivation of Magnetite by Reaction with Aqueous Cr(VI): XAFS and TEM Results. *Environ. Sci. Technol.* **31**, 1573–1576.

Polshettiwar V., Luque R., Fihri A., Zhu H., Bouhrara M. and Basset J.-M. (2011) Magnetically Recoverable Nanocatalysts. *Chem. Rev.* **111**, 3036–3075.

Quinto C. A., Mohindra P., Tong S. and Bao G. (2015) Multifunctional superparamagnetic iron oxide nanoparticles for combined chemotherapy and hyperthermia cancer treatment. *Nanoscale* **7**, 12728–12736.

Răcuciu M., Creangă D. E. and Airinei A. (2006) Citric-acid-coated magnetite nanoparticles for biological applications. *Eur. Phys. J. E* **21**, 117–121.

Rahim Pouran S., Abdul Raman A. A. and Wan Daud W. M. A. (2014) Review on the application of modified iron oxides as heterogeneous catalysts in Fenton reactions. *Journal of Cleaner Production* **64**, 24–35.

Ramos-Guivar J. A., López E. O., Greneche J.-M., Jochen Litterst F. and Passamani E. C. (2021) Effect of EDTA organic coating on the spin canting behavior of maghemite nanoparticles for lead (II) adsorption. *Applied Surface Science* **538**, 148021.

Ravikumar C. and Bandyopadhyaya R. (2011) Mechanistic Study on Magnetite Nanoparticle Formation by Thermal Decomposition and Coprecipitation Routes. *J. Phys. Chem. C* **115**, 1380–1387.

Revia R. A. and Zhang M. (2016) Magnetite nanoparticles for cancer diagnosis, treatment, and treatment monitoring: recent advances. *Materials Today* **19**, 157–168.

Rodríguez-Carvajal J. (1993) Recent advances in magnetic structure determination by neutron powder diffraction. *Physica B: Condensed Matter* **192**, 55–69.

Rodríquez-Carvajal J. and Roisnel T. (2004) Line Broadening Analysis Using FullProf*: Determination of Microstructural Properties. *Materials Science Forum* **443–444**, 123–126.

Roldan Cuenya B. (2010) Synthesis and catalytic properties of metal nanoparticles: Size, shape, support, composition, and oxidation state effects. *Thin Solid Films* **518**, 3127–3150.

Rossi L. M., Costa N. J. S., Silva F. P. and Wojcieszak R. (2014) Magnetic nanomaterials in catalysis: advanced catalysts for magnetic separation and beyond. *Green Chem.* **16**, 2906.

Roth H.-C., Schwaminger S., Fraga García P., Ritscher J. and Berensmeier S. (2016) Oleate coating of iron oxide nanoparticles in aqueous systems: the role of temperature and surfactant concentration. *J Nanopart Res* **18**, 99.

Sahoo Y., Goodarzi A., Swihart M. T., Ohulchanskyy T. Y., Kaur N., Furlani E. P. and Prasad P. N. (2005) Aqueous ferrofluid of magnetite nanoparticles: Fluorescence labeling and magnetophoretic control. *J. Phys. Chem. B* **109**, 3879–3885.

Sartori K., Cotin G., Bouillet C., Halté V., Bégin-Colin S., Choueikani F. and Pichon B. P. (2019) Strong interfacial coupling through exchange interactions in soft/hard core–shell nanoparticles as a function of cationic distribution. *Nanoscale* **11**, 12946–12958.

Schwaminger S. P., Bauer D., Fraga-García P., Wagner F. E. and Berensmeier S. (2017) Oxidation of magnetite nanoparticles: impact on surface and crystal properties. *CrystEngComm* **19**, 246–255.

Schwaminger S. P., García P. F., Merck G. K., Bodensteiner F. A., Heissler S., Günther S. and Berensmeier S. (2015) Nature of Interactions of Amino Acids with Bare Magnetite Nanoparticles. *J. Phys. Chem. C* **119**, 23032–23041.

Shailaja M. and Narasimhan S. V. (1991) Dissolution Kinetics of Nickel Ferrite in Chelating and Reducing Agents. *Journal of Nuclear Science and Technology* **28**, 748–756.

Sherman D. M. (1987) Molecular orbital (SCF-Xα-SW) theory of metal-metal charge transfer processes in minerals. *Phys Chem Minerals* **14**, 355–363.

Signorini L., Pasquini L., Boscherini F., Bonetti E., Letard I., Brice-Profeta S. and Sainctavit P. (2006) Local magnetism in granular iron/iron oxide nanostructures by phase- and site-selective x-ray magnetic circular dichroism. *Phys. Rev. B* **74**, 014426.

Silva A. M. N., Kong X., Parkin M. C., Cammack R. and Hider R. C. (2009) Iron(iii) citrate speciation in aqueous solution. *Dalton Trans.*, 8616.

Silvester E., Charlet L., Tournassat C., Géhin A., Grenèche J.-M. and Liger E. (2005) Redox potential measurements and Mössbauer spectrometry of FeII adsorbed onto FeIII (oxyhydr)oxides. *Geochimica et Cosmochimica Acta* **69**, 4801–4815.

Singer D. M., Chatman S. M., Ilton E. S., Rosso K. M., Banfield J. F. and Waychunas G. A. (2012) U(VI) Sorption and Reduction Kinetics on the Magnetite (111) Surface. *Environ. Sci. Technol.* **46**, 3821–3830.

Soenen S. J. H., Brisson A. R. and De Cuyper M. (2009) Addressing the problem of cationic lipid-mediated toxicity: The magnetoliposome model. *Biomaterials* **30**, 3691–3701.

Stephen Z. R., Kievit F. M. and Zhang M. (2011) Magnetite nanoparticles for medical MR imaging. *Materials Today* **14**, 330–338.

Stoerzinger K. A., Pearce C. I., Droubay T. C., Shutthanandan V., Liu Z., Arenholz E. and Rosso K. M. (2019) Structure, Magnetism, and the Interaction of Water with Ti-Doped Fe_3O_4 Surfaces. *Langmuir* **35**, 13872–13879.

Sun Z.-X., Su F.-W., Forsling W. and Samskog P.-O. (1998) Surface Characteristics of Magnetite in Aqueous Suspension. *Journal of Colloid and Interface Science* **197**, 151–159.

Sweeton F. H. and Baes C. F. (1970) The solubility of magnetite and hydrolysis of ferrous ion in aqueous solutions at elevated temperatures. *The Journal of Chemical Thermodynamics* **2**, 479–500.

Teasdale P. R., Minnett A. I., Dixon K., Lewis T. W. and Batley G. E. (1998) Practical improvements for redox potential (Eh) measurements and the application of a multiple-electrode redox probe (MERP) for characterising sediment in situ.

Teja A. S. and Koh P.-Y. (2009) Synthesis, properties, and applications of magnetic iron oxide nanoparticles. *Progress in Crystal Growth and Characterization of Materials* **55**, 22–45.

Tombácz E., Tóth I. Y., Nesztor D., Illés E., Hajdú A., Szekeres M., and L.Vékás (2013) Adsorption of organic acids on magnetite nanoparticles, pH-dependent colloidal stability and salt tolerance. *Colloids and Surfaces A: Physicochemical and Engineering Aspects* **435**, 91–96.

Turcu R., Socoliuc V., Craciunescu I., Petran A., Paulus A., Franzreb M., Vasile E. and Vekas L. (2015) Magnetic microgels, a promising candidate for enhanced magnetic adsorbent particles in bioseparation: synthesis, physicochemical characterization, and separation performance. *Soft Matter* **11**, 1008–1018.

Unni M., Uhl A. M., Savliwala S., Savitzky B. H., Dhavalikar R., Garraud N., Arnold D. P., Kourkoutis L. F., Andrew J. S. and Rinaldi C. (2017) Thermal Decomposition Synthesis of Iron Oxide Nanoparticles with Diminished Magnetic Dead Layer by Controlled Addition of Oxygen. *ACS Nano* **11**, 2284–2303.

Usman M., Byrne J. M., Chaudhary A., Orsetti S., Hanna K., Ruby C., Kappler A. and Haderlein S. B. (2018) Magnetite and Green Rust: Synthesis, Properties, and Environmental Applications of Mixed-Valent Iron Minerals. *Chem. Rev.* **118**, 3251–3304.

Usman M., Martin S., Cimetière N., Giraudet S., Chatain V. and Hanna K. (2014) Sorption of nalidixic acid onto micrometric and nanometric magnetites: Experimental study and modeling. *Applied Surface Science* **299**, 136–145.

Vukosav P., Mlakar M. and Tomišić V. (2012) Revision of iron(III)–citrate speciation in aqueous solution. Voltammetric and spectrophotometric studies. *Analytica Chimica Acta* **745**, 85–91.

Walz F. (2002) TOPICAL REVIEW: The Verwey transition - a topical review. *Journal of Physics Condensed Matter* **14**, R285–R340.

Wang D., Kou R., Choi D., Yang Z., Nie Z., Li J., Saraf L. V., Hu D., Zhang J., Graff G. L., Liu J., Pope M. A. and Aksay I. A. (2010) Ternary Self-Assembly of Ordered Metal Oxide−Graphene Nanocomposites for Electrochemical Energy Storage. *ACS Nano* **4**, 1587–1595.

Wang M., Wang N., Tang H., Cao M., She Y. and Zhu L. (2012) Surface modification of nano-Fe_3O_4 with EDTA and its use in H_2O_2 activation for removing organic pollutants. *Catal. Sci. Technol.* **2**, 187–194.

Wei H., Bruns O. T., Kaul M. G., Hansen E. C., Barch M., Wiśniowska A., Chen O., Chen Y., Li N., Okada S., Cordero J. M., Heine M., Farrar C. T., Montana D. M., Adam G., Ittrich H., Jasanoff A., Nielsen P.

and Bawendi M. G. (2017) Exceedingly small iron oxide nanoparticles as positive MRI contrast agents. *Proc Natl Acad Sci USA* **114**, 2325–2330.

Weissleder R., Nahrendorf M. and Pittet M. J. (2014) Imaging macrophages with nanoparticles. *Nature Mater* **13**, 125–138.

White A. F., Peterson M. L. and Hochella M. F. (1994) Electrochemistry and dissolution kinetics of magnetite and ilmenite. *Geochimica et Cosmochimica Acta* **58**, 1859–1875.

Woo K., Hong J., Choi S., Lee H. W., Ahn J. P., Kim C. S. and Lee S. W. (2004) Easy synthesis and magnetic properties of iron oxide nanoparticles. *Chem. Mat.* **16**, 2814–2818.

Wu S., Sun A., Zhai F., Wang J., Xu W., Zhang Q. and Volinsky A. A. (2011) Fe3O4 magnetic nanoparticles synthesis from tailings by ultrasonic chemical co-precipitation. *Mater. Lett.* **65**, 1882–1884.

Wu W., He Q. and Jiang C. (2008) Magnetic Iron Oxide Nanoparticles: Synthesis and Surface Functionalization Strategies. *Nanoscale Res. Lett.* **3**, 397–415.

Xu M., Zhang Y., Zhang Z., Shen Y., Zhao M. and Pan G. (2011) Study on the adsorption of Ca2+, Cd2+ and Pb2+ by magnetic Fe3O4 yeast treated with EDTA dianhydride. *Chemical Engineering Journal* **168**, 737–745.

Xu P., Zeng G. M., Huang D. L., Feng C. L., Hu S., Zhao M. H., Lai C., Wei Z., Huang C., Xie G. X. and Liu Z. F. (2012) Use of iron oxide nanomaterials in wastewater treatment: A review. *Science of The Total Environment* **424**, 1–10.

Yang J. B., Zhou X. D., Yelon W. B., James W. J., Cai Q., Gopalakrishnan K. V., Malik S. K., Sun X. C. and Nikles D. E. (2004) Magnetic and structural studies of the Verwey transition in Fe3−δO4 nanoparticles. *Journal of Applied Physics* **95**, 7540–7542.

Yang L., Steefel C. I., Marcus M. A. and Bargar J. R. (2010) Kinetics of Fe(II)-Catalyzed Transformation of 6-line Ferrihydrite under Anaerobic Flow Conditions. *Environ. Sci. Technol.* **44**, 5469–5475.

Yew Y. P., Shameli K., Miyake M., Ahmad Khairudin N. B. B., Mohamad S. E. B., Naiki T. and Lee K. X. (2020) Green biosynthesis of superparamagnetic magnetite Fe3O4 nanoparticles and biomedical applications in targeted anticancer drug delivery system: A review. *Arabian Journal of Chemistry* **13**, 2287–2308.

Yi Y., Zhang Y., Wang Y., Shen L., Jia M., Huang Y., Hou Z. and Zhuang G. (2014) Ethylenediaminetetraacetic acid as capping ligands for highly water-dispersible iron oxide particles. *Nanoscale Res Lett* **9**, 27.

Yuan K., Lee S. S., Cha W., Ulvestad A., Kim H., Abdilla B., Sturchio N. C. and Fenter P. (2019) Oxidation induced strain and defects in magnetite crystals. *Nat Commun* **10**, 1–10.

Zanganeh S., Hutter G., Spitler R., Lenkov O., Mahmoudi M., Shaw A., Pajarinen J. S., Nejadnik H., Goodman S., Moseley M., Coussens L. M. and Daldrup-Link H. E. (2016) Iron oxide nanoparticles inhibit tumour growth by inducing pro-inflammatory macrophage polarization in tumour tissues. *Nature Nanotech* **11**, 986–994.

Zhang T., Lowry G., Capiro N., Chen J., Chen W., Chen Y., Dionysiou D., Elliott D., Ghoshal S., Hofmann T., Hsu-Kim H., Hughes J., Jiang C., Jiang G., Jing C., Kavanaugh M., Li Q., Liu S., Ma J. and Alvarez P. (2019) In situ remediation of subsurface contamination: Opportunities and challenges for nanotechnology and advanced materials. *Environmental science. Nano.* **6**.

Zhao H., Saatchi K. and Häfeli U. O. (2009) Preparation of biodegradable magnetic microspheres with poly(lactic acid)-coated magnetite. *Journal of Magnetism and Magnetic Materials* **321**, 1356–1363.

Zhu X., Zhu Y., Murali S., Stoller M. D. and Ruoff R. S. (2011) Nanostructured Reduced Graphene Oxide/Fe $_2$ O $_3$ Composite As a High-Performance Anode Material for Lithium Ion Batteries. *ACS Nano* **5**, 3333–3338.

UNIVERSITÉ DE RENNES 1

Titre : Impact des conditions environnementales sur la stœchiométrie de nanoparticules de magnétite

Mots clés : magnétite, maghémite, stœchiométrie, solubilité, solution-solide, modèle de spéciation géochimique, XMCD.

Résumé : Les nanoparticules de magnétite (MNs, 10 nm) sont présentes au cœur de la Zone Critique : le sol. Les MN ont été largement utilisés dans de nombreuses applications (la dépollution, la catalyse, le stockage d'énergie, l'imagerie et la thérapie médicale, etc.) en raison de leurs propriétés physiques et chimiques (optiques, magnétiques, semi-conducteurs et large surface spécifique). Cependant, les MNs stœchiométriques sont extrêmement sensibles à l''O_2 et aux conditions de pH. Ce projet de thèse visait à étudier l'évolution de la stœchiométrie de la magnétite (R = Fe(II)/Fe(III)) par utilisation du rayonnement synchrotron et à développer des modèles prédictifs de la solubilité de la magnétite dans des conditions environnementales pertinentes (pH, condition redox, concentration en Fe(II) dissous et présence de ligands organiques). Bien que la recherche à ce jour ait eu tendance à se concentrer sur les taux de réduction des contaminants en fonction de la stœchiométrie initiale de la magnétite (R_{ini}), aucun travail ne s'est préoccupé du rapport effectif (R_{eff}) et de la solubilité du Fe. Ici, cette thèse démontre que les MNs stœchiométriques ne peuvent pas exister à pH < 7 malgré une concentration élevée de magnétite et un excès de Fe(II) dissous. L'ajout de molécules organiques (citrate, EDTA, etc.) peut modifier de manière significative les propriétés de surface des MNs. Par conséquent, des précautions doivent être prises lorsque l'on travaille avec des MNs en présence de ligands.

Title: Impact of the environmental conditions on the stoichiometry of magnetite nanoparticles

Keywords: magnetite, maghemite, stoichiometry, solubility, solid-solution, geochemical speciation model, XMCD

Abstract: Magnetite nanoparticles (MNs,10 nm) are present at the heart of the Critical Zone: the soil. MNs has been broadly used in numerous applications (e.g. environmental remediation, catalysis, energy storage, magnetic resonance imaging, medicine therapy) due to their physicochemical properties (e.g. magnetic, highly surface areas, optic, semiconductor). However, stoichiometric MNs are extremely sensitive to the presence of oxygen and pH condition. This thesis project aimed to study the evolution of the stoichiometry of magnetite (R =Fe(II)/Fe(III)) and to develop predictive models of magnetite solubility under environmentally relevant conditions (pH, redox condition, oxidation, recharge, overloading of dissolved Fe(II), and the presence of organic ligands). Although the research to date has tended to focus on the rates of contaminant reduction by initial magnetite stoichiometry (R_{ini}) rather than the effective ratio (R_{eff}), no work concerns about the R_{eff} and solubility of Fe. Here, this study demonstrates that stoichiometric MNs cannot exist at pH < 7 despite a high magnetite concentration and an excess of dissolved Fe(II). Adding of organic molecules (e.g. citrate, EDTA) can change significantly the surface properties of MNs. Therefore, caution should be taken when working with MNs in presence of ligands.